Chromatin: a playground of drug interaction

by Dr. Erfaneh Firouzi Niaki (Pharm.D.)

Supervisor: Prof. Dr. Gabor Szabo, M.D., Ph.D.

UNIVERSITY OF DEBRECEN

DOCTORAL SCHOOL OF MOLECULAR CELL AND IMMUNE BIOLOGY

DEBRECEN, 2021

TABLE OF CONTENTS

ABBREVIATIONS…….....4

Part A. INTERACTIONS OF CISPLATIN AND DAUNORUBICIN

1. INTRODUCTION…….....5

1.1. Cisplatin…….....6

1.1.1. Chemistry of Cisplatin…….....6

1.1.2. Cisplatin and DNA……..….8

1.1.3. Effect of adducts on DNA and nucleosome structure…….....9

1.1.4. Cisplatin and other cellular molecules…….....9

1.1.5. Cytotoxicity……10

1.1.6. Effect of DNA topology on adduct formation……..……..……...11

1.2. Superhelicity …….....14

1.2.1. Why does it matter?.....14

1.2.2. What is it?.....15

1.3. Anthracycline..……..…….....19

1.3.1. Chemistry of anthracyclines…….....19

1.3.2. Daunorubicin and its mechanisms of action…….....20

1.3.3. Interaction of Daunorubicin with chromatin……...……..……23

1.4. Combination therapy……...……...24

1.4.1. Chou-Talaly (Dose-Effect) Analysis……..24

2. AIM AND OBJECTIVES OF THE STUDY…….....26

3. MATERIALS AND METHODS……..…….....……27

3.1. Materials…….....27

3.2. Methods……27

3.2.1. Cytotoxicity assay……..28

3.2.2. Urea-agarose gel electrophoresis……..……...…..……28

3.2.3. Measurement of Daunorubicin fluorescence…….....28

3.2.3.1. Determination of total intracellular Daunorubicin fluorescence……...28

3.2.3.2. Determination of total nuclear Daunorubicin fluorescence…….…….29

3.2.3.3. Determination of DNA-bound Daunorubicin fluorescence.…..…….....29

3.2.3.4. Flow cytometry……..29

3.2.4. Measurement of Histone eviction.….…….....29

3.2.5. Measurement of total Cisplatin-DNA and interstrand crosslink levels by Laser scanning cytometry……..30

3.2.5.1. Preparation of comets and halos..……..…….....30

3.2.5.2. Determination of total amount of total Cisplatin-DNA crosslinks…….….....31

3.2.5.3. Laser scanning cytometry.…… …….....31

3.2.6. Determination of amount of Platinum in the nuclei of agarose-embedded cells using quantitative laser ablation-inductively coupled plasma mass spectrometry spot analysis……...….....32

3.2.6.1. LA-ICP instrumentation..…….....…….....…….....32

3.2.6.2. Spot analysis.....32

3.2.7. Statistical analysis.....32

4. RESULTS…….....34

4.1. Cisplatin and Daunorubicin synergize or antagonize each other depending on cell type and applied dose…….....34

4.2. Co-treatment of Dauno with Cisplatin differentially alters the amount of total cellular, chromatin-bound and DNA-bound Dauno.… ……..44

4.3. Cisplatin facilitates Dauno-induced histone eviction..…….....44

4.4. Detection of ICLs using a modified alkaline comet assay.…….....46

4.5. Co-treatment of Cisplatin with Dauno alters Cisplatin-DNA adduct level…….....48

4.6. Effect of nucleosome eviction on Cisplatin-DNA crosslinks level…….....49

5. DISCUSSION…….…….....……52

6. SUMMARY…….....58

Part B. THE RELEVANCE OF HISTONE LEVELS FOR DNA-TARGETED THERAPY

I. INTRODUCTION…….....60

II. AIM OF THE STUDY...…….....……..….64

III. METHODS……...…….....……64

IV. RESULTS……..…….....……66

V.DISCUSSION.....69

VI.SUMMARY.....70

7. REFERENCES……..…….....71

8. KEY WORDS.....92

9. ACKNOWLEDGEMENTS…….....93

10. APPENDIX.....94

ABBREVIATIONS

AMD1	Adenosylmethionine Decarboxlase 1
BSA	Bovine serum albumin
CI	Combination index
Cis-Pt	Cisplatin
Dauno	Daunorubicin
Dox	Doxorubicin
E.coli	*Esherchia coli*
EBr	Ethidium bromide
Fa-CI	Drug effect level%-Combination index
GFP	Green fluorescent protein
ICL	Interstrand cross-link
LA-ICP-MS	Laser Ablation Inductively Coupled plasma Spectrometry
LMP	Low melting point
LSC	Laser scanning cytometry
MEE	Median dose-effect equation
ODC1	Ornithine Decarboxylase 1
PA	Polyamine
PBS	Phosphate buffer saline
PI	Propidium iodide
QINESIn	Quantitative Imaging of Nuclei after Elution with Salt/Intercalators
ROS	Reactive oxygen species
TES	Transcription End Sites
Top2	Topoisomerase II
TSS	Transcription Start Sites

Part A. Interactions of Cisplatin and Daunorubicin

1. INTRODUCTION

The application of multiple anticancer drugs with a diverse mode of actions that target different cell components might lead to a desirable outcome to treat particular cancer types more effectively. A synergy of the drugs could lead to 1) increment in the effectiveness of therapy; 2) reduction in the dosage to decrease side effects while improving or maintaining efficacy; 3) mitigate or delay the development of resistance to the drug. In this matter it is questionable what strategies and approaches are best for choosing candidates to be combined and tested even at the pre-clinical state of research. It also seems challenging to interpret and evaluate the results of pre-clinical tests, what is crucial to move forward to the clinical trials. A combination is considered efficient if it generates enhanced response compared to the individual drugs by themselves. Because numerous drug combinations only have additive or slight synergistic effects, it is the extent of synergy that becomes vital to be determined. This task demands high throughput methods. On the other hand, the choice of the drugs to be combined must fit some rationale based on the mechanisms of action involved.

Anticancer drugs that target chromatin are some of the most effective agents in combating cancer. Anthracyclines and platinum-based drugs have been exploited in combination chemotherapy to treat a broad variety of different types of cancer, such as ovarian carcinoma[1,2], small cell lung cancer[3], and in endometrial carcinoma[4], among others.

Cisplatin (Cis-Pt) is a component of the standard treatment of testicular, ovarian, cervical, head and neck, lung and bladder cancer, also lymphomas, myelomas, and melanoma. Daunorubicin (Dauno), a member of the anthracyclines family, is used in the treatment of acute myeloid leukemia (AML), acute lymphoblastic leukemia (ALL), and lymphomas. Doxorubicin (Dox), a congener derivative of Dauno, is indicated in treating several cancer types such as ALL, AML, breast cancer, lung cancer, Hodgkin and non-Hodgkin lymphomas, and ovarian cancer. (https://www.cancer.gov/about-cancer/treatment/drugs/)

Although many of the cellular targets of these anticancer agents are known, their involvement in cytotoxicity is poorly understood. Therefore, how they interact with each other when used in combination is even more difficult to predict. On the other hand, long-term benefits of

combination treatments include overcoming the emergence of resistant cell clones. Therefore, although anthracyclines and Cis-Pt e.g., the drugs most frequently used in the treatment regimens of ovarian cancer, exhibit a combined effect no greater than additivity[5], the advantages of combination treatment may still be significant.

My focus, however, is interaction of these drugs at the level of primary toxicity. For both Cis-Pt and Dauno, the main drug target is chromatin and both influence DNA topology; thus the possibility arises that they may mutually influence each other's binding to their chromatin targets. Therefore, we set out to determine how the Dauno evoked changes in chromatin structure and DNA topology affect the formation of Cis-Pt-DNA adducts, and vice versa how Cis-Pt influences Dauno binding.

1.1. Cisplatin

1.1.1. Chemistry of Cisplatin

Cisplatin (Cis-Pt), *Cis*-(Pt $(NH3)_2Cl_2$), formerly known as Peyrone's chloride, was first synthesized by Michele Peyrone in 1844; a century later, subsequent to investigations addressing the effect of electric fields on *Escherichia coli (E.coli)* growth, it was observed by Barnett Rosenberg[6] that electrolyzed platinum derived from the electrodes formed a platinum complex which inhibited bacterial cell proliferation. The discovery that Cis-Pt treatment elicited a decrease of sarcoma mass in rats[7] established its anti-cancer activity. Cis-Pt consists of two ammine and two chloride ligands in the *cis* configuration, bound to a single atom of platinum in a square planar complex. The molecular structure is shown in **Figure 1**.

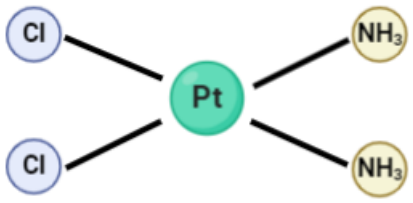

Figure 1. Molecular structures *Cis*-diamminodichloroplatinum (II)

Cis-Pt is a small uncharged molecule thus its uptake into cells prominently occurs via passive diffusion[8]. Once inside the cell, it is converted to cationic species which may not cross over the lipid bilayer of the cell membrane readily. In addition to passive diffusion, a series of studies have indicated that Cis-Pt is imported to tumor cells by transporters such as copper transporter 1 (Ctr1)[9,10] as well as organic cation transporters (OCT2)[11], while the copper-transporting P-type transporter ATP7B[12] and the ATP-binding cassette transporter ABCC2[13] are associated with the active efflux of Cis-Pt.

Cis-Pt is administered intravenously. Extracellular fluids contain high concentrations of chlorides (~100 mM), in which Cis-Pt exists in stable, inert, dichloro-form. Following its entry into the cell, due to the decrease of chloride concentration to ~2-10 mM, the diammino*dichloro*platinum (II) undergoes a nucleophilic substitution (SN_2)[14] reactions in which the chloro ligands are substituted with water molecules in two consecutive steps while preserving *cis* configuration, to become the chemically active *cis* diammined*iaqua*platinum (II) species. The chemical reaction is shown in **Figure 2**. This hydrolysis reaction is the rate-limiting step for DNA binding, and the half-life ($t_{1/2}$) for substitution of the first chloride ligand with water is about 2 hours (hrs)[15].

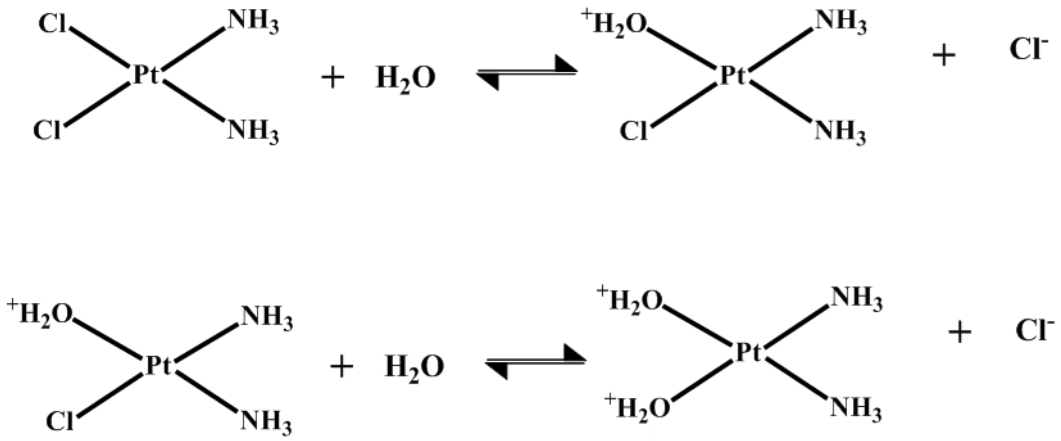

Figure 2. *Aqua*tion reactions involving Cis-Pt in the cell

1.1.2. Cis-Pt and DNA

The cationic aquated Cis-Pt species behave as electrophilic reagents and interact with nucleophilic sites on the DNA. The water molecule of the mono-aquated species is readily substituted by the N7 of guanine or adenine, forming a monofunctional adduct ($t_{1/2}$ of formation = 2 hrs)[15]. Due to the presence of the potentially reactive sites in the vicinity, the monofunctional adduct reacts and rearranges to form intra- and interstrand cross-links (ICL) ($t_{1/2}$ of formation= 2.1-3.5 hrs)[15,16]. Through the reaction of the bifunctional platinum compound with adjacent purines, different types of adducts form, as shown in **Figure 3**. The DNA isolated from white blood cells of patients treated with Cis-Pt contained intrastrand cross-links formed by the binding of Cis-Pt to two neighboring guanines (1,2-d(GpG)) comprises ~65% of the total Cis-Pt-DNA adducts, ~22% of the adducts formed on adenine and guanine in the 1,2-d(ApG) sequence but not in pGpA, ~13% on two guanines separated by one or more nucleotides (1,3-d(GpNpG))[17], while ICLs forming between the guanine bases at complementary strands were present at a frequency of about 1-5%[18]. Based on calculated electrostatic potentials of the bases, it was postulated that the G-G sequence is the most electronegative region in double-stranded DNA[19] and, therefore, represent the most reactive site toward the positively charged, aquated Cis-Pt intermediate; this explains why platination at G-G sequence comprises the majority of the adducts. Reactivity of the individual nucleobases according to the calculated electrostatic potentials in a decreasing order : guanine-N7>>adenine-N7 > cytosine-N3[20].

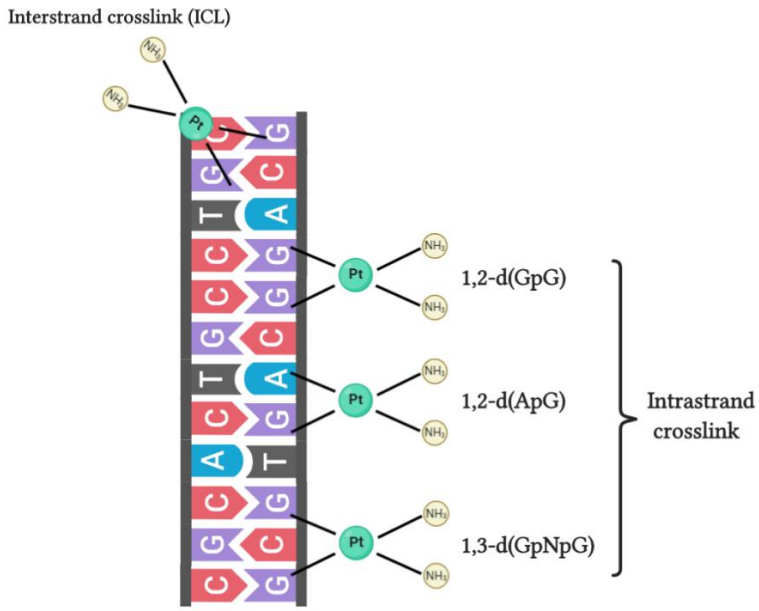

Figure 3. Types of DNA-Cis-Pt crosslinks

1.1.3. Effect of adducts on DNA and nucleosome structure

The formation of Cis-Pt-DNA adducts causes distortions of the DNA conformation. The structural alterations induced in DNA after binding of Cis-Pt have been extensively studied. Gel electrophoretic[21-23], X-ray crystallographic[24,25], and NMR spectroscopic[26,27] studies demonstrated that intrastrand cross-linking adducts tend to bend the DNA toward the major groove[21], while ICLs cause DNA bending toward the minor groove[28]. Cis-Pt adducts also unwind the DNA helix: 1,2- and 1,3- intrastrand adducts by 13˚ and 23˚ [22], respectively, whereas a single ICL unwinds DNA by approximately 79˚ [29]. These adduct-induced distortions are recognized by various classes of proteins, including high-mobility group (HMG) box proteins, repair proteins, transcription factors[30] and several other proteins including histone H1 that preferentially recognizes the 1,2-intrastrand cross-linked platinum–DNA adducts as reviewed in ref.[31]. The effect of Cis-Pt on post-translational modifications (PTM) of H3 and H4 histones has also been studied[32]: According to Western-blot analyses of Cis-Pt-treated HeLa cells, the drug induces phosphorylation of H3 at Ser-10 and acetylation of H4. These changes may be biologically relevant since phosphorylation of H3 at interphase correlates with chromatin relaxation and gene expression, while in mitosis it correlates with compaction[33]; on the other hand, acetylation of H4 (on K_{16} in particular) results in a disruption in internucleosomal interactions thus having a profound impact on chromatin structure[34].

1.1.4. Cis-Pt and other cellular molecules

Cis-Pt target the vast majority of biological macromolecules. It reacts with and impairs the proper functioning of several RNA molecules, including the whole pool of mRNAs[35] , rRNA[36] and the RNA component of telomerase[37], to mention just a few. Recent studies on interactions of Cis-Pt with ribosome constituents have found that Cis-Pt targets pivotal parts of the ribosome like the mRNA channel, the GTPase activating center, the peptide exit tunnel, and a functionally important "bridge" (named B7a) between the two ribosomal subunits. These data suggest that Cis-Pt stabilizes mRNA binding to the ribosomal P site and prevents mRNA/tRNA translocation, thus inhibiting protein synthesis[38]. Cis-Pt binds also to lipid components of plasma membrane (phosphatidylserine and phospholipids) that results in plasma membrane disruption[39]. Furthermore, by binding to tubulin and G-actin, Cis-Pt inhibits polymerization of microtubules and microfilaments, respectively[39,40]. Reactions of proteins with the drug have been extensively investigated as reviewed in refs. [41,42]. Proteins, notably those containing cysteine and methionine residues, readily bind to Cis-Pt.

Cis-Pt mainly reacts with thiol-containing polypeptide species such as metallothioneins[43]. It also reacts with the tripeptide glutathione; in some platinum-resistant cancer cells, glutathione and metallothionein levels are relatively high, therefor Cis-Pt is soaked up in the cytoplasm before DNA binding can occur, thus causing resistance[44,45].

1.1.5. Cytotoxicity

There are strong pieces of evidence that DNA is the critical therapeutic target of Cis-Pt among its many potential cellular targets. For instance, when the number of platinum atoms binding to DNA, RNA, and protein molecules was measured in the case of HeLa cells treated with ^{195m}Pt-radiolabeled Cis-Pt used at a lethal dose[46], the ratio of Cis-Pt modified molecules to the total number of the same molecular species in the cell was much higher in the case of DNA than for the other classes of molecules. Based on this study, binding of Cis-Pt to the DNA is generally perceived as the leading cause of its toxicity[46]. Other studies on *E.coli* and human cells demonstrated that DNA repair-deficient cells were 3-10x more susceptible to Cis-Pt than wild type cells[31] suggesting that DNA is indeed the primary therapeutic target of Cis-Pt.

In experiments performed on human HL-60 cells ~48,000 Pt-DNA adducts (i.e., ~ 1Pt/125 kilobase pairs (kbp)) per cell gave rise to 50 % inhibition of cell growth. Considering that the number of 1,2-intrastrand cross-links is predicted to occur at a frequency of ~65% of total Pt-DNA adducts, it was concluded that there were ~31000 1,2- intrastrand cross-links/cell, while the number of ICLs was estimated to be only 480/cell[47]. The contribution of the various types of cross-links to toxicity has not been clarified fully. Nonetheless, as intrastrand cross-links comprise the major form of adducts, it is suggested that this type of lesion may be responsible for the cytotoxic action of Cis-Pt. In line with this notion, transplatin, the trans-isomer of Cis-Pt that is ineffective in chemotherapy is unable to form 1,2-intrastrand cross-links; therefore, intrastrand cross-links. On the other hand, ICLs are deemed not to be the primary cytotoxic lesions in conformity with the observation that transplatin, despite of the fact that it is ~ 6 fold more apt to form ICLs than Cis-Pt, is clinically ineffective[48]. However, based on the hypersensitivity of Fanconi anemia cells (defective in the repair of ICLs) to ICL forming reagents their impact on cytotoxicity may still be considerable[48,49].

Cis-Pt induced DNA adducts were mapped genome-wide using a new generation sequencing-based “Damage-seq” protocol *in vivo* and *in vitro* in human B-lymphoblast[50] and mouse internal organs[51]. The results showed that these adducts are evenly distributed throughout the genome and were only slightly more abundant at the promoters than at the enhancers. While

these regions are known to be nucleosome-free regions, the question was raised whether enrichment of Cis-Pt adducts at promoters was due to the structure of the chromatin or it was a reflection of the elevated G-G (i.e., the preferred target for Cis-Pt to form 1,2-intrastrand adducts) frequency here. To answer this, the authors compared the G-G frequency at the Transcription Start Sites (TSSs) and Transcription End Sites (TESs) of the genes, and it was shown that the dinucleotide G-G frequency at TSSs is generally higher relative to TES regions; thus, they attributed the higher incidence of Pt-d (GpG) adducts formed in promoters to this rather than the open chromatin structure. As opposed to the study described above, Cis-Pt binding to linker region was shown to be preferred over binding to nucleosomal DNA and the ratio of the DNA damage caused by Cis-Pt was ~ 1.3 times higher at linker regions than within the core region of nucleosomes[52].

While the above and most other similar studies examined the formation of all types of the Cis-Pt-DNA adducts together[52-54], in another publication specifically the formation of ICLs[50,51] was measured in reconstituted nucleosomal and naked DNA. According to these latter results, Cis-Pt forms ICLs with naked and nucleosomal DNA at a similar efficiency[55]. Taken together the above results, it is unlikely that Cis-Pt would prefer linker DNA over nucleosomal DNA to a degree what could have biological significance, as it binds rather uniformly along the chromatin fiber most probably due to its small size.

1.1.6. Effect of DNA topology on adduct formation

Regarding the question whether DNA topology plays a role in the formation Cis-Pt-DNA adducts, indirect evidence was obtained in experiments where the influence of DNA supercoiling on the cytotoxicity of Cis-Pt in *E.Coli* K12 bacteria was studied. Bacteria carrying mutations in the Gyrase gene were treated with Cis-Pt. (In Eubacteria, the Gyrase enzyme introduces negative superhelical turns into the genomic DNA and Gyrase defects are known to decrease superhelical density by ~ 25% in comparison with the level of supercoiling in the wild-type). An ~1.5x increase in the amount of total Cis-Pt bound to DNA, measured by atomic absorption spectroscopy, was observed in the mutant strains, implying an influence of DNA supercoiling on DNA platination[56]. In *in vitro* experiments, the number of ICLs was compared in supercoiled and linear plasmid DNA[57]. The results showed that at relatively low levels of total modification by Cis-Pt (< 1 Pt /500 bp), ICLs were formed in negatively supercoiled DNA at approximately 3x higher frequency than in linear or relaxed DNA[57]. In these studies ICLs

comprised 30%-40% of the total adducts. In theory, the increase of ICL incidence in supercoiled DNA could also be due to the formation of cross-links between distant bases, when DNA loops form by the cross-links mediated by ICL. In other words, two remote bases could be brought to the vicinity of each other so that Cis-Pt could cross-link them leading to formation of covalently closed loops. Upon exposure of such loops to γ-irradiation, the loops are expected to relax and remain compact, thus migrating in non-denaturing agarose gels in the same fashion as intact supercoiled plasmids. However, following induction of nicks, DNA co-migrated similarly to relax non-platinated DNA, suggesting that ICLs in negatively supercoiled DNA did not significantly form between remote bases. Instead, ICLs were shown to preferentially form between residues that are in proximity[57]. The kinetics of ICL formation were also faster in supercoiled DNA (formation $t_{1/2}$ ~ 2 hrs) than in linearized DNA ($t_{1/2}$~ 4 hrs), suggesting that negative supercoiling indeed enhances ICL formation[57]. ICL formation by another interstrand cross-linker, Psoralen[58], is also favored in negatively supercoiled as compared to linear or relaxed DNA. However, based on work in our lab, it is likely that psoralen intercalation between the adjacent base pairs and not cross-linking, is facilitated by negative supercoiling[59]. Since ICLs are minor adducts formed by Cis-Pt, their detection and measurement in cells at clinically relevant doses of the agent are challenging. Several techniques have been used, including denaturing electrophoresis, mass spectrometry, and alkaline single-cell gel electrophoresis (Comet) assay. These methods and their advantages and limitation are well reviewed in ref.[60]. The basis of these methods in brief is that the complementary strands of the DNA cannot be separated due to the covalent cross-links formed by Cis-Pt.

The alkaline comet assay, originally used to measure DNA strand breaks, is an established method for detection of ICLs also. It is based on the preferential re-association of alkali-denatured genomic DNA derived from Cis-Pt-treated cells. Upon electrophoresis of single cells embedded in low melting point agarose under denaturing condition, DNA without ICLs migrates in its denatured, single-stranded form, whereas the complementary strands do not separate when the DNA is cross-linked by Cis-Pt and will migrate more slowly[61].

In summary, the Cis-Pt-induced DNA cross-links, intrastrand and interstrand alike, appear to be sensitive to DNA topology. As I will describe it in section 1.3, anthracyclines, often used in cancer chemotherapy in combination with Cis-Pt, elicit changes in DNA conformation upon their intercalation between the adjacent base-pairs. Therefore, their co-administration with Cis-Pt may result in major consequences on Cis-Pt toxicity. Conversely, the Cis-Pt-elicited cross-links may fix genomic DNA in constrained conformational states antagonizing intercalation.

In view of these complexities, we set out to determine how the Dauno evoked changes in chromatin structure and DNA topology affect the formation of Cis-Pt-DNA adducts, and how Cis-Pt influences Dauno uptake and binding.

1.2 Superhelicity

1.2.1. Why does it matter?

The hierarchical packaging of the genomic DNA is eukaryotes involves formation of the nucleosomal structure (beads-on-a-string), then further packaging into a continuum of zigzag and ~30 nm fibers, formation of chromatin loops and further, higher order compaction[62]; all these structural changes involve changes of DNA supercoiling[63]. In bacterial systems, supercoiling appears to be essential for viability and is finely tuned by the antagonistic activities of DNA gyrase and topoisomerase I. Alterations in the level of supercoiling by more than 25% subsequent to mutation in corresponding genes are lethal[64]. DNA supercoiling, affecting the conformation of larger DNA regions, as well as locally influencing DNA structure is an important player in the regulation of gene expression as reviewed in[64-68]. For efficient transcription as well as replication, negative supercoiling facilitates the separation of DNA double strands. Such a topology is introduced into the bacterial systems in an ATP-dependent manner by gyrase enzymes (see section 1.1); in eukaryotes, nucleosomal structure entails negative supercoiling. Toroidal writhes composed of 145-147 bp of DNA wrapped around the histone octamer, forms 1.65 turns[69]. Upon unwrapping of DNA from nucleosomes, the constrained toroidal writhe is converted to unconstrained plectonemic writhe[70]. When the constrained, negative supercoils form upon the assembly of the nucleosomes, compensatory positive supercoils are generated in the linker DNA[64] that are assumed to be relaxed by topoisomerases. (See section 1.3). Upon the binding of large proteins and their subsequent translocation along the DNA (like DNA and RNA polymerases), the baseline supercoiled state is altered transiently: overwound and underwound supercoils are generated in front and behind the elongating polymerase[71,72], respectively. In other words, instead of one helical turn per 10.5 bp, there is one helical turn per < 10.5 bp ahead of RNA polymerase, whereas, in the rear, there is one helical turn per >10.5 bp. If the positive supercoils ahead of DNA- or RNA polymerases remain unrelaxed, it leads to replication and transcription blockade. Negative supercoils behind the polymerases favor formation of unconventional DNA conformations (non-B DNA), including Z-DNA, D-loops, and R-loops and G-quadruplexes[73]. The strategy applied by both pro- and eukaryotes to resolve polymerase-induced supercoiling is recruiting topoisomerases. Over- or underwound DNA behaves as a substrate for topoisomerases. Topoisomerases, upon forming “cleavage complexes” with the DNA, introduce transient single- or double-strand breaks thus removing the replication or transcription blockade, as reviewed in[73,74]. In prokaryotes, DNA is usually negatively supercoiled (excepting the thermophile archaea).

Writhe exists in both toroidal and plectonemic form. When in the toroidal form, DNA is wrapped around nucleoid-associated proteins including HU and FIS[75, 76].
In eukaryotes, changes of supercoiling are effortful challenges for DNA replication and transcription. Also, the superhelical state of DNA in chromatin and the enzymes involved in the regulation of DNA topology are among the most effective targets in combating cancer. However, due to its complexity, supercoiling and its biological significance in human genomes is not yet well appreciated.

1.2.2. What is it?

In order to understand DNA topology, we need to tackle some key mathematical concepts: superhelical density (σ), linking number (*Lk*), twist (*Tw*), and writhe (*Wr*).

Twist (*Tw*): is the number of times one DNA strand crosses the other strand in a double helix (number of helical turns), which is one turn every 10.5 bp under physiological conditions (0.2 M NaCl, pH 7, 37 ◦C), in the case of DNA exhibiting no supercoiling, and since it is a right-handed helix, it is a positive number. It is calculated from eq (1) below where N is the length of DNA in base pairs divided by the number of base pairs per turn of helix (*h).*

Writhe (*Wr*): is the number of times the double helix crosses itself (plectoneme) or the number of times it coils around (toroid). Right-handed plectoneme and left-handed toroid are indicated by a negative number.

Linking number (*Lk*): is the number of times complementary strands in the DNA double helix are wound around each other. It is always a positive integer value.
Superhelical density (σ): is the fractional change in linking number. It is a positive value in positive supercoils and a negative value in negative supercoils.
These concepts are expressed in equations as shown below (the meaning of subscript 0 is discussed below):

eq(1)

$$Tw_0 = N/10.5$$

eq(2)

$$Lk_0 = Tw_0 + Wr$$

eq(3)

$$\sigma = \frac{(Lk - Lk_0)}{Lk_0}$$

The above concepts are best demonstrated describing the topology of covalently closed circular DNA, like plasmids. However, genomic DNA is also considered as closed-end DNA because, on the one hand, the excessive length of DNA causes high degree of friction which hampers its rotation, on the other, genomic DNA is tethered to itself via protein linkages or to scaffolds[77]. For a better understanding and simplicity let's focus on a particular relaxed linear DNA segment that has N = 2100 bp. From *eq (1)* twist can be calculated:

$$Tw_0 = 2100/10.5 = 200$$

And Lk_0 can be calculated from *eq (2):*

$$Lk_0 = 200 + 0$$

Since we assume that the DNA is relaxed, in the absence of writhe $Lk_0 = Tw_0$. However, N/10.5 might not necessarily be an integer number; thus, Lk_0 cannot be a true linking number, it is an imaginary (also referred to as 'hypothetical'[67]) linking number that serves as a reference point helping to measure the actual level of supercoiling. *Lk* always has an integer value, and it is constant unless strand breaks occur. Conventionally, the sign of *Lk* in right-handed B-DNA is positive. In both prokaryotes and eukaryotes, DNA is globally underwound by ~6%[78,79]. Returning to our example, this means that for 2100 base pairs, there are 188 turns of the helix instead of the expected 200 turns. In other words, there is 1 helical turn for every ~11 bp. The term ΔLk (linking difference) denotes this difference, and it is equal to the actual linking number (*Lk*) of a molecule minus the hypothetical linking number (Lk_0). Hence for the above example:

$$\Delta Lk = Lk\,(188) - Lk_0\,(200) = -12$$

Underwound and overwound DNA are called negatively and positively supercoiled, respectively.

The underwound ($\Delta Lk < 0$) and overwound ($\Delta Lk > 0$) states produce torsional stress within the DNA. This stress distributes along the length of the DNA and induces the molecule to either coil around itself and generate plectonemes (in a right-handed direction) or writhe about a protein core forming a toroid (in a left-handed direction).

Considering that *Lk* is constant, supercoiling leads to changes in *Tw* and/or *Wr*. Referring to the above example, since *Lk* = 188 and does not change, the negative supercoiling ($Lk < Lk_0$) should manifest in changes of twist and writhe. One possibility would be a reduction in twist and increase in writhe.

$$Lk = Tw + Wr$$

$$188 = 190 + (-2)$$

In order to study the partitioning of supercoil into changes in *Tw* and *Wr*, two strategies are applied. One is using simulated molecules (Monte Carlo simulation) which involves calculation of free energy of different DNA superhelical conformations. Another one is an experimental strategy to analyze supercoiling by e.g. electron microscopy or gel electrophoresis as reviewed in[67,78,80]. The results of both strategies are consistent with each other and imply that change in the supercoiling level in small DNA molecules (< 2.5 kb) is partitioned mostly to twisting[75]. However, in large DNA molecules (> 2.5 kb), a higher proportion (~70%)[78] of supercoiling is partitioned into writhing rather than twisting (*Wr* : *Tw* = 2.6 : 1)[81]. Supercoil portioning into changes in *Tw* and *Wr* leads to crucial biological consequences[82,83] .

Finally, in order to compare the supercoiling level of a particular DNA molecule, a parameter called supercoiling density (σ) can be used. It is a function of ionic strength and temperature. Since it is independent of the length of DNA, the degree of supercoiling in the case of DNA molecules of different length can be compared. Supercoiling density is defined as the ratio of the ΔLk to Lk_0. Referring to our example, from *eq (3)*:

$$\sigma = -12/200$$

$$\sigma = -0.06$$

As described in the section 1.1, binding of Cis-Pt (and many other compounds; see section 1.3) causes the DNA double helix to unwind. This unwinding is either a direct consequence of the binding of the agent to DNA (e.g., Cis-Pt, intercalators) or of binding to enzymes responsible for altering DNA topology (agents targeting topoisomerases).

Regarding direct DNA binding, another parameter described for the alteration of supercoiling by a drug is unwinding angle (θ); in standard conditions it is calculated as:

$$\theta = 18\ \sigma / rb_{(c)}$$ [84,85]

Where $rb_{(c)}$ is the amount of bound drug that is necessary for complete removal of all supercoils from the DNA.

Intercalators like ethidium bromide, chloroquine, psoralen, and anthracyclines are planar, mainly polycyclic, aromatic/heteroaromatic ring structures. They intercalate between two adjacent base pairs of a double-stranded DNA, perpendicular to the helical axis of DNA. Upon intercalation, they increase the distance between adjacent base pairs (in order to accommodate the aromatic ring structure). The increase in distance between base pairs leads to local unwinding (decrease in *Tw, increase in -Wr*) of the DNA helix, and an increase in its length. Following the addition of a higher concentration of intercalators the DNA reaches a relaxed state (*Wr=0, Tw=Lk*), and above this concentration it will overwind (increase in *+Wr*).

A recent study performed in our lab demonstrated that both constrained and unconstrained superhelicity impedes intercalation[59]. This is in line with the conclusions of another study investigating damage caused by platinum-intercalator compounds denoted that a Pt-acridine complex binds to the linker region at twice higher frequency than to nucleosomal DNA[52].

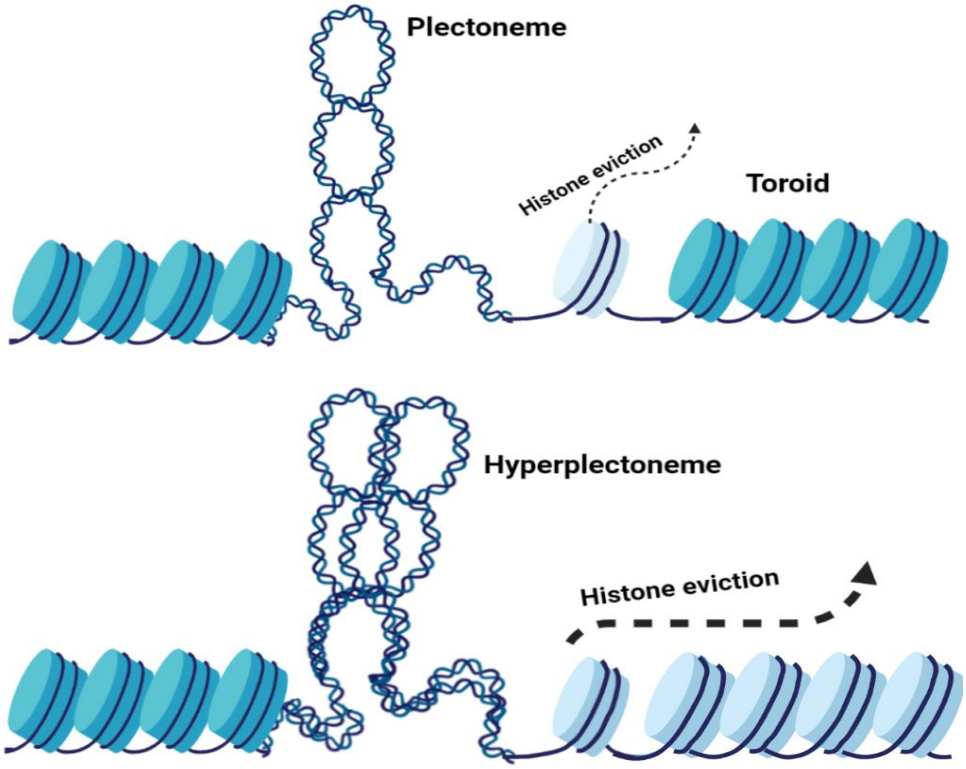

Figure 4. Schematic representation of chromatin topology

1.3. Anthracyclines

1.3.1. Chemistry of anthracyclines

The anthracyclines (including daunorubicin, doxorubicin, epirubicin, idarubicin and aclarubicin) belong to a class of chemotherapeutics with similar structures that are widely used for treatment of several types of cancer.

Daunorubicin (Dauno) and Doxorubicin (Dox) were isolated from a soil bacterium called streptomyces peucetius. Dauno and Dox consist of planar tetracyclic (A, B, C, D) ring and sugar moieties as shown in **Figure 5**. The C-9 of ring A carries a short side chain (R_1), and the sugar moiety called daunosamine, is bound to the C-7 of ring A.

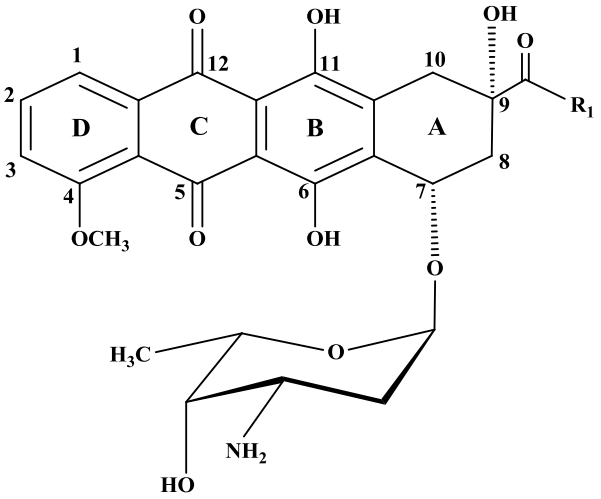

	Daunorubicin	Doxorubicin
R_1 :	$-CH_3$	$-CH_2OH$

Figure 5. Molecular structure of Dauno- and Dox.

Dauno and Dox vary only in the R_1 side chain: In Dauno, R_1 is a methyl group, whereas in Dox it is a hydroxymethyl group. The minor difference in the structure of Dauno and Dox has an impact on the spectrum of diseases where they are applied. Dox is used in the treatment of breast cancer, soft tissue sarcomas, lymphomas and solid tumors arising in endometrial tissue, whereas Dauno is applied in myeloblastic or acute lymphoblastic leukemia[86].

1.3.2. Daunorubicin and its mechanisms of action

Dauno, the first discovered anthracycline compound, in its uncharged form, enters the cell via passive diffusion[87]. Under physiological pH, most of the Dauno molecules are positively charged, probably limiting uptake only to a small extent due to the equilibrium between the ionized and neutral form. On the other hand, entry of the charged Dauno molecules appears also to be possible by a flip-flop mechanism[88]. Dauno affects a broad range of biochemical processes, and a several of different mechanisms have been proposed to be responsible for Dauno-elicited cytotoxicity. These include inhibition of DNA and RNA synthesis (mainly due to binding of the drug to the DNA), topoisomerase II poisoning (by trapping the enzyme at cleavage sites), oxidative stress (due to formation of reactive oxygen species), also involving lipid peroxidation (by chelating iron).

- **Direct effect on plasma- and mitochondrial membrane**

Dauno is a lipophilic compound, so it binds to the different lipid components of cellular membranes partly through hydrophobic interactions. On the other hand, cationic Dauno interacts with anionic-charged moieties in phosphatidylserine[89], G-Protein coupled receptor[90], cardiolipin[91] and sphingomyelin[92]. As a consequence of these varied interactions, Dauno alters plasma membrane structure and disrupts lipid-lipid and lipid-protein interactions involved in signaling pathways[93].

- **Free radical formation is elicited by Dauno and stabilizes Dauno-DNA intercalation**

Quinone moiety (ring C) is a substrate for several oxidoreductases. These enzymes, including xanthine dehydrogenase, mitochondrial NADH dehydrogenase, and endothelial nitric oxide synthase, consume NAD(P)H to oxidize the quinone[94]. The produced semiquinone radical reduces oxygen containing molecules, to regenerate its stable parent quinone structure. Through the redox process, reactive oxygen species (ROS) like superoxide, hydrogen peroxide, and hydroxyl radicals are formed[94]. Moreover, semiquinone oxidizes the bond between ring A and the daunosamine moiety resulting in detachment of daunosamine from the polycyclic ring[86] (as presented in **Figure 6**). This will increase the lipophilicity of the polycyclic ring, thus facilitating its insertion into cellular membranes what will lead to further free radical formation[86]. ROS are known to cause DNA breaks; however, ROS formed by Dauno were only observed in cells treated at supraclinical doses of Dauno[95]. Therefore, at clinically relevant doses, alluding to the formation of free radicals as the primary cytotoxic action of anthracyclines is a matter of debate[86,95].

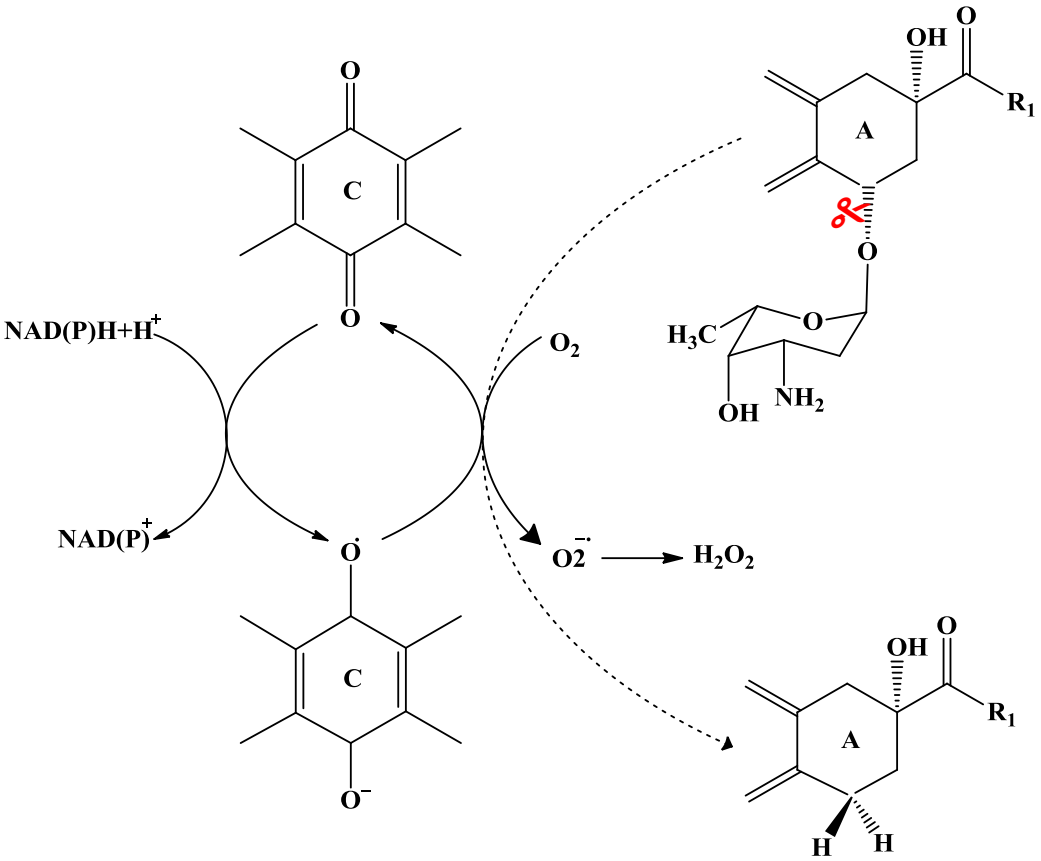

Figure 6. Oxidation-reduction reaction of the Dauno quinone structure

Anthracyclines chelate iron (III) what causes lipid peroxidation, what is true especially for Dox-Fe^{3+} [96]. Anthracyline-Fe^{3+} complexes also catalyze the formation of formaldehyde (CH_2O) from lipids and other carbon-containing cellular constituents, and CH_2O conjugates with Dauno covalently. The intercalating CH_2O-drug conjugate forms a covalent bond between the amino group of the daunosamine and the guanine base in one strand and forms a hydrogen bond between Dauno and another guanine base on the complementary strand[97]. These covalent Dauno-DNA adducts that are formed at clinically relevant doses account only for a minor fraction of total Dauno in cell; nevertheless, they might contribute to their cytotoxicity[98]. The higher levels of CH_2O in Dauno-sensitive tumor cells compared to resistant and healthy cells support the contribution of Dauno-DNA adducts to Dauno cytotoxicity[99]. This notion is further supported by the observation that co-administration of Dauno or Dox with subtoxic doses of CH_2O-releasing drugs *in vivo* and *vitro* lead to an increase in Dauno/or Dox-DNA adducts and

to ~3-fold greater cytotoxic response than treatment with Dauno/or Dox alone was observed[100,101].

- **Daunorubicin as topoisomerase II poison/inhibitor**

One of the mechanisms proposed for the cytotoxicity of Dauno (at clinically relevant doses) is topoisomerase II (Top2) poisoning. Top2 introduces transient breaks in both strands of the DNA, thus relaxing positively and negatively supercoiled domains that have been generated during replication and transcription processes[68,75]. Top2 has two isoforms, Top2α and Top2ß. In proliferating cells, it is Top2α which is expressed at higher levels, while Top2ß is prevalent in the quiescent cell (e.g. cardiomyocytes)[73]. Top2α relaxes positively supercoiled DNA with greater efficiency than negatively supercoiled DNA, whereas Top2ß relaxes both negative and positive supercoils with the same efficiency[102]. Dauno can affect both isoforms of Top2. The effect of Dauno on Top2α seems to be most relevant for its anti-cancer activity, whereas the effect on Top2ß may be responsible for its cardiotoxicity[73].

The Top2 catalytic cycle involves the following steps, as reviewed in[73,103]. The Top2 homodimer binds to DNA, and in the presence of ATP, undergoes through extensive conformational changes. A tyrosine residue in both monomers reacts and breaks the phosphodiester backbone of the DNA independently in the two strands, four bases apart[73]. Next, the double-strand-cleaved segment allows another DNA segment pass through, altering the linking number and superhelical density of the DNA. Following strand passages, the broken strands are religated and released from the enzyme. The transient covalent complex composed of DNA and Top2 is called cleavage complex. Dauno, depending on its concentration, exerts its inhibitory effect on Top2 in two ways: (a) Top2 poisoning: at lower concentration, upon its intercalation, the daunosamine and ring A form a ternary complex composed of Dauno-DNA-Top2 which stabilizes the cleavage complex; thus DNA cannot be released from the Top2[104] and Top2-induced double strand breaks remain unsealed; (b) Top2 inhibition: at higher Dauno concentrations, Dauno directly binds to Top2 and inhibits the formation of the cleavage complex.

In other words, at lower Dauno concentrations the formed cleavage complexes are trapped in this state, while at higher Dauno concentration these complexes do not form at all[73].

1.3.3. Interactions of Dauno with chromatin

In addition to Top2 inhibition, Dauno inhibits both DNA and RNA synthesis possibly due mainly to direct binding to and inhibition of the polymerases[105-108]. Inhibition of DNA synthesis has been observed at concentrations of Dauno as low as ~0.25 μM[109]. The fused tetracyclic (A-D) structure (shown in **Figure 5)** intercalates between adjacent base pairs, while daunosamine extends into the minor groove[110]. Dauno intercalation is slightly preferred at GC base pairs[111]. Single-molecule measurements denote that the intercalation of one Dauno molecule untwists (unwinds) the double helix by 8°-12°[112,113]. In negatively supercoiled DNA, such an alteration in *Tw* would generate compensatory positive torsional stress in the neighboring parts of the DNA, what makes the DNA resist further intercalation more-and-more as intercalator concentration is increased[59]. Importantly, single-molecule magnetic tweezers studies showed that the assembly of a nucleosome on positively supercoiled DNA is inhibited[114]. The torsional stress exerted by the compensatory positive supercoiling can weaken histone-histone and histone-DNA interactions in the nucleosome core particle and favor dissociation of the H2A/H2B dimers from the H3/H4 tetrasome (at low salt conditions)[115]. Likewise, Cis-Pt unwinds DNA locally, thus induces positive torsional stress around, what would also act to destabilize the nucleosomes. Published results by our lab as well as another lab showed that Dox induces eviction of histones independently from Top2 inhibition[116,117]. Furthermore, it was shown that Doxorubicinone (Dox lacking the sugar moiety) was unable to evict histones, suggesting the importance of sugar group and its extension into the minor groove[116]. The postulated mechanism for histone eviction is a competition of the sugar moiety with histone residues critical for nucleosome stability like the arginine side chain of H4 (H4-R45)[69,116]. Dauno preferentially binds to linker DNA[118] and nucleosome depleted regions like active promoters[118]. Binding of Dauno to the linker DNA regions induces an unfolding followed by aggregation of chromatin fiber[118] thereby influencing higher-order chromatin conformation. Dauno also binds to H1 and H5 linker histones with preference for H1 over H5[119]. Recent work from our lab suggests that the anthracyclines evict then aggregate the H2A-H2B dimers[120].

1.4. Combination therapy

1.4.1. Chou-Talalay (Dose-Effect) Analysis

Synergy between two drugs (when the observed effect is greater than the effects of the individual agent added), vs. antagonism (when the observed effect is smaller than what is expected when the effects add up), are not readily determined by comparison of the individual effects with those of the combinations, due mainly to the non-linearity of the dose-effect relationships. Therefore, we used the combination index (CI) method based on the median-effect principle of the mass-action law performed according to Chou-Talalay to determine the mode of drug interaction.

Chou and Talalay, based on the mass-action law and employing mathematical deductions, generated the Median dose-effect equation (MEE) and the formula of CI for biological systems. A widely used computer software for dose-effect analysis was also developed[121,122] and published online (http://www.combosyn.com/).

MEE delineates the behavior of many biochemical systems and is shown below:

$$\frac{f_a}{f_u} = \left(\frac{D}{D_m}\right)^m$$

Where *D* denotes the dose of a particular drug, *fa* and *fu* are the fractions of the cells affected and unaffected, respectively, by the dose *D; Dm* is the median-effect dose, which is the dose needed to induce the "median effect". The median effect depends on the context of the study, can be IC_{50}, ED_{50}, or LD_{50}. In other words, D_m is the dose that inhibits the system under study by 50%. *m* is a coefficient that accounts for the shape of the dose-effect curve. $m > 1$, $= 1$, and < 1 indicate sigmoidal, hyperbolic and flat sigmoidal dose-effect curves, respectively. The median-effect equation is closely related to well-known biochemical equations, including Henderson- Hasselbalch for pH ionization, Hill[123] for higher-order ligand binding occupancy of receptors, Michaelis-Menten[124] for first–order enzyme kinetics (m=1) and Scatchard for receptor binding. Detailed explanation of how this method was developed is reviewed in[125].

The CI equation was derived from the MEE[125] and can be calculated as:

$$CI = \frac{(D)_1}{(D_x)_1} + \frac{(D)_2}{(D_x)_2}$$

Where CI < 1, = 1, and > 1 indicate antagonism, additive effect, and synergism, respectively. In the denominator $(Dx)_1$ is a dose of drug 1 (e.g., Cis-Pt) that affects *x*% of the cells when

applied alone, and $(Dx)_2$ is the dose of drug 2 (e.g., Dauno) that affects *x*% of the cells when applied alone. In the numerators, $(D)_1$ is the dose of drug 1 that, in combination with $(D)_2$ dose of drug 2, affects *x*% of the cells.

A plot of *fa* (indicating drug effect level %) on the *x*-axis and CI on the *y*-axis is the "Fa-CI plot" (**Figure 7**). A horizontal line drawn from 1 on the y-axis represents simple additive effect and any point above and under this line represent antagonism and synergism, respectively. The ranges of CI corresponding to the extent of synergy or antagonism are shown in **Table.1**.

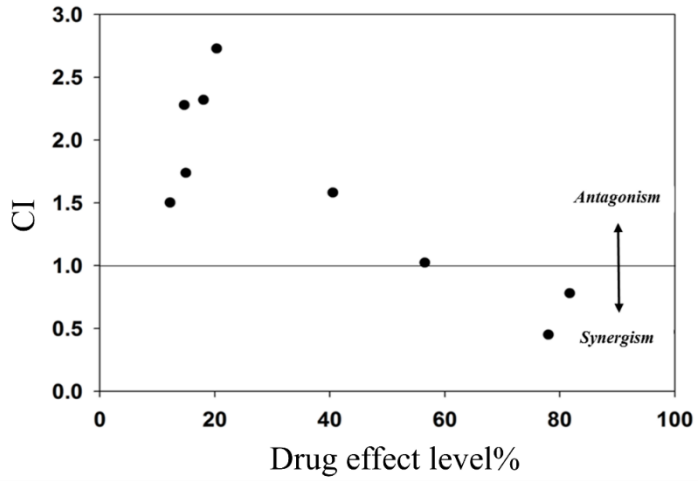

Figure 7. Fa-CI plot. HeLa cells treated with Cis-Pt and Dauno

Table.1

Range of IC	Description
<0.1	Very strong synergism
0.1-0.3	strong synergism
0.3-0.7	synergism
0.7-0.85	moderate synergism
0.85-0.9	slight synergism
0.9-1.1	nearly additive
1.1-1.2	slight antagonism
1.2-1.45	moderate antagonism
1.45-3.3	antagonism
3.3-10	strong antagonism
>10	very strong antagonism

Ranges of CI corresponding to the extent of synergy or antagonism

2. AIM AND OBJECTIVES OF THE STUDY

Since the primary target of Cis-Pt and Dauno is chromatin and they alter DNA topology, the possibility arises that they may mutually affect each other's binding to their chromatin target when applied in combination. Therefore, we aimed to elucidate if and how Dauno and Cis-Pt, influence each other's binding to chromatin components.

Objectives

1) To determine if Dauno and Cis-Pt synergize or antagonize each other's cytotoxicity *in vitro*.
2) To establish techniques for the measurement of the drugs bound in the different cell compartments.
3) To determine how the changes in chromatin induced by Dauno affect the amount of Cis-Pt-DNA adduct levels.
4) To determine how Cis-Pt affects the cellular uptake and chromatin binding of Dauno.

3. MATERIALS AND METHODS

3.1. Materials

All reagents were purchased from Sigma-Aldrich (St. Louis, Missouri, USA), with the exception of what are listed below:

- Penicillin from Gibco, Grand Island, NY
- Cis-Pt from Accord-UK Ltd, United Kingdom, purchased as 1 mg/ml stock solution
- Dauno from Pfizer, Budapest, 2mg/ml stock solution
- Anti-Cisplatin modified DNA antibody (ab103261) from Abcam, Cambridge, UK; 1 mg/ml
- Donkey anti-rat IgG antibody, Proteinase K, S1 endonuclease and SYBR Green I from Thermo Fisher Scientific, Waltham, Massachusetts, USA
- Agarose from SeaKem® LE Agarose, Lonza
- Nicking endonuclease Nt.CviPII from New England Biolabs Inc., Ipswich, MA, USA
- Blotto Non-Fat Dry Milk from Santa Cruz Biotechnology Inc., Santa Cruz, California, USA

3.2. Methods

3.2.1 Cells, treatments, cytotoxicity assay

HeLa cells expressing H2B-GFP or H3-GFP, control HeLa, HCT-116 and T47-D cells were cultured in DMEM, where Jurkat cells in RPMI1640, supplemented with 10% FCS, 2 mM L-glutamine, 100 µg/ml streptomycin and 100 U/ml penicillin in T-150 tissue culture flasks in 5% CO_2. Treatment with cytotoxic agents was performed in 24-well plates. Dauno was used in a concentration range of 0 –15 µM. Cis-Pt was applied at 0–80 µM. For median effect analyses, Cis-Pt was added to the cells at 40 µM final concentration together with a concentration series of Dauno, for 16 hrs. Cytotoxicity was measured based on mitochondrial function, assessed using the Resazurin based assay[126]. 100 µl aliquots of the drug treated cells were re-suspended in colorless media and added to 96-well flat-bottom microplates to 20,000 cells per well. For each drug combination four parallel wells were prepared. 100 µl of freshly prepared Resazurin solution in colorless medium was added to each well to a final concentration of 18 µM. The plates were incubated at 37 °C for 24 hrs and fluorescence signals were measured at an excitation wavelength of 560 nm and an emission wavelength of 590 nm using Synergy H1 microplate reader (BioTek). The fluorescence signal of Resorufin was recorded. The untreated cells reduce Resazurin (non-fluorescent) to Resorufin (fluorescent) fully, thus giving the

maximal fluorescence emission. The maximum fluorescence signal signified 100% viable cells, which shows 0% cytotoxicity of the drug. Cytotoxicity (Drug effect %) is detected by decreased reduction reaction of Resazurin to its fluorescent product Resorufin. Viability was expressed in the experimental groups in relation to untreated cells (control). The average concentrations of four wells were determined per dose. To determine synergism, additivity or antagonism, median effect analysis was performed using the method of Chou-Talalay[127], using CompuSyn ver. 1.0 (ComboSyn Inc., Paramus, NJ, USA). The CI reflects synergism, additivity or antagonism when CI < 1; CI = 1 or CI > 1, respectively. All indicated values are the averages of at least three independent experiments. The method involves recording of dose-effect curves for the individually applied drugs, and measurement of the cytotoxic effect at a fixed dose of one drug, varying the concentration of the other. Typical dose-effect curves are demonstrated in **Figures 8, 12, and 14**.

3.2.2. Urea-agarose gel electrophoresis

Jurkat cells were treated with 9 μM Dox, known to bind to the DNA covalently[128], and 10 or 25 μM Cis-Pt for 16 hrs. The DNA of the samples was analyzed by urea-agarose gel electrophoresis, the method of Materna et al., further developed in our lab[129,130]. Briefly, the cells were embedded into Low melting point (LMP) agarose plugs, deproteinized and treated with the Nt.CviPII nickase enzyme. This was necessary to allow the entry of part of the DNA, after heat-denaturation, into the gel. The samples of agarose plugs were equilibrated with 9 M urea-containing loading buffer, denatured at 90 ˚C for 5 min, allowed to cool to RT then loaded onto an agarose gel also containing urea. The denatured fragments stay single-stranded in these conditions thus will not be stained by ethidium bromide (EBr). However, after electrophoresis, the gel was submerged in TAE buffer supplemented with EBr (5 μg/ml) overnight, so ample time was given to the samples to be renatured when urea has been washed away from the agarose gels.

3.2.3. Measurement of Dauno fluorescence

3.2.3.1. Determination of total intracellular Dauno fluorescence

In order to assess Dauno fluorescence in live cells and in isolated nuclei by flow-cytometry, HeLa cells were treated with 1.5 μM of Dauno alone or in combination with 40 μM of Cis-Pt

for 16 hrs. After trypsinization and re-suspension of the cells, Dauno fluorescence intensity distributions were recorded in a flow-cytometer.

3.2.3.2. Determination of nuclear Dauno fluorescence

Aliquots of the drug treated cells above were suspended in 500 µl PBS (150 mM NaCl, 3.3 mM KCl, 8.6 mM Na_2HPO_4, and 1.69 mM KH_2PO_4, pH = 7.4) and lysed in 500 µl ice-cold 0.2% (v/v) Triton X-100 dissolved in 1 × PBS/EDTA (5 mM EDTA in PBS), for 20 minutes (min). After lysis, nuclei were washed twice with 4 ml ice-cold PBS/EDTA then re-suspended in 1 ml PBS/EDTA and Dauno fluorescence intensity distributions were recorded by flow-cytometry.

3.2.3.3. Determination of DNA-bound Dauno via Hoechst-quenching

HeLa cells were treated with 1.5 µM of Dauno alone or in combination with 40 µM of Cis-Pt for 16 hrs, then, without washing the samples, stained with 35 µM Hoechst 33342 for 30 min. After trypsinization, the cells were analyzed by flow-cytometry.

3.2.3.4. Flow-cytometry

A Becton Dickinson FACSAria III Cell Sorter (Becton Dickinson, Mountain View, CA, USA) was used. Dauno was excited using the 488 nm line of a solid-state laser and the emitted light was detected using a 695/40 nm band-pass filter. Hoechst 33342 fluorescence was measured by excitation at 375 nm and emission detection using a 450/50 nm band-pass filter. Fluorescence signals were collected in logarithmic mode and the flow-cytometric data were analyzed by the Reflex software[131].

3.2.4. Measurement of histone eviction

The histone H2B gene was fused to the gene encoding the green fluorescent protein (GFP) and transfected into human HeLa cells to generate a stable line constitutively expressing H2B–GFP[132] . Histone eviction was measured by the QINESIn assay developed in our lab[117]. Briefly, the agarose-embedded GFP-histone expresser HeLa cells at the bottom of ibidi wells were permeabilized with 500 µl ice cold 1% (v/v) Triton X-100 dissolved in 1x PBS/EDTA, washed with 500 µl ice-cold 1x PBS/EDTA and these samples of nuclei were treated with different concentrations of Dauno. The histones remaining chromatin-bound were determined cell-by-cell using Laser scanning cytometry (LSC) scans (see below) of the samples.

3.2.5. Measurement of ICLs and total Cis-Pt-DNA adduct levels by LSC

3.2.5.1. Preparation of comets and halos

Following exposure to drugs, the cells were centrifuged at 175 g for 5 min at 4 °C, then re-suspended to a final concentration of 1 × 106 cells/ml in PBS, kept at 37 °C and mixed at a v/v ratio of 1: 3 with 1% LMP agarose dissolved in PBS. 100 µl of the cell-agarose suspension was pipetted onto Superfrost microscope slides and were covered with coverslips. The slides were pre-coated by submerging them in molten 1% agarose dissolved in water, and then allowed to dry overnight at room temperature. The cells were left to sediment on the surface of the slides for 4 min at 37 °C, then kept on ice for 5 min. After polymerization of the agarose, the coverslips were gently removed, then the slides were submerged in glass staining tanks containing ice-cold PBS/EDTA for 5 min, then submerged in ice-cold TRIS/EDTA (Tris-HCl 20 mM pH = 7.5, 5mM EDTA), 150 mM NaCl and 1% v/v Triton X-100 for 10 min, next in PBS/EDTA containing 1% Triton X-100 for another 10 min. After washing in PBS/EDTA for 10 min, the samples were equilibrated with nickase buffer (10 mM Tris-HCl pH 8.0, 50 mM NaCl, 10 mM $MgCl_2$, 1 mg/ml BSA), then nickase treatment was performed covering the slides with 500 µl of nickase buffer containing the frequent cutter nicking endonuclease Nt.CviPII at a final concentration of 0.001 U/ml and incubated in a wet chamber at 37 °C, for 20 min. After washing with ice-cold PBS/EDTA three times for 10 min, the slides were submerged in freshly made alkaline lysis buffer (2.5 mM NaCl, 1% N-Laurylsarcosine sodium salt, 10 mM Tris, 150 mM NaOH, 100 mM EDTA, 10% DMSO, and 1% Triton X-100; pH = 10) at room temperature, for 1h. After alkaline denaturation, the slides were placed in an electrophoresis tank filled with alkaline running buffer (300 mM NaOH, 1 mM EDTA, pH = 13). After electrophoresis (for 20 min at 200 mA), the samples were neutralized with 0.4 M Tris (pH = 7.5) for 10 min before staining with SYBR Green I, 1: 5000 diluted in PBS/EDTA. Since no background fluorescence was detected following S1 digestion (see **Figure 20**), simple intensity measurements instead of calculating tail-moments sufficed, so the steps related to comet formation (nickase digestion and electrophoresis) were omitted and the experiments were performed in ibidi 8-wells microslide. These halo preparations allowed comparison of samples in ibidi slides that proved to be more convenient and reliable, also improving throughput. The samples were equilibrated with S1 buffer (280 mM NaCl, 50 mM CH_3COONa and 4.5 mM $ZnSO_4$, pH = 4.4) for 30 min, then the samples were covered with 500 µl of S1 enzyme solution. The enzyme was diluted to 1000 U/ml concentration in S1 nuclease buffer in the working solution. The samples were incubated on ice for 5 min with the enzyme for equilibration, then

digestion was performed at 37°C, for 20 min. After washing in PBS/EDTA, the samples were stained with SYBR Green I as described above, for 1 h.

3.2.5.2. Determination of total amount of Cis-Pt-DNA adducts

Nuclear halos were labeled by indirect immunofluorescence using anti-Cisplatin primary antibody as described below. Agarose-embedded nuclei on ibidi slides were exposed to the combinations of Cis-Pt and Dauno at 4°C for 16 hours, washed with ice-cold PBS/EDTA three times for 5 min each, treated with Proteinase K dissolved in 0.4 M EDTA, 1% Sodium lauroyl sarcosinate, 10mM Tris, pH = 8 at 0.5 mg/ml final concentration, at 42 °C, for 24h. The enzymatic reaction was stopped by incubating the samples with 1:10 dilution of 10mM PMSF (Serin protease inhibitor) at room temperature, for 10 min. Then the samples were denatured and renatured as described above; electrophoresis was skipped. Immunofluorescence labeling was performed at 4°C, overnight, using rat monoclonal anti-Cisplatin modified DNA antibody diluted at a titer of 1:800 in 150µl of PBS/EDTA/1% BSA. Samples were washed 6 times for 10 min each, followed by incubating the samples with 500µl 5% (m/v) Blotto Non-Fat Dry Milk in PBS/EDTA on ice for 30 min. Labeling with the secondary antibody was performed using Alexa Fluor 488 (A488) conjugated Donkey anti-rat IgG, at a titer of 1:800, diluted in PBS/EDTA/3% BSA, from 2 mg/ml stock solutions. After labeling with the secondary antibody, nuclei were washed with 500µl ice-cold PBS/EDTA 3 times for 10 min each. Then the samples were fixed using 1% formaldehyde at 4 °C, overnight. After fixation, the nuclei were washed with 500µl ice-cold PBS/EDTA three times for 5 min and fluorescence intensity distributions were recorded by LSC. For studying the effect of salt induced histone eviction on total Cis-Pt-DNA adduct formation (**Figure 22a**), the agarose embedded nuclei of HeLa cells were prepared on the slides as described above and were treated with 1.1 M or 1.6 M of NaCl in PBS/EDTA 6 times for 10 min each and subsequently washed with PBS/EDTA. These samples were exposed to 40 µM of Cis-Pt, for 16 hrs, then treated with proteinase K followed by PMSF and washing steps, then labelled by immunofluorescence for the LSC measurements, as described above. Then the same samples were dehydrated with an ascending series (20–95%) of ethanol for subsequent LA-ICP-MS analysis.

3.2.5.3. Laser scanning cytometry (LSC)

Automated microscopic imaging was performed using an iCys instrument (iCys® Research Imaging Cytometer; CompuCyte, Westwood, MA, USA). Green fluorescent protein (GFP), SYBR Green I, A488, and propidium iodide (PI) were excited using a 488nm Argon ion laser. A647 was excited with a 633nm HeNe laser. The fluorescence signals were collected via an

UPlan FI 20x (NA 0.5) objective. GFP and A488 and SYBR Green fluorescence were detected through 510/21nm, 530/30nm and 550/30nm filters respectively, while A647 and PI were detected through a 650 nm/LP filter. Each field (comprising 1000 × 768 pixels) was scanned with a step size of 1.5 µm. Data evaluation was performed using the iCys 7.0 software for Windows XP. Gating of G1 phase cells was based on the fluorescence intensity distribution curves of the DNA stained with PI.

3.2.6. Determination of Pt in the nuclei of agarose-embedded cells using quantitative LA-ICP-MS

3.2.6.1. LA-ICP-MS instrumentation

The LA-ICP-MS measurements were conducted by our collaborators at the Chemistry Department of Ghent University, using an Analyte G2 193 nm ArF* excimer-based LA-unit (Teledyne Photon Machines Inc., Bozeman, MT, USA), equipped with a low-dispersion Cobalt ablation cell, what was coupled to a quadrupole-based Agilent 7900 ICP-mass spectrometer (Agilent Technologies Inc., Tokyo, Japan) *via* the ARIS (Aerosol Rapid Introduction System, Teledyne Photon Machines Inc., Bozeman, MT, USA), providing fast aerosol transport[133-135].

3.2.6.2. Spot analysis

This is also our collaborators' work. The determination of Pt in the nuclei of agarose-embedded cells was performed using a quantitative LA-ICP-MS spot analysis approach, derived from the single-cell LA-ICP-MS analysis method described in a previous work by Van Acker *et al*.[136]

3.2.7. Statistical analysis

The results of the LSC, flow-cytometry and mass spectrometry imaging experiments contain the means of the investigated features characterizing the cell populations based on cell-by-cell measurements encompassing many cells. These range from a few hundred to a few thousand, as indicated in the legends of the relevant figures. A particular parameter (e.g., the level of total platination; Fig.20 **a**) were measured at least 3 times (as specified in the legends) and the averages of the population means were used in the figures, with the bars representing the SD calculated from the 3 or more means. The observations in Fig. 20 **a** and **c** were also confirmed using two alternative cytometric approaches as shown in Fig. **21 d** and **e**, each performed once. The means of the different samples were compared by the unpaired two-sample Student's t-test based on the assumption that the parameters followed normal distribution, when the

variances of the compared averages proved not to be significantly different in the F-test. The condition on the normality of the statistics was experimentally supported by the cytometric distributions. In addition, one way ANOVA test followed by a post hoc (Tukey) test was also performed.

4. RESULTS

4.1. Mode of interaction (synergism vs. antagonism) between Cis-Pt and Dauno is cell-type and dose dependent

I made a comprehensive pre-titration of concentrations, using the two drugs in several combinations and selected the conditions based on data shown in **Figures 8, 10** and **Table.2.** Based on literature data[98,97] treatment of cells with Dauno for 3 hrs sufficed to detect covalent Dauno-DNA crosslinks. The duration of treatment and level of crosslinks directly relate to each other[137]. As for Cis-Pt, the time that is required for Cis-Pt to form crosslinks was estimated ≥10hrs[15] (as mentioned in section 1.1). The time constraints of repair dynamics in the case of Cis-Pt and anthracyclines crosslinks[138,139,140,141] are thought to be within 24 hrs. There are many protocols in clinical practice[2,142,143,144,145] with a time window making interaction possible, especially given that the formed adducts keep the agents fixed to the DNA until the cell dies or the lesions are repaired. As shown in **Figure 9**, when the agarose gel is stained with EBr, in the samples containing Dox, EBr is quenched or prevented to bind to DNA. Since preparation of the DNA samples in the agarose blocks took 48 hrs and involved detergent treatment, we concluded that the drug must be rather tightly bound. Due to co-treatment with Cis-Pt, Dox-binding is increased, which was inferred from the further decrease in EBr staining.

Considering all these dynamic aspects, I chose the simultaneous addition of the two drugs for 16 hrs. The concentrations of both drugs were systematically varied in a matrix spanning 0.3 – 30 μM of Dauno and 10 – 100 μM of Cis-Pt, and the combination indices (CI values) were determined for each combination. To determine the mode of drug interaction I calculate the CIs based on the median-effect principle of the mass-action law[146], performed according to the Chou-Talalay method. Cytotoxicity was evaluated by performing a Resazurin cell viability assay[126]. These studies were performed in Jurkat cells that exhibited high sensitivity to both drugs. The results were consistent with the general expectation of synergy. Since the differences in CI values between 40 and 50 μM of Cis-Pt combined with 3 μM of Dauno were negligible (See Table. 2), I considered them equivalent and chose to work with the lowest concentration in this range. Therefore, 40 μM of Cis-Pt was used in the further experiments that included other cells as well. Unexpectedly, in sharp contrast with the Jurkat cells, as shown in **Figure 11 and Table. 3**, in HeLa antagonism (CI > 1) was observed at the subtoxic Dauno concentration range of 0.3–1.8 μM, and synergism (CI < 1) at toxic Dauno concentrations ranging between 3–12 μM, using 40 μM Cis-Pt.

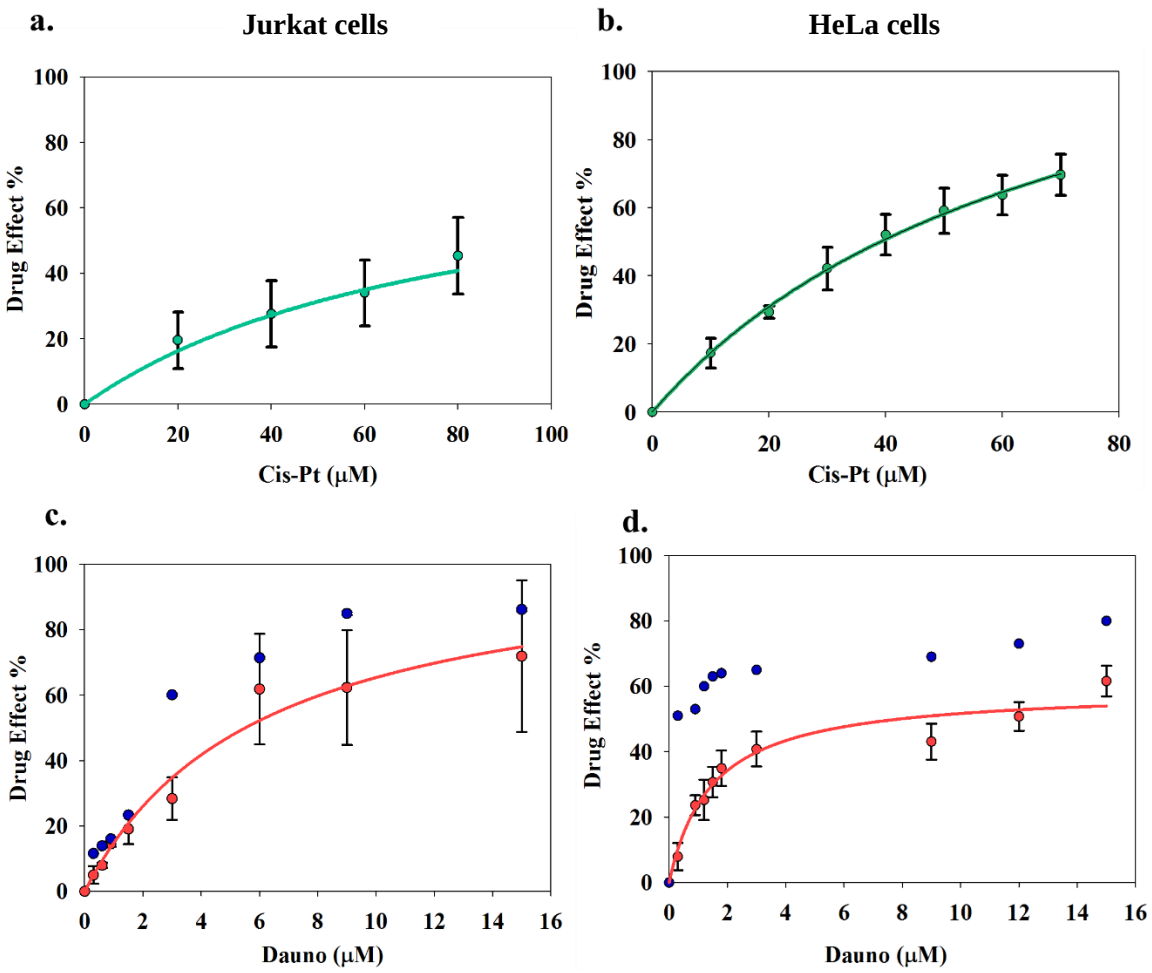

Figure 8. Dose-effect curves of Cis-Pt and Dauno treatment of HeLa and Jurkat cells

*Panels **(a)** and **(c)**: Jurkat cells were treated with Dauno (red line) or Cis-Pt (green line) in a concentration range of 0.3-15 µM and 10-70 µM, respectively. Averaged dose-effect curves of 4 independent samples (a triplicate and an independent biological experiment).*

*Panels **(b)** and **(d)**: HeLa cells treated with Dauno and Cis-Pt at a concentration range of 0.3-15 µM and 20-80 µM, respectively. Blue circles: dose-effect values of treatment with Dauno in combination with 40 µM Cis-Pt. Averaged dose-effect curves of 4 independent experiments. Error bars represents SDs. Cytotoxicity (Drug effect %) is detected by decreased reduction of Resazurin to its fluorescent product Resorufin.*

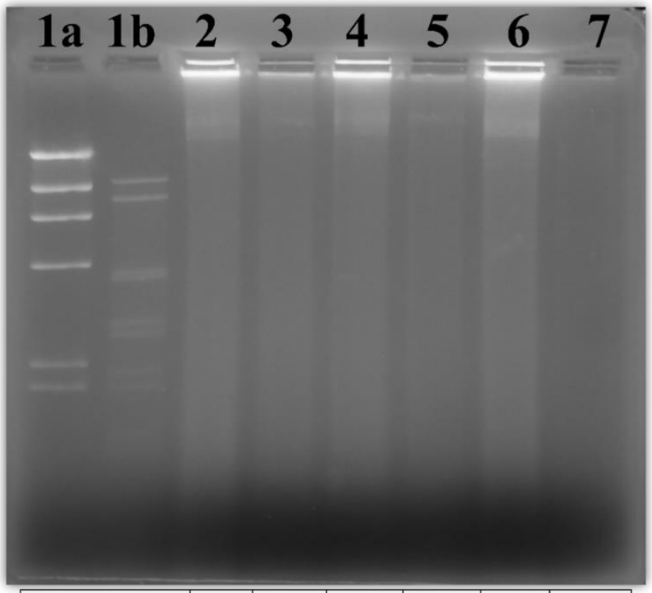

	2	3	4	5	6	7
Dox	-	+	-	+	-	+
Cis-Pt	-	-	+	+	++	++

Figure 9. DNA binding of Dox is augmented when co-administered with Cis-Pt

Jurkat cells were treated with 9 µM Dox, known to bind to the DNA covalently[128]*, and 10 (+) or 25 µM (++) Cis-Pt for 16 hrs. The DNA of the samples was analyzed by urea-agarose gel electrophoresis, as described in section 3.2.2* [129]*. Following conventional electrophoresis, the gel was stained with 5 µg/ml EBr, overnight. Lanes 1a, b: Lambda Hind III fragments run without (a) and with (b) heat-denaturation. The uncropped picture of the gel is depicted, recolored to grayscale.*

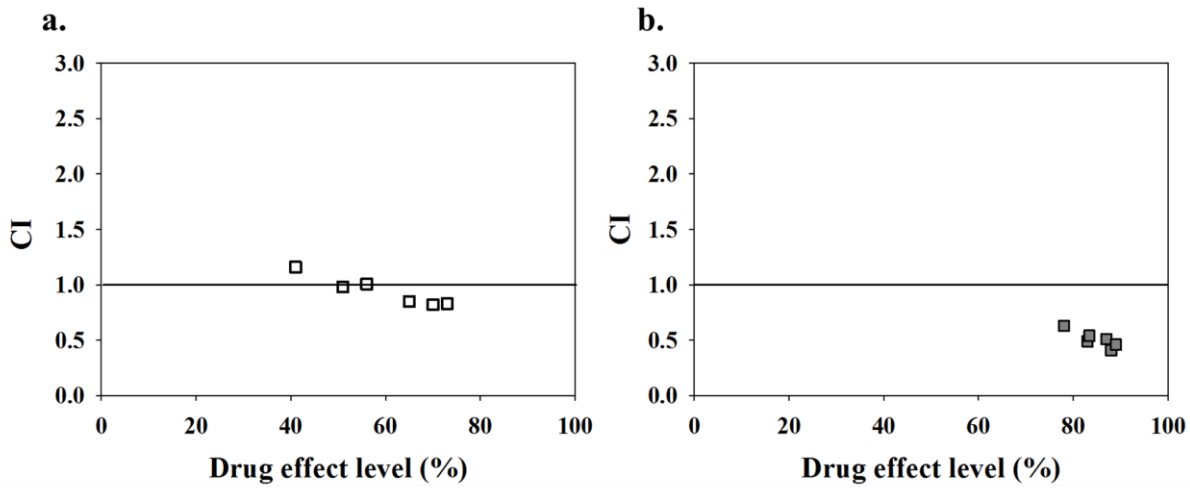

Table. 2

Dauno (μM)	Cis-Pt (μM)	Drug effect level ± SD	CI
3	10	0.415 ± 0.03	1.16
3	20	0.519 ± 0.09	0.98
3	30	0.567 ± 0.06	1.00
3	40	0.657 ± 0.06	0.85
3	50	0.708 ± 0.06	0.82
3	60	0.735 ± 0.06	0.83

Dauno (μM)	Cis-Pt (μM)	Drug effect level ± SD	CI
18	10	0.78 ± 0.04	0.63
18	20	0.83 ± 0.05	0.49
18	30	0.834 ± 0.05	0.54
18	40	0.87 ± 0.05	0.41
18	50	0.89 ± 0.05	0.51
18	60	0.92 ± 0.06	0.46

Figure 10. Dependence of CI values on Cis-Pt concentration

*CI values determined for Jurkat cells treated with 3 μM Dauno (**a**) and 18 μM Dauno (**b**) in combination with Cis-Pt varied between 10 and 60 μM. The tables below the graphs show the specific CI values plotted. The matching values of CI and Dauno concentrations are shown in **Table. 2.***

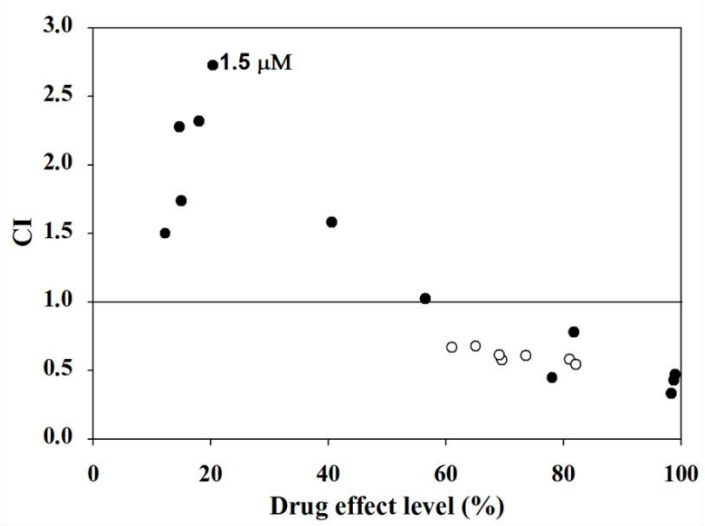

Table.3

		HeLa		Jurkat	
Dauno (μM)	**Cis-Pt (μM)**	**Effect ± SEM**	**C.I. ± SEM**	**Effect ± SEM**	**C.I. ± SEM**
0.3	40	0.12 ± 0.03	1.5 ± 0.2	0.61 ± 0.08	0.67 ± 0.24
0.6	40	0.14 ± 0.01	1.7 ± 0.2	n.d.[a]	n.d.
0.9	40	0.14- ± 0.01	2.2 ± 0.4	0.65 ± 0.11	0.68 ± 0.27
1.2	40	0.18 ± 0.03	2.3 ± 0.1	0.69 ± 0.09	0.57 ± 0.19
1.5	40	0.2 ± 0.05	2.7 ± 0.5	0.69 ± 0.06	0.61 ± 0.11
1.8	40	0.40 ± 0.004	1.5 ± 0.1	n.d.	n.d.
2.1	40	0.56 ± 0.07	1.02 ± 0.04	n.d.	n.d.
2.4	40	0.78 ± 0.06	0.4 ± 0.02	n.d.	n.d.
3.0	40	0.817 ± 0.09	0.7 ± 0.2	0.73 ± 0.085	0.61 ± 0.14
6.0	40	0.983 ± 0.003	0.3 ± 0.04	0.81 ± 0.11	0.58 ± 0.29
9.0	40	0.98 ± 0.003	0.4 ± 0.1	0.81 ± 0.11	0.58 ± 0.29
12.0	40	0.98 ± 0.005	0.4 ± 0.1	0.82 ± 0.08	0.54 ± 0.27

Figure 11. Fa-CI plot of Cis-Pt and Dauno treatment of HeLa and Jurkat cells

HeLa (●) and Jurkat (○) cells were co-treated with 40 μM Cis-Pt and different concentrations of Dauno for 16 h, and the viability of the cells was measured by the Resazurin assay. The dose-effect profiles were used to calculate CI values as described in sections 1.4 and 3.2.1. The data represent averages of three independent experiments. The dose-effect data of the averages are shown in ***Figure 8****. The toxicity values obtained at the different Dauno concentrations combined with a constant dose of Cis-Pt are represented on the X axis (drug effect levels). The matching values of CI and Dauno concentrations are shown in* ***Table.3.*** *The concentration of Dauno where the highest degree of antagonism was observed (1.5 μM) is indicated on the figure.[a] n.d. indicates no data.*

To further investigate the cell type dependence of the effects, HCT-116 and T47D cells were treated with Dauno or Cis-Pt at a concentration range of 0.3-15 µM and 10-160 µM, respectively, as the Dose–effect curves are shown in **Figure 12**. Also, cells were treated with the combination of 0.3-15 µM of Dauno and 40 µM of Cis-Pt**.** I again observed that synergism vs. antagonism between Dauno and Cis-Pt is a dose- and cell-line-dependent phenomenon. HCT-116 and T47D cells exhibited synergism between Cis-Pt and Dauno at low Dauno concentration ($\leq$ 6 µM) and additivity or even antagonism at high Dauno concentrations. The Fa-CI plot is depicted in **Figure 13**.

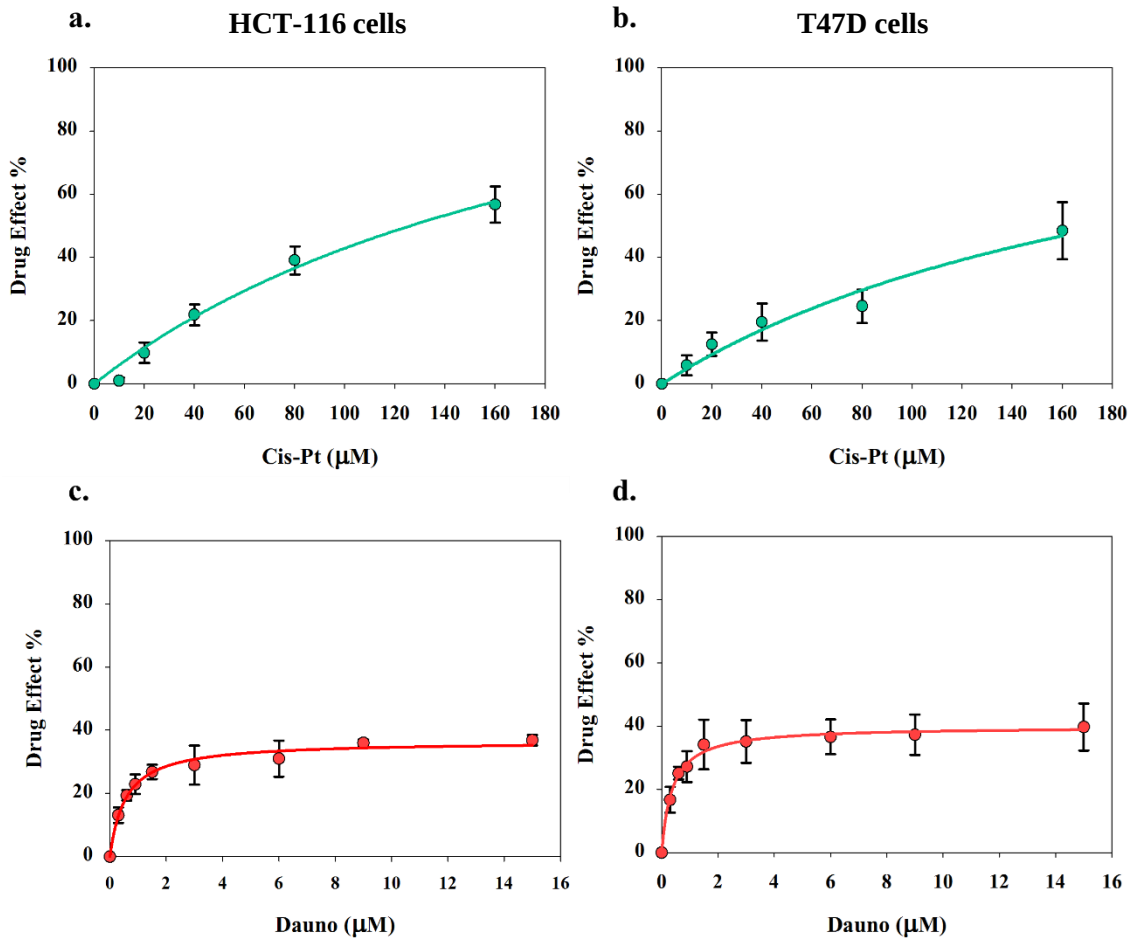

Figure 12. Dose-effect curves of Dauno and Cis-Pt treatment of HCT 116 and T47D cells

*Panels **(a)**, **(c)**: HCT-116 and Panels **(b)** , **(d)** : T47D cells were treated with Dauno (red line) or Cis-Pt (green line) in a concentration range of 0.3-15 µM and 10-160 µM, respectively. Average dose-effect values of 6 independent samples (two independent biological experiments measured in triplicates) were used to construct the graphs. Error bars represents SDs.*

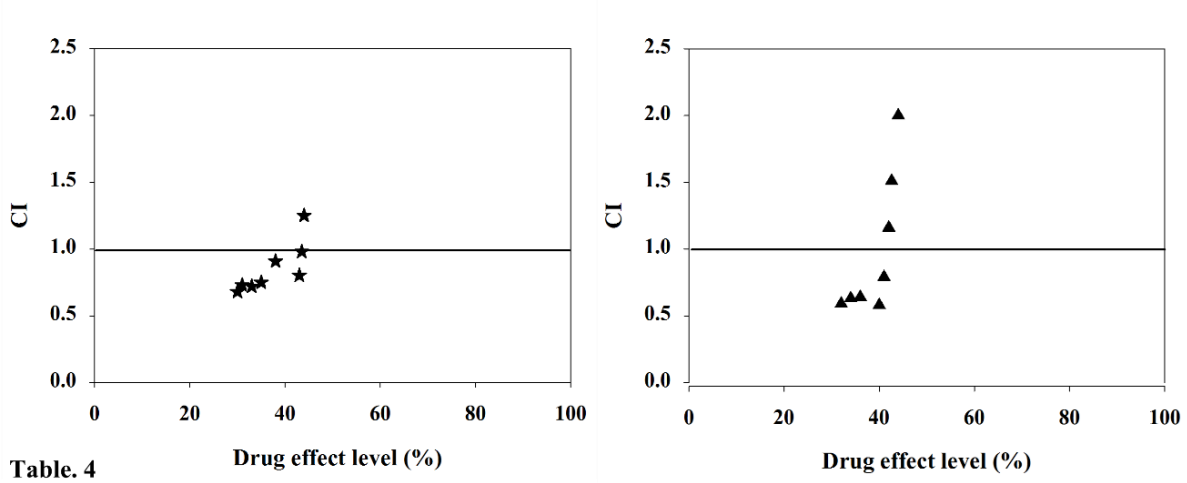

Table. 4

Dauno (µM)	*Cis*-Pt (µM)	Drug effect level ± SD	CI
0.3	40	0.3 ± 0.05	0.68
0.6	40	0.31± 0.01	0.73
0.9	40	0.33± 0.04	0.72
1.5	40	0.35 ± 0.01	0.75
3	40	0.38 ± 0.07	0.90
6	40	0.43 ± 0.04	0.80
9	40	0.43±0.03	0.98
15	40	0.44±0.04	1.25

Dauno (µM)	*Cis*-Pt (µM)	Drug effect level ± SD	CI
0.3	40	0.32 ± 0.11	0.59
0.6	40	0.34± 0.14	0.63
0.9	40	0.367 ± 0.13	0.64
1.5	40	0.4 ± 0.12	0.58
3	40	0.41 ± 0.12	0.79
6	40	0.42 ± 0.10	1.16
9	40	0.426±0.12	1.51
15	40	0.44±0.11	2.01

Figure 13. Fa-CI plot of Cis-Pt and Dauno treatment of HCT-116 and T47D cells

HCT-116 (★) and T47D (▲) cells were co-treated with 40 µM Cis-Pt and different concentrations of Dauno for 16 h, and the viability of the cells was measured by the Resazurin assay. The data represent average dose-effect values of 6 independent samples (two independent biological experiments measured in triplicates). The corresponding dose-effect data of the averages are shown in ***Figure 12.*** *The toxicity values obtained at the different Dauno concentrations combined with a constant dose of Cis-Pt are represented on the X axis. The matching values of CI and Dauno concentrations are shown in* ***Table. 4*** *.*

Considering the highly similar chemical structure of Dauno and Dox, the question is raised whether the observed effects for the combination of Dauno and Cis-Pt holds true also for the combination of Dox with Cis-Pt. Therefore, to assess the role of drug-specificities in our findings, I also performed experiments using Dox. Jurkat and HeLa cells were treated with Dox or Cis-Pt at a concentration range of 0.3-32 µM and 5-160 µM, respectively, and using a combination of 40 µM of Cis-Pt with different Dox concentrations. The dose-response curves

are shown in **Figure 14**. The cells showed a varied response to the combination of Dox and Cis-Pt, which recapitulated the dose- and cell line-dependence of synergy vs. antagonism found in the case of Dauno and Cis-Pt. The Fa-CI plot obtained is shown in **Figure 15**.

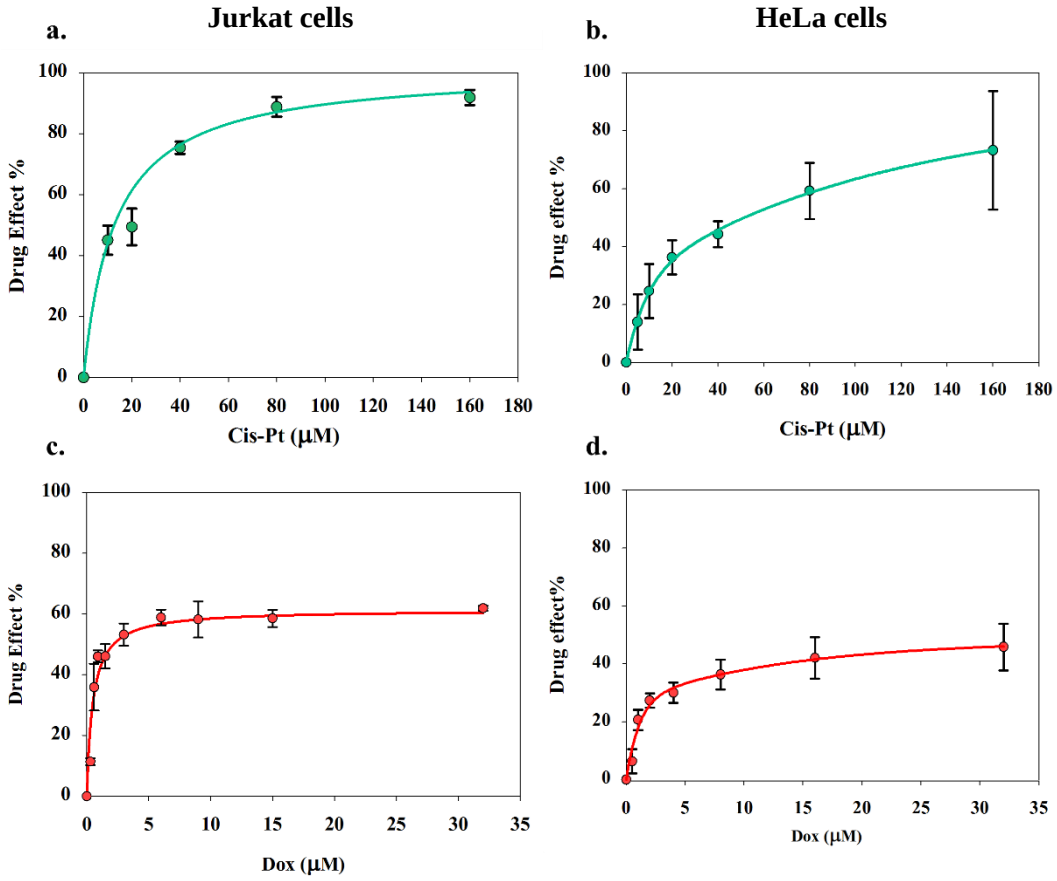

Figure 14. Dose-effect curves of Dox and Cis-Pt treatment on Jurkat and HeLa Cells

*Panels **(a)**, **(c)**: Jurkat cells and HeLa cells Panels **(b)**, **(d)** were treated with Dox (red line) or Cis-Pt (green line) in a concentration range of 0.3-32 µM and 5-160 µM, respectively. Averaged dose-effect curves of a triplicate experiment on HeLa and of a single experiment on Jurkat cells are drawn. Error bars represent SDs.*

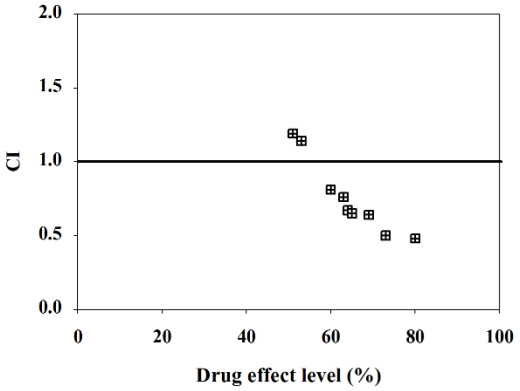

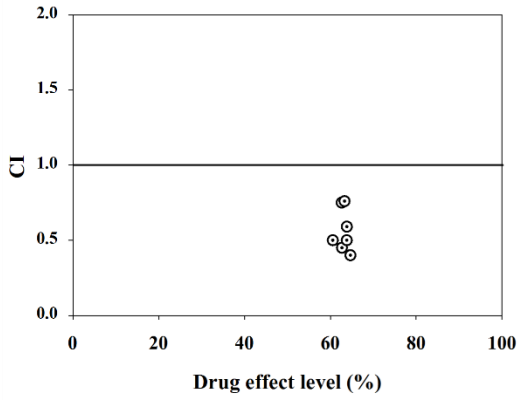

Table. 5

Dox (μM)	*Cis*-Pt (μM)	Drug effect level	CI
0.3	40	0.73	1.19
0.6	40	0.74	1.14
0.9	40	0.8	0.81
1.5	40	0.81	0.76
3	40	0.830	0.67
6	40	0.835	0.65
9	40	0.839	0.64
15	40	0.87	0.5
32	40	0.98	0.48

Dox (μM)	*Cis*-Pt (μM)	Drug effect level ± SD	CI
0.5	40	0.60± 0.07	0.5
1	40	0.62± 0.09	0.45
2	40	0.64±0.07	0.4
4	40	0.62±0.1	0.75
8	40	0.63±0.06	0.5
16	40	0.63±0.04	0.5
32	40	0.63±0.05	0.76

Figure 15. Fa-CI plot of Dox and Cis-Pt treatment of Jurkat and HeLa cells

Jurkat (⊞) and HeLa (⊙) cells were co-treated with 40 μM Cis-Pt and different concentrations of Dox for 16 h, and the viability of the cells was measured by the Resazurin assay. The data represent average dose-effect values of 3 independent samples (HeLa cells) and of a single experiment (Jurkat cells). The corresponding dose-effect data of the averages are shown in ***Figure 12.*** *The matching values of CI and Dox concentrations are shown in* ***Table. 5.***

I also tested if Dox exhibits a concentration-dependent synergy/antagonism when combined with another drug that interferes with protein degradation pathways, which has come to the focus of our interest *via* another project, focusing on aggregation/redistribution phenomena involving the H2A and H2B histones upon Dox treatment of Jurkat cells[120]. In those experiments, Jurkat cells were treated with Dox and PYR-41 alone at a concentration range of 2.25-36 μM and 6.25-100 μM, respectively, or in a combination of 50 μM of PYR-41 with various concentration of Dox. As shown in **Figure 16** (The dose-effect curve and Fa-CI plot)**,** the combination of Dox and PYR-41 treatments on Jurkat cells is synergistic. Dox exhibits concentration-independent synergism when combined with PYR-41, an agent that interferes

with protein degradation, a process implicated in the nucleocytoplasmic transport process following Dox-induced H2B eviction. Here, in the context of the interactions of Dauno and Cisplatin, I use it to demonstrate that the concentration-dependence of a synergy/antagonism relationship is specific for the drugs whose main target is chromatin, and it does not occur between Dox and a drug with a chromatin-*un*related target. Such a concentration dependence may arise as a result of multiple interactions involving any of the drugs. In the case of the anthracyclines, they change (relax) the superhelicity of internucleosomal DNA at smaller, then also evict nucleosomes at larger concentrations. This can explain Dox concentration dependence in the case of Dox/Cisplatin combination. No such interaction is expected in the case of Dox and PYR-41, hence the concentration independent synergy. My contribution to the publication of Nanasi et al. was to derive the conclusion that the observed synergy raises the possibility that combined administration of Dox and PYR-41 may be exploited in cancer chemotherapy, since PYR-41 is already considered as a potential anticancer agent[120].

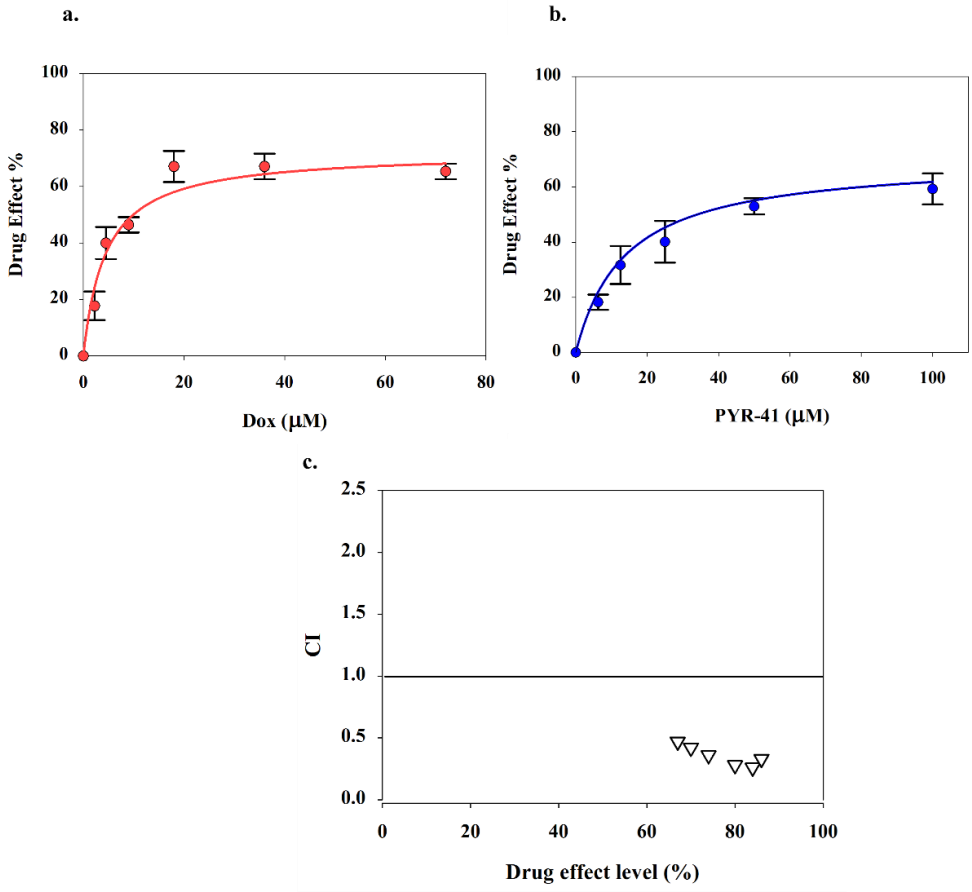

Figure16 . Fa-CI plot of Dox and PYR-41 treatment of Jurkat cells

*Panels **(a)**, **(b)**: Jurkat cells were treated with Dox (red line) or PYR-41 (blue line) in a concentration range of 2.25-72 µM and 6.25-100 µM, respectively. Panel **(c) :** Jurkat (▽) cells were co-treated with 50 µM PYR-41 and different concentrations of Dox for 2 h, and the*

viability of the cells was measured by the Resazurin assay. The data represent average dose-effect values of 3 independent samples. Error bars represent SDs.

4.2. Co-treatment with Cis-Pt differentially alters the amount of total cellular, chromatin-bound and DNA-bound Dauno

I first evaluated whether the antagonism between the two drugs might be related to an effect of Cis-Pt on the amount of Dauno taken up into the cells, accumulating in the acidic endosomal compartment[147], by assessing Dauno fluorescence in live HeLa cells using flow-cytometry. In parallel, the total nuclear fluorescence of Dauno, accounting for the chromatin-bound drug, was also measured. Dauno fluorescence was significantly decreased in Cis-Pt-Dauno co-treated cells as compared to cells incubated with Dauno only, both measured in live cells (**Figure 17a**) and nuclei (**Figure 17b**). Since Dauno also binds to histones[119] in addition to DNA, I performed an assay to directly measure the effect of Cis-Pt co-treatment on DNA-bound Dauno in live cells via the quenching of Hoechst 33342 fluorescence[148]. Hoechst 33342 enters live cells and becomes brightly fluorescent upon binding through the minor groove of the DNA to tandem AT base pairs[149-151]. The green emission of Hoechst dye is absorbed by Dauno, thus quenching of Hoechst fluorescence can be utilized as a measure of DNA-bound anthracycline. The decrease of Hoechst fluorescence in the presence of Dauno was stronger when Cis-Pt was also added. This difference can be partly accounted for by the influence of Cis-Pt on Hoechst fluorescence (see Table inset of **Figure 17c**). However, an increased level of DNA-bound anthracycline in the presence of Cis-Pt co-treatment was corroborated in experiments when the DNA of cells treated with Dox was isolated, run on agarose gels and visualized by EBr staining, see **Figure 9**.

4.3. Cis-Pt facilitates Dauno-induced histone eviction

A newly discovered effect of anthracyclines, also implicated in their cytotoxicity, is induction of nucleosome eviction due to intercalation[116,117]. I investigated whether this effect may be influenced by Cis-Pt. Live HeLa cells or their isolated nuclei were co-treated with the intercalator and Cis-Pt and populations of cells were assessed on a cell-by-cell basis by flow cytometry. The intercalator-induced eviction of the histone dimers and tetrasomes were both substantially augmented, see **Figure 18-19**. Thus, the amount of histone-bound Dauno is

expected to decrease in the nucleus when cells are co-treated with Dauno and Cis-Pt, apparently in the entire concentration range of the intercalator.

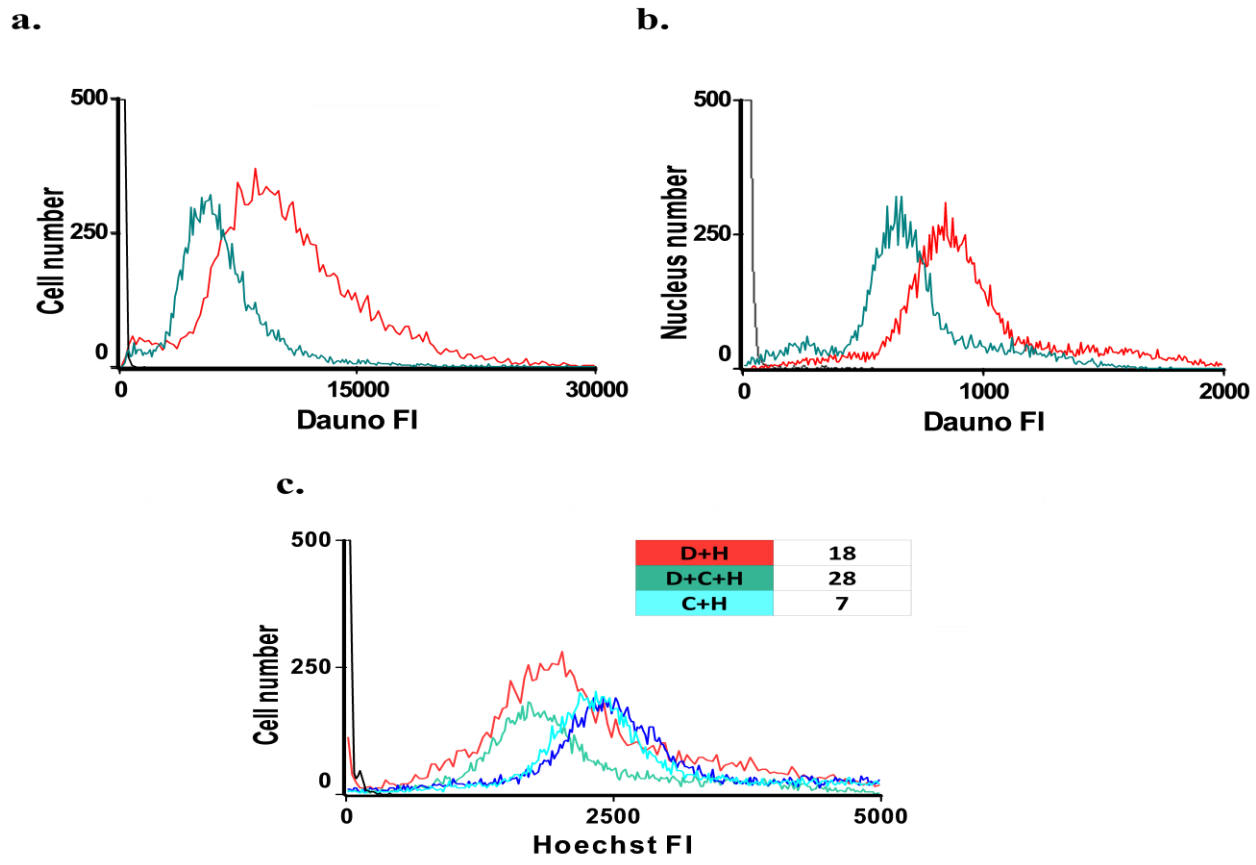

Figure 17. Effect of Cis-Pt on Dauno uptake

*Total cellular (**a**) and nuclear (**b**) fluorescence intensity distributions of Dauno, and of Hoechst 33342 (**c**), measured by flow-cytometry. Fluorescence intensity distributions of 20,000 events were recorded in a representative experiment.*

***a, b** Distribution curves of Dauno fluorescence of HeLa cells (a), or nuclei (b), after treatment of live cells with 1.5 µM Dauno only (red line), with 1.5 µM Dauno in combination with 40 µM Cis-Pt (green), or left untreated (black).*

***c** Hoechst 33342 fluoresence intensity distributions of live HeLa cells. The Hoechst dye (H) was added to the cells at 35 µM concentration following incubation with Dauno and/or Cis-Pt at different combinations: Dauno and Hoechst (red), Dauno, Cis-Pt and Hoechst (green), Hoechst 33342 only (blue), Hoechst 33342 and Cis-Pt (turquoise). The table inset shows the*

decrease of the mean Hoechst fluorescence in the samples co-treated with Dauno (D+H), Dauno + Cis-Pt (D+C+H) and Cis-Pt only (C+H), in % of the control (blue).

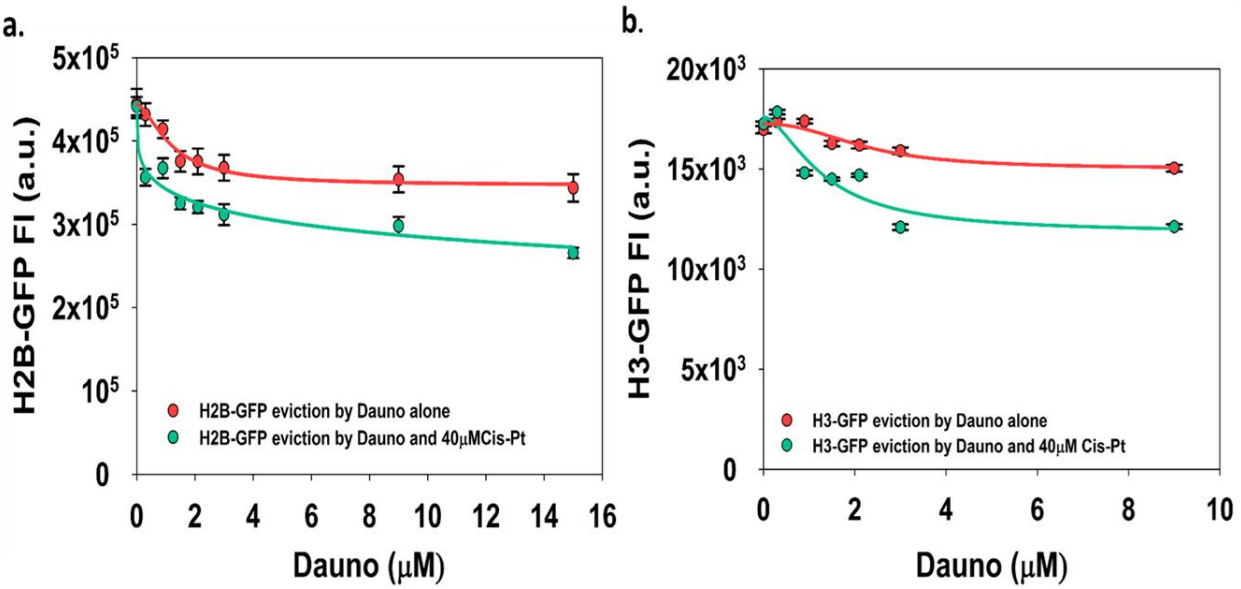

Figure 18. Effect of Cis-Pt on Dauno-induced histone eviction

(a) *QINESIn assay of histone eviction[117]. Nuclei of H2B-GFP-expressor HeLa cells were treated with a concentration series of Dauno only (red) or with Dauno in combination with Cis-Pt (green). The GFP fluorescence intensity of the individual nuclei was recorded by LSC.* ***(b)*** *Live H3-GFP-expresser HeLa cells were treated with Dauno only or with Dauno in combination with Cis-Pt (red and green line, respectively). Subsequently nuclei were prepared and their histone-GFP levels measured by LSC. The mean values of ~1,000 nuclei were plotted as a function of the Dauno concentration used. For both panel* ***(a)*** *and* ***(b)****, the means of the fluorescence distribution curves, recorded for the samples treated and run in parallel, are plotted. Error bars denote SEM of ~1000 nuclei of a representative experiment which has been repeated 3 times.*

4.4. Detection of ICLs using a modified alkaline comet assay

Another possible mode of interaction between the two classes of drugs is relaxation of supercoiling by the intercalator, mitigating ICL formation[57] . In order to study this possibility, I modified this assay to improve its specificity and throughput. Also, in collaboration with the Ghent University, we applied Quantitative Laser Ablation Inductively Coupled plasma Mass

Spectrometry (LA-ICP-MS) spot analysis to yield absolute numbers for total Cis-Pt-DNA adducts and ICLs per nucleus.

We employed a modified version of the alkaline comet assay where the ICL-dependent increment in the renaturation of alkali-denatured samples of nuclei is measured[152]. In view of the rather high background of renatured DNA in the absence of cross-linker in that procedure (**Figure 19a**), we used S1 nuclease treatment to remove any non-renatured DNA, and the SYBR Green I dye to stain double-strand DNA (**Figures 19c, d**). Using these modifications and employing LSC to measure the fluorescence of nuclear comets (or, with equivalent results, nuclear halos; see Materials and Methods), ICL detection was made possible in a wide concentration range of Cis-Pt added to live cells, as low as ~5 µM (**Figure 19e**). In the subsequent experiments we used this modified assay to detect ICLs.

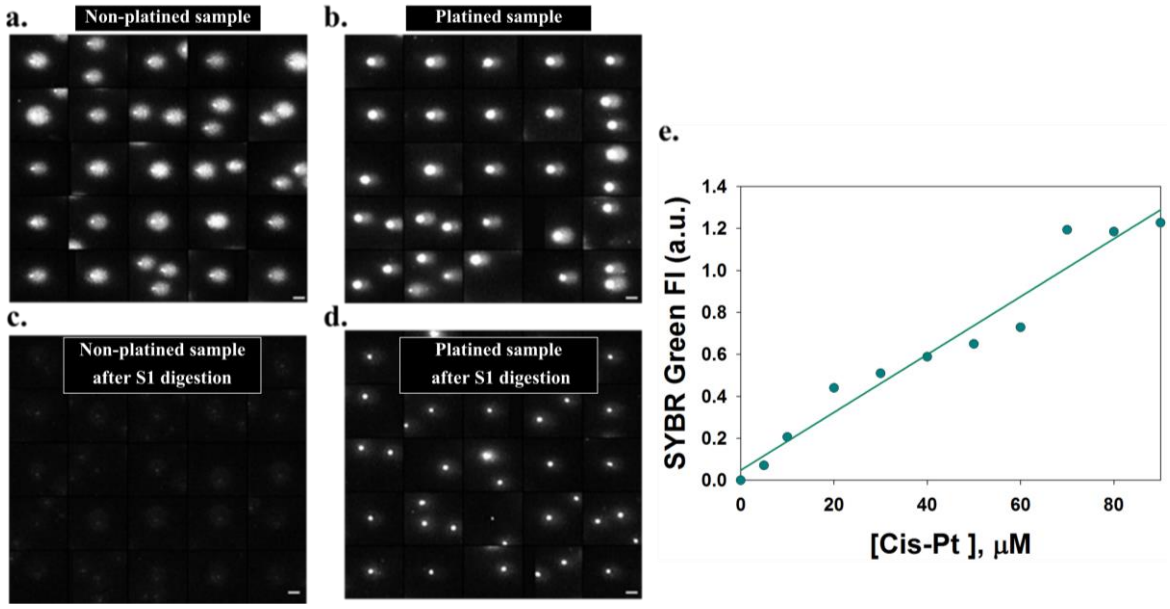

Figure 19. Measurement of ICLs using the alkaline comet assay combined with S1 endonuclease treatment and SYBR Green I staining

(a, c) Alkaline comets of Jurkat cells in the absence of drug treatment. (b, d) Alkaline comets after treatment with 40 µM Cis-Pt. The effect of S1 endonuclease treatment performed after renaturation is shown in (c) and (d). (e) Jurkat cells were treated with different concentrations (1-90 µM) of Cis-Pt, and the mean fluorescence intensities of the renatured comets were recorded by LSC after being digested with S1 endonuclease and stained with SYBR Green I. The median values of the fluorescence intensity distributions of ~ 400 nuclei were plotted as a function of Cis-Pt concentration. ICL levels measured in the lower concentration range of Cis-Pt in a separate experiment are shown in the inset. Fluorescence intensities are shown in arbitrary units (a.u.). Scale bars=10µm

4.5. Co-treatment with Dauno influences Cis-Pt-DNA adduct levels

In order to assess the effects of Dauno intercalation on the formation of Cis-Pt-DNA adducts, nuclei of HeLa cells were exposed to combinations of 40 µM of Cis-Pt and Dauno used at various concentrations. ICL levels were assessed employing the modified comet assay described above (**Figure 19**), while total Cis-Pt DNA adducts were measured via immunofluorescence using an antibody recognizing all Cis-Pt-DNA adducts. I observed no change in the level of total DNA-Pt adduct levels (**Figures 20a and c**), while there was an apparent reduction in ICL formation (**Figures 20b and d**). Notably, this effect was detected already in the low concentration range of the intercalator.

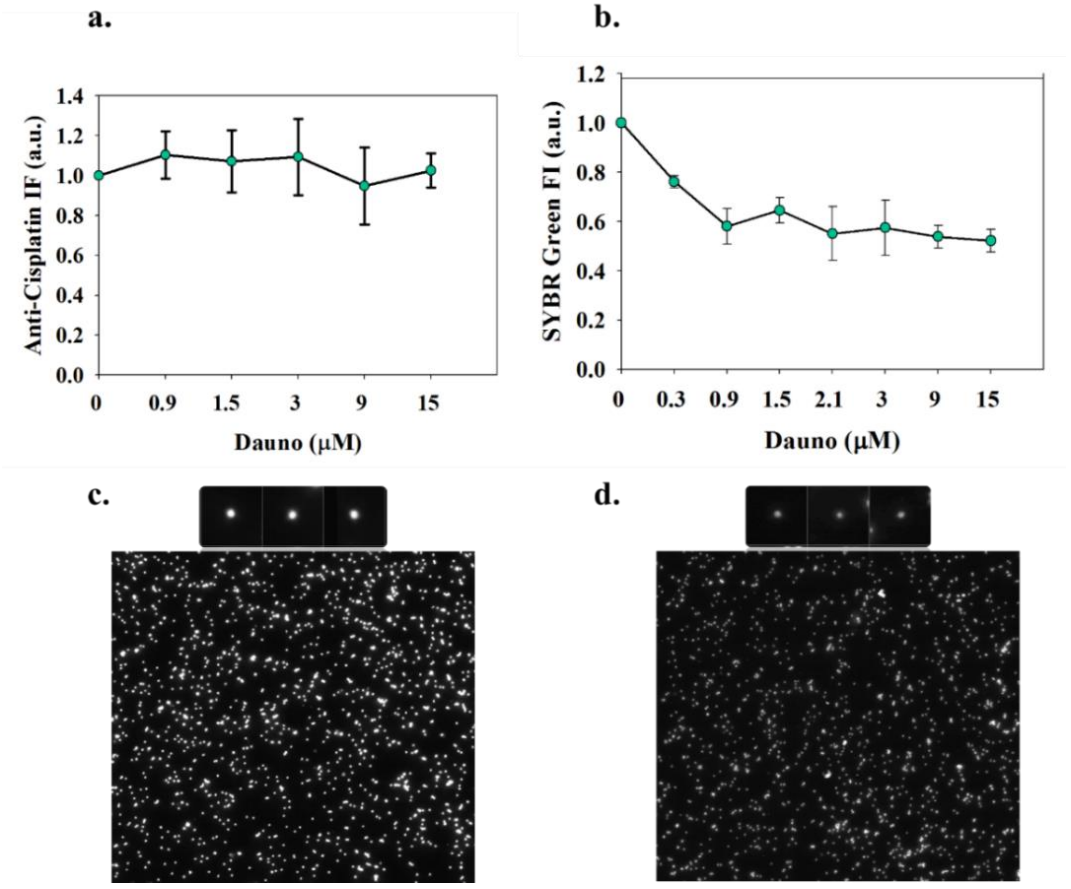

Figure 20. Effect of Dauno treatment of nuclei on the formation of Cis-Pt-DNA adducts

Agarose-embedded nuclei of HeLa cells co-treated with 40 µM Cis-Pt and Dauno used at the concentrations indicated, for 16 hrs (a, b). The amount of all Cis-Pt-DNA adducts (a) and ICLs (b) were measured by LSC. (a) Total Cis-Pt-DNA adduct levels detected by indirect immunofluorescence using an anti-Cisplatin primary and Alexa 488 conjugated secondary

*antibody on deproteinized nuclear halo samples. (b) ICL levels measured by SYBR Green I staining of dsDNA. The nuclear halos were deproteinized after renaturation of the alkaline-denatured DNA strands and the un-denatured DNA molecules were removed by S1 nuclease treatment. (c, d) Field-images of the LSC scans of alkaline halo samples in the case of nuclei treated with Cis-Pt only (c), or with Cis-Pt and 15 μM Dauno (d). Fluorescence intensities are shown in arbitrary units (a.u.). Representative nuclei of each sample are shown in the insets. Error bars in panel **a** and **b** represent SEM values calculated based on two independent biological experiments, each in duplicate.*

4.6. Effect of nucleosome eviction on Cis-Pt-DNA adduct levels

Dauno can cause an increase of total Cis-Pt-DNA adduct levels as well as of ICLs due to increased accessibility of the DNA in the wake of nucleosomal eviction. ICL levels may be increased just because total adduct levels are increased. On the other hand, they can be decreased as a result of the relaxation of the superhelical twist accompanying intercalation[117] and also as a result of nucleosome eviction allowing for free twist-writhe inter-conversion. In view of the complexity of possible scenarios of drug interactions, a model system was set up to learn how nucleosome eviction, in the absence of any other effects of Dauno, might influence Cis-Pt binding to the DNA. I measured total Cis-Pt adduct levels and ICLs in nuclei pre-treated with salt to remove the dimers (1.1 M NaCl), or all the histones (1.6 M NaCl). Total adduct levels were assessed by three independent methods: by measuring the fluorescence intensity of SYBR Green I staining dsDNA in the renatured samples when S1 digestion step was omitted so as to detect all the Cis-Pt adducts renaturing into ds DNA when (any) two strands are covalently linked by Cis-Pt (**Figure 21a**), by immunofluorescence using the anti-Cis-Pt antibody (**Figure 21b**), and also by LA-ICP-MS (**Figure 21d**). ICLs were measured by the modified comet assay described above (**Figure 21c**) as well as by LA-ICP-MS following the treatments performed in the comet assay (**Figure 21e**). The different approaches yielded results that were in agreement with each other. Total DNA platination was increased at intermediate salt levels only, while ICLs were decreased, moderately at 1.1 M, and to a greater extent at 1.6 M salt concentration. The fluorescence intensity distribution histograms corresponding to **Figure 21b-c** of the LSC data are shown in **Figure 22.**

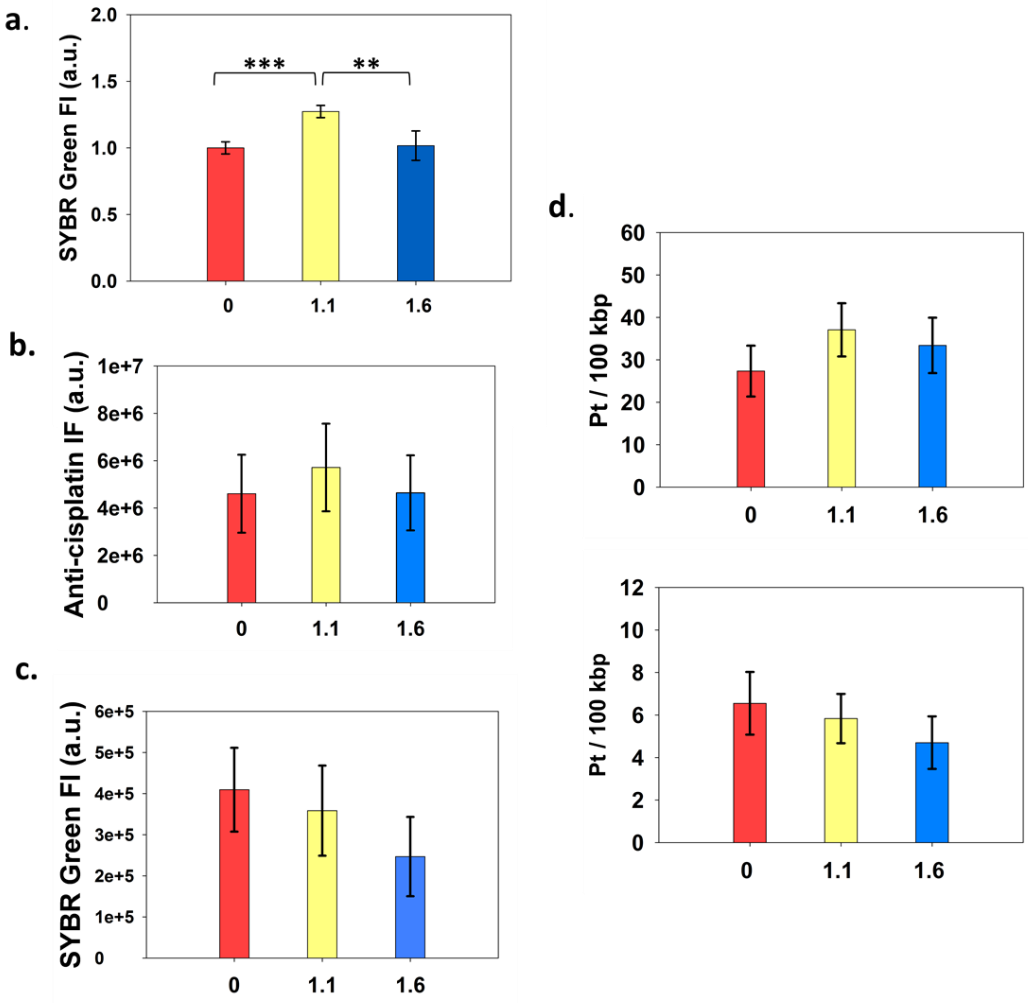

Figure 21. Effect of histone eviction on the formation of DNA-Cis-Pt adducts

*Total Cis-Pt-DNA adduct (**a**, **b, d**) and ICL levels (**c**, **e**) formed in HeLa nuclei after pre-treatment with 1.1 M and 1.6 M of NaCl, or with PBS only (indicated as 0), followed by incubation with 40 µM Cis-Pt for 16 h.*

***(a,b** and **d)** Total Cis-Pt-DNA adduct levels were measured (a) by SYBR Green I staining of the renatured nuclear halos (without S1 nuclease treatment), by immunofluorescence (b), or by LA-ICP-MS (d).*

***(c,e)** ICLs were measured after S1 endonuclease digestion of the renatured, deproteinized halo samples, by SYBR Green I staining (c) or by ICP-LA-MS (e). Fluorescence intensities are shown in arbitrary units (a.u.). In (d) and (e) the absolute number of Pt atoms per 100 kbp of*

*DNA are shown. In panel (a) error bars denote SD of the means of 4 independent experiments. In case of panel (b) and (c) error bars denote SD of mean fluorescence intensty of ~2500 events in a representative experiment. For panel (d) and (e) error bars denote SD of the mean fluorescence intensty of ~100 events. One of the samples represented by panel (a) and the same sample shown in (c) were also measured by ICP-LA-MS (panels d and e, respectively). Statistical calculation for panel (a) is unpaired two sample student t-test and one way ANOVA test followed by post hoc (Tukey) test. *** and ** designates statistical significance at p<0.001 and p<0.005 respectively. Representative distribution curves for panels* ***b*** *and* ***c*** *are shown in* ***Figure 22****. Fluorescence intensities are shown in arbitrary units (a.u.).*

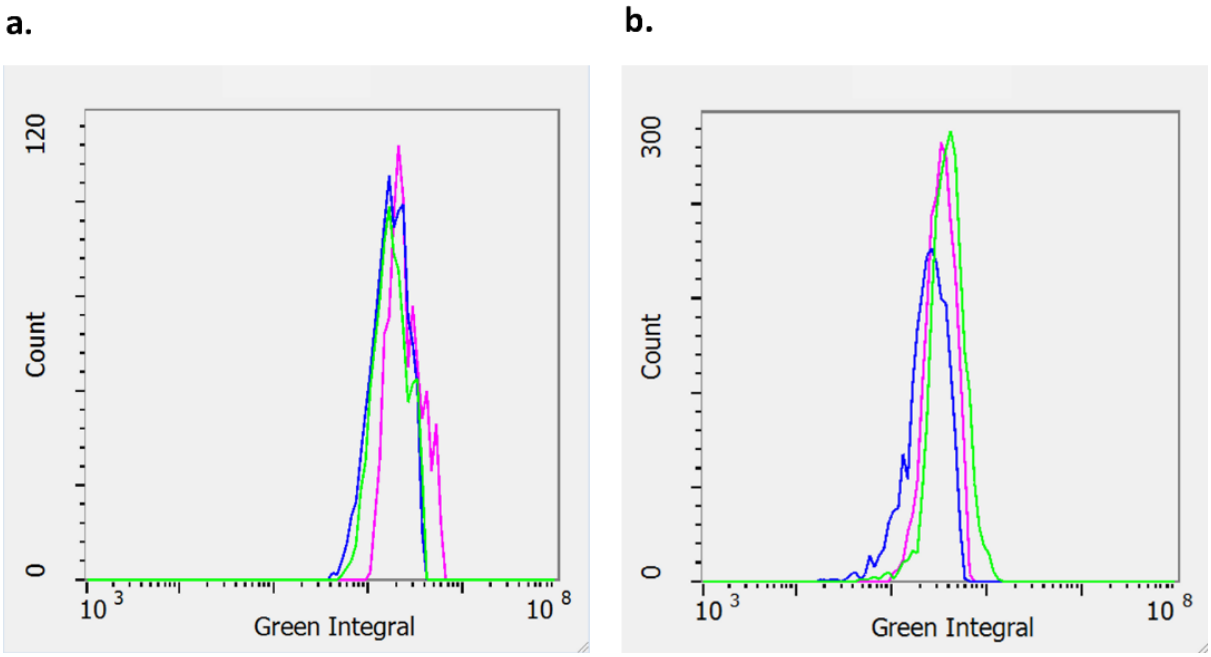

Figure 22. Fluorescence intensity distribution curves of total Cis-Pt adduct and ICL levels

Fluorescence intensity distribution histograms of the LSC data shown in ***Figure 21****. Panel (a) shows the total Cis-Pt adduct levels and corresponds to* ***Figure 21b****; panel (b) represents ICLs and corresponds to* ***Figure 21c****. Green lines: 0 salt; pink lines: 1.1 M salt; blue lines: 1.6 M salt. Fluorescence is shown in log scale.*

5. DISCUSSION

We have observed interaction between Dauno and Cis-Pt is cell type- and dose-dependent phenomenon (see **Figures 8-15** and **Tables 2-4**), which warrants a detailed analyses of the mechanistic components of the interactions in the case of their combined application in cancer chemotherapy. In brief, on HeLa and Jurkat cells, the toxic concentrations of Dauno synergize with Cis-Pt. Nevertheless, on T47D and HCT-116 cells at the same concentration range of Dauno (>6 μM), antagonism was observed between the two drugs. Furthermore, at the concentration of Dauno where synergism was observed on Jurkat and T47D cells, the two drugs antagonize each other on HeLa cells. Reminiscent of our findings, cell type and dose-dependent synergism vs. antagonism was described for the combination of Cis-Pt with a deoxycytidine analogue[153].

In view of the fact that both Dauno and Cis-Pt appear to primarily target the chromatin[46,105], we set out to assess how they affect each other's binding to particular cellular components, focusing on the chromatin. There is little doubt that the mode of Cis-Pt action most relevant to cytotoxicity is its binding to the DNA[46]. Although the effects of Dauno are more diverse, its interaction with the different components of the chromatin are generally considered of primary importance for its toxicity[95]. Also in line with the hypothesis that Dauno exerts its cytotoxicity mainly in the nucleus, a shift in its cellular distribution was observed toward higher cytoplasmic/nuclear ratios in resistant cells[154]. To investigate the possible scenarios of interactions that may lead to synergism or antagonism we employed a web-based resource (https://discover.nci.nih.gov/cellminercdb/) that integrates multiple forms of pharmacological and genomic analyses, and also unifies the cancer cell line datasets[155]. CellminerCDB analyses shown in **Figure 23**, revealed that despite the highly similar chemical structure and mechanisms of action of Dauno and Dox, there are differences even among cell lines of the same tissue type regarding their individual sensitivity to the two drugs. Hence the complexity of cell biological features influencing the toxicity of drugs must be enormous, which makes it difficult to pinpoint the target most relevant for cytotoxicity for any of the drugs studied herein. Thus, the cell line-specific differences in the mode of interactions observed in the combination of Dox and Cis-Pt shown in **Figures 14-15** may not be surprising.

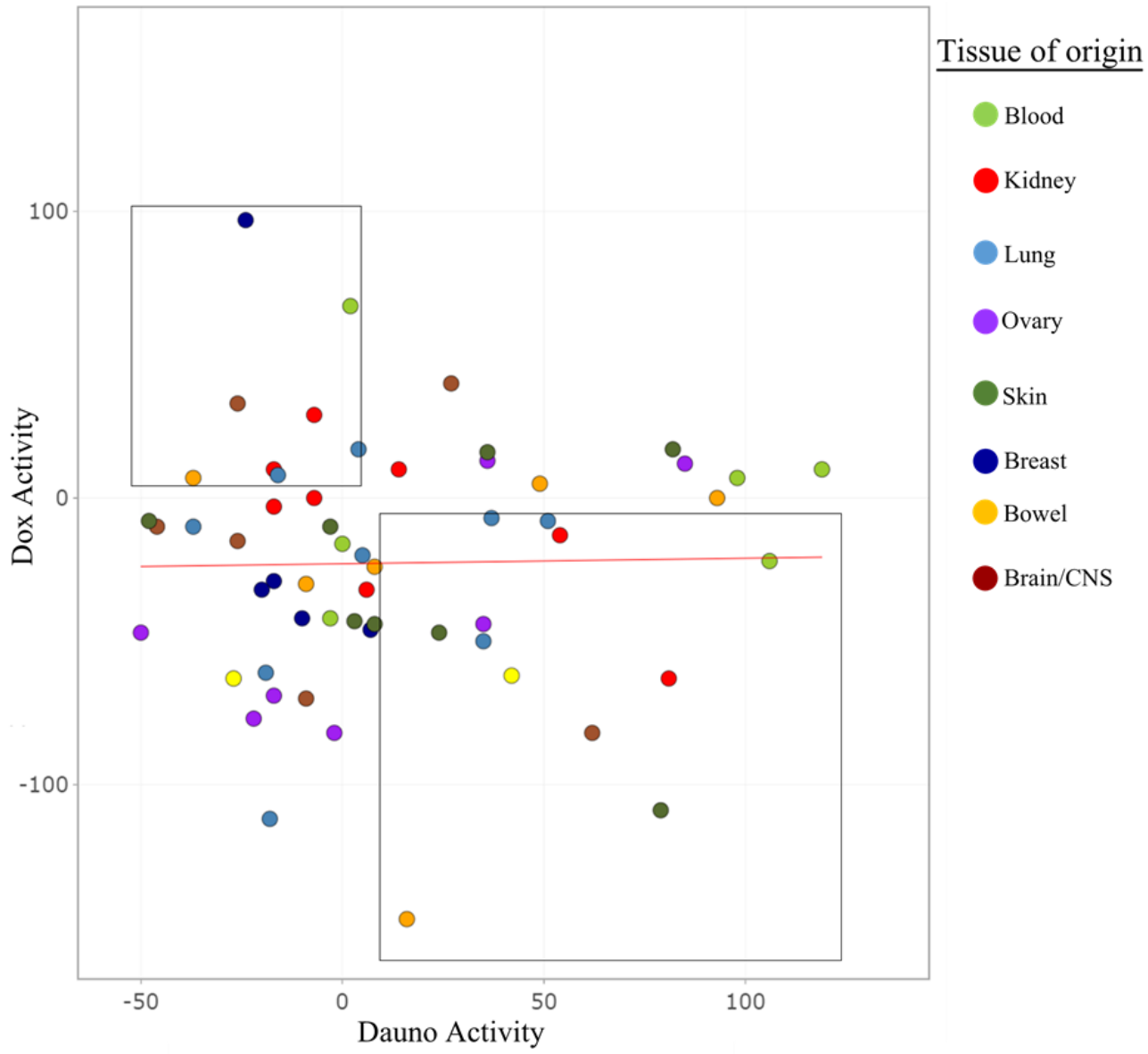

Figure 23. Activity of Dauno, Dox across 60 cell lines

Activity of Dauno (x axis) and Dox (y axis) across 60 cell lines of various tissues of origin is presented. Data are extracted from CellminerCDB, NCI60-DTP-Almanac data set[156]. Cell lines falling in the lower right quadrant are sensitive to Dauno but resistant to Dox, whereas cell lines of the upper left quadrant are sensitive to Dox but not to Dauno.

Regarding the effect of Cis-Pt co-treatment on Dauno levels (**Figures 17a-b**), total Dauno fluorescence representing mainly the acidic endosomal compartment where amphiphylic compounds spontaneously accumulate, decreases upon co-treatment. Therefore, if extra-nuclear effects are also important factors in Dauno toxicity, Cis-Pt could antagonize them by reducing the cytoplasmic Dauno levels. The mechanism of decreased uptake was not further investigated in this study focusing on possible chromatin level interactions. Cis-Pt also decreased total nuclear Dauno fluorescence (**Figure 17b**). Dauno binds more avidly to DNA than to histones[157], but its fluorescence is quenched only by DNA[158]. Therefore, the fluorescence intensities measured probably reflect the presence of both Dauno-DNA and Dauno-histone complexes, but in an unknown ratio. Therefore, we applied an assay that can directly measure DNA-bound Dauno, based on the quenching of Hoechst 33342 fluorescence by Dauno when they are in molecular proximity[148]. The data of **Figures 17c** and **9** reveal that upon Cis-Pt co-treatment the levels of DNA-bound Dauno or Dox do not decrease (**Figure 17c**), rather increase (**Figure 9**). Dimming of the EBr fluorescence in the presence of the Dox was stronger when more Cis-Pt was added to the cells together with the intercalator. Thus, Cis-Pt indeed increases the amount of the DNA-bound anthracycline, also demonstrated in a visually convincing manner, what could only be suspected through the spectacles of the less sensitive Hoechst experiment. In view of the fact that DNA-bound anthracycline levels certainly did not decrease (rather increased based on **Figure 9**), the decreased nuclear fluorescence of Dauno in the presence of Cis-Pt (**Figure 17b**) may reflect a significantly decreased presence of histone-bound Dauno levels, likely due to histone eviction elicited by the anthracycline. In summary, Cis-Pt decreased the amount of anthracycline accumulating in the cytoplasmic acidic compartment (comprising the dominant species of the drug), it also decreased the amount of the histone-bound Dauno, while the amount of DNA-bound anthracycline increased.

As **Figure 18** shows, Dauno-induced eviction of histones was augmented in the nuclei co-treated with Cis-Pt. Two possible explanations for this augmentation by Cis-Pt were considered: 1) Increase of DNA-bound Dauno despite a decrease in its cellular uptake (as concluded from the Hoechst quenching and from the agarose gel data of **Figures 9** and **17c**); 2) Cis-Pt unwinds DNA locally, thus inducing compensatory positive torsional stress around, what would also act to destabilize the nucleosomes enhancing Dauno–induced histone eviction. In other words, Cis-Pt causes distortions in the DNA structure which may be an important factor in its influence on Dauno-induced histone eviction: DNA containing a Cis-Pt 1, 2-

intrastrand d(GpG) adduct is bent by 60° toward the major groove[159]. Eviction occurs also when live cells are treated with anthracyclines in line with the work of Pang.et.al[116] and also with the results of Imre et al from our lab[117]. The Cis-Pt elicited increase in the eviction of H2B was detected already at low, while H3 eviction was augmented only at higher Dauno concentrations. Thus, interaction of the two drugs in terms of histone eviction appears to be synergistic in the whole concentration range of the anthracycline. In summary, Cis-Pt augments the binding of anthracyclines to the genomic DNA in spite of the overall decrease of cellular uptake in its presence. Taken together, from these results we can conclude that histone eviction is a multifactorial process. Although Cis-Pt unwinds DNA much more than Dauno, we do not see eviction in only Cis-Pt treated samples. However, upon addition of also Dauno, eviction is augmented. On the other hand, the increment in the formation of covalent Dauno-DNA adducts in the case of treatment with a combination of Dox and Cis-Pt (**Figure 9**) may contribute to the synergistic toxicity of the two drugs.

In respect to the effect of Dauno on Cis-Pt-DNA cross-links levels, total platination was not affected (**Figure 20a**), while the level of ICLs, assessed using a modified version of the alkaline renaturation assay (**Figure 19**; see also section 4.4), was significantly decreased (**Figure 20b**). The decreased ICL levels observed at low Dauno concentration were not further changed using higher concentrations of the anthracycline; thus, the antagonistic effect of Dauno on ICL formation appears to be similar in the entire Dauno concentration range tested. Therefore, if ICLs significantly contribute to Cis-Pt toxicity, Dauno co-treatment could mitigate these consequences in the low Dauno concentration range, while the synergistic other effects may overrule this at higher concentrations. The decrease of ICL formation is likely due to relaxation of negative supercoiling of the chromatin loops, in line with reference[57] and with data on psoralen cross-linking[58]. Based on the above, the antagonism of low Dauno concentration with Cis-Pt in HeLa cells is suggestive of the importance of ICL formation in the cytotoxicity of Cis-Pt in certain experimental and treatment regimens[48,49].

I have set up a model system comprising isolated nuclei treated with moderate and high salt concentration, to evict nucleosomes and elicit topological changes of the DNA in a controlled manner and in the absence of topological changes induced directly by intercalators. The LA-ICP-MS approach let us obtain absolute numbers for the total adduct levels and for ICLs and these are comparable to the numbers determined in other studies[47]. The changes in total platination levels (mainly intrastrand cross-links[18]) and ICLs were comparable to the changes observed when nuclei were treated with Cis-Pt and Dauno (**Figure 20**). The eviction of

nucleosomes by salt or Dauno increases the target size for Cis-Pt binding. Furthermore, intrastrand crosslinks that involve bending of the DNA[26,160] must be severely antagonized by any constrainment of its structure and augmented by the release of such constraints. On the other hand, the increase of free DNA regions upon nucleosome eviction is expected to favor formation of highly constrained, hyperplectonemic structures likely to occur in the case of long superhelical DNA molecules[161]. These antagonistic effects can explain the changes observed in total Cis-Pt-DNA adduct formation in our model system (**Figure 21**). The increase of target size upon histone eviction may be dominant at moderate salt concentration, increasing adduct levels, while the hyperplectonemic constrainment in the naked DNA produced by high salt pre-treatment may prevent the bending of DNA required for intrastrand crosslinking[26,160]. On the other hand, ICL formation is strongly favored by negative Tw[162]. The superhelicity of the linker regions is generally assumed to be negative[163]. About 30% of the overall linking number difference is estimated to partition as twist[164]. The nucleosomal structure entails slightly overwound DNA (Tw =10.3 bp/turn compared to 10.5 bp/turn for B-DNA[165]. The negative twist in the linker regions together with the slightly positive twist inside the nucleosomes can account for the linker-preference of ICL formation[52]. At moderate salt treatment, upon eviction of H2A and H2B[117], the enlarged nucleosome-free regions are expected to adopt a topology with higher degree of freedom to redistribute twist and writhe. As a consequence, Wr likely becomes more, and Tw less negative in the widening linker regions, in comparison with their state before eviction. Such changes would lead to a decrease in ICL numbers after treatment with 1.1 M salt. At high salt, upon complete eviction, the hyperplectoneme imposed topological constraints would antagonize proper apposition of the bases involved in ICL formation, further decreasing the chances of their generation. The data obtained in this model system are in line with the interpretation that the Dauno evoked decrease of ICL formation observed in isolated nuclei (**Figure 20**) is, at least partly, due to Dauno induced eviction of the histone dimers (**Figure 18**). To what extent Dauno-elicited Tw relaxation directly contributes to a decreased ICL formation could not be determined because nucleosome eviction necessarily accompanies intercalation. The scenario of complete eviction modeled by high salt concentration pre-treatment of isolated nuclei does not occur even at high Dauno concentrations. However, eviction may not be uniform along the genome, affecting certain chromatin regions more than others. Local stretches of naked DNA may be present when live cells are treated with Dauno. The formation of ICLs is expected to be reduced in these regions based on the data of **Figure 21**. In summary, histone eviction by itself is expected to diminish ICL formation, while total adduct formation may not change due to the complexity of effects involving increased target

size represented by a more relaxed naked DNA on the one hand, and constraints emerging in the wake of DNA-DNA interactions upon hyperplectoneme formation, on the other. These observations on the model system are in line with the effect of Dauno on total Cis-Pt adduct formation and on ICL formation (**Figure 20**). Since both drugs have multiple targets in the cell, antagonism as well as synergy could involve multitudes of factors. However, as both drugs are considered to primarily target the chromatin[46,157], their interactions here may be important determinants of the pharmacological outcome of co-treatment. It remains to be determined if inhibition of Top II by Dauno, which was initially perceived as the primary cytotoxic effect of anthracyclines[166], influences Cis-Pt toxicity. However, apoptosis induction by the DNA-Dauno adducts rather than Top II inhibition appears to be appears to be the crucial factor in the cytotoxicity of anthracycline[101].

6. SUMMARY

The widely used anticancer agents Cis-Pt and Dauno exhibited cell type- and concentration-dependent synergy or antagonism *in vitro*. In HeLa cells, the mode of interaction between Dauno used at subtoxic concentrations and Cis-Pt was antagonism, yet, at a toxic concentration of Dauno combined with Cis-Pt, synergism was observed. In the case of Jurkat cells, Dauno and Cis-Pt synergize with each other through the whole applied concentration range. In contrast with HeLa cells, in T47D and HCT 116 cells the mode of interaction between the subtoxic concentration of Dauno and Cis-Pt was synergism, while antagonism was observed when toxic concentrations of Dauno were combined with Cis-Pt. I attempted to interpret these effects in terms of the changes elicited by the drugs in the chromatin, the target held primarily responsible for the cytotoxicity of both agents. I measured the effect of Cis-Pt on the levels of Dauno in different cell compartments, the effect of Cis-Pt on Dauno-induced nucleosome eviction, and assessed the influence of Dauno on DNA platination by flow- and laser scanning cytometry as well as in laser ablation-inductively coupled plasma-mass spectrometry assays. As summarized in **Figure 24**, Dauno and Cis-Pt antagonize one another through a decrease of ICLs in the presence of Dauno (at its low and high cc. alike), and, also via the diminished Dauno uptake in the presence of Cis-Pt. They could synergize with each other through enhanced histone eviction by Dauno in the presence of co-treatment with Cis-Pt, accompanied by an increment of DNA bound anthracycline. These drug interactions have not been described before to the best of our knowledge and may impact cytotoxicity reached by combination treatment regimens *in vivo*.

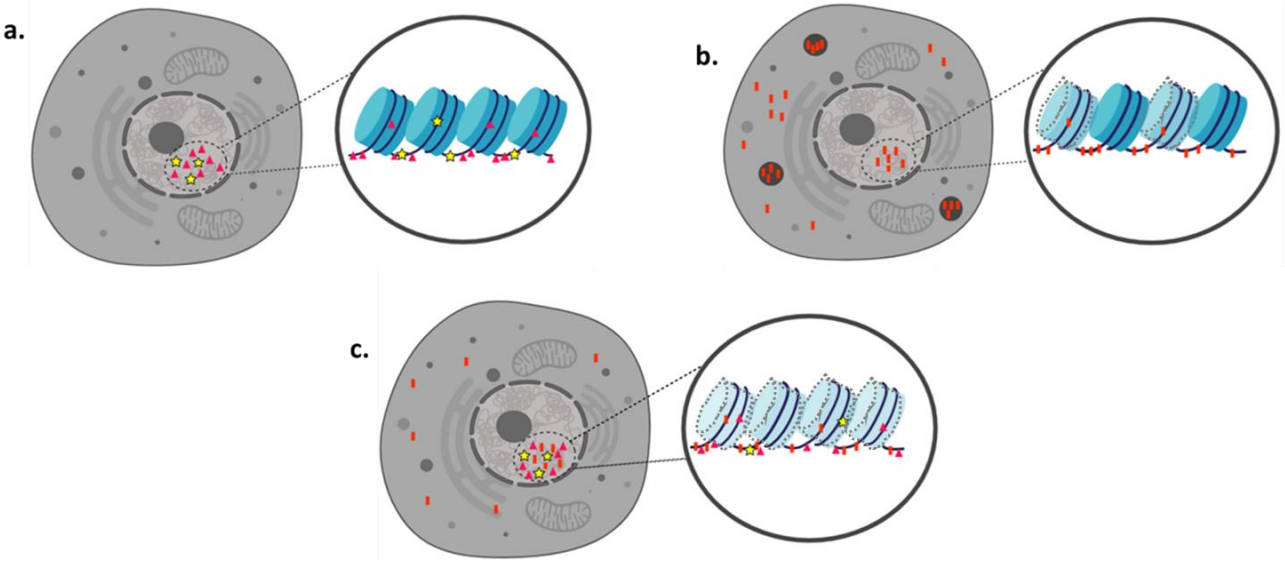

Figure 24. Schematic interpretation of the interactions observed

(a) *In DNA, Cis-Pt forms mainly intrastrand (pink triangle) crosslinks and, less frequently, ICLs (yellow star). DNA (navy blue line) is wrapped around histone octamer (dark blue).*

(b) *Dauno (orange rectangle) is present in cytoplasm mainly in the endosomal compartment. In the nucleus it intercalates into the DNA and evicts histones (eviction is demonstrated as a light blue histone octamer).*

(c) *In the presence of Cis-Pt, Dauno concentration decreases in the cytoplasm (due to decreased uptake into the cell and/or the endosomal compartment). In the nucleus, its total amount is not affected by Dauno co-treatment, but the number of ICLs is decreased. The number of DNA bound Dauno is increased when Cis-Pt is co-administered. Histone eviction is represented by the faded color of the core histones (very light blue). Figures are created with BioRender.com*

Part B. The Relevance of Histone Levels for DNA-Targeted Therapy

I. INTRODUCTION

As mentioned in section 1.3, Dauno binds to the linker histones[119]. Moreover, in **Figure 18**, I showed that binding of Dauno alone, as well as its combination with Cis-Pt led to histone eviction. Since eviction mattered for anthracyclines binding and how the two drugs interact with each other, we systematically used CellminerCDB to analyze how sensitivity to these drugs correlates with the expression level of the different histones. In contrast with the experimental observation of Braunestin. *et al*[167], we, by using CellminerCDB to explore the NCI-60 database, found no correlation between the sensitivity of Dauno and Dox with the expression level of H2A (HISTH2AC) and H2B (HISTH2BD) and H1.5 (HIST1H1B) histones, as shown in **Figure B1**. However, we stumbled on an interesting phenomenon. We have observed that 10 out of 60 cell lines from 9 different tissue types have markedly decreased mRNA expression levels of the H1.5 variant linker histone gene, concomitant with mRNA overexpression of ODC1 (Ornithine Decarboxylase 1) and AMD1 (Adenosylmethionine Decarboxlase 1); see **Figure B2**. I investigated two scenarios, trying to interpret this phenomenon: First, based on the assumption that the linker histone variants, unexpressed in the 10 cell lines and expressed in 50, may provide a selective advantage for the latter by shielding the linker DNA to drugs, I tested if cell lines with inducible H1.5 expression may exhibit any dependence of drug sensitivity on H1.5 expression levels. For this purpose, drugs differentially toxic for the 50 and the 10 cell lines were selected based on Cellminer analyses. These studies have led to negative results, not demonstrated here. I also investigated another option: whether the elevated level of the enzymes involved in polyamine synthesis might have a nucleosome destabilizing effect, potentially influencing drug sensitivity. If it were so, then the overexpression of ODC1 in the 10 cell lines could make them more vulnerable to DNA-targeted drugs. This aspect, a fortuitous side-product in our attempt to interpret the strange dichotomies among the NCI60 cell lines, has led us to realize that at high enough concentration polyamines destabilize nucleosomes.

ODC1 and AMD1 are the genes of the key enzymes for polyamine (PA) synthesis[168,169]. PAs (Putrescin, Spermidine and Spermine) are polycationic alkylamines (structures are shown in

Figure B3). Putrescin is generated from ornithine catalyzed by the ODC1 enzyme, and it is a precursor for the production of Spermidine and Spermine. AMD1 is generated as a pro-enzyme (proAMD1), which, as a result of self-cleavage and heterotetramerization, becomes an active enzyme[169]. The active AMD1 enzyme catalyzes the conversion of *S*-adenosylemethionine to *S*-adenosyl-5′-(3-methylthiopropylamine) which is fully engaged to polyamine biosynthesis[170]. Investigations on the activity of ODC1 in brain cancer, as well as AMD1 activity in prostate cancer unveiled that their activity leads to the potentiation of these malignancies[169,171]. Expression and activity of ODC1 and AMD1 are closely related to each-other (based on CellminerCDB not shown) and to the cellular concentration of the polyamines[172]. Furthermore, PAs are involved in the pathologies of several parasitic diseases such as Trypanosomiasis[173] and Leishmaniasis[174]. It is also worth noting that PAs are associated with neurodegenerative diseases such as Alzheimer's[175], Parkinson's[176] and certain age-related conditions, as polyamines are known to decrease with age[177]. Since PAs levels and the enzymes involved in their metabolism proved to play a role in cancer and several other diseases, inhibitors of PA synthesis or transport are in the focus of attention in view of the therapeutic prospects. Preclinical and clinical studies on polyamine antagonist regimens including Eflornithine and Sardomozide (ODC1 and AMD1 inhibitors, respectively), showed promising results in certain types of cancer[178-180]. Combination of Eflornithine and some of the non-steroidal anti-inflammatory drugs such as Indomethacin[178], Sulindac[181] and Celecoxib[182] synergized with each other resulting in the suppression of polyamine-dependent cell proliferation and tumor growth. The transport system of PAs is another therapeutic target for decreasing the PAs level in cancer cells. Synthetic, lipophilic polyamine analogues restrict the cellular PA uptake system and when in combination with Eflornithine, they synergize each other strongly resulting in PA depletion[183]. At physiological pH, positively charged (basic) PAs associate with negatively charged (acidic) sites on proteins, nucleic acids as well as phospholipid membranes[184]. PAs are required for cells to proceed from G1 to S phase and they are directly involved in the DNA synthetic phase of the cell cycle[185,186]. PAs bind to DNA and cause DNA aggregation[187]. The stoichiometry of PA binding which leads to condensation of DNA is ~2 PA molecules per one helical turn of DNA[188]. PAs appear to stabilize also nucleosomes[189] and condense chromatin[190,191,192] in the ~ 0.1-3 mM concentration range. The nucleosome destabilizing effect discussed below, an unexpected observation with possible ramification not contemplated earlier, appears at slightly higher, still biologically relevant PA concentrations[193].

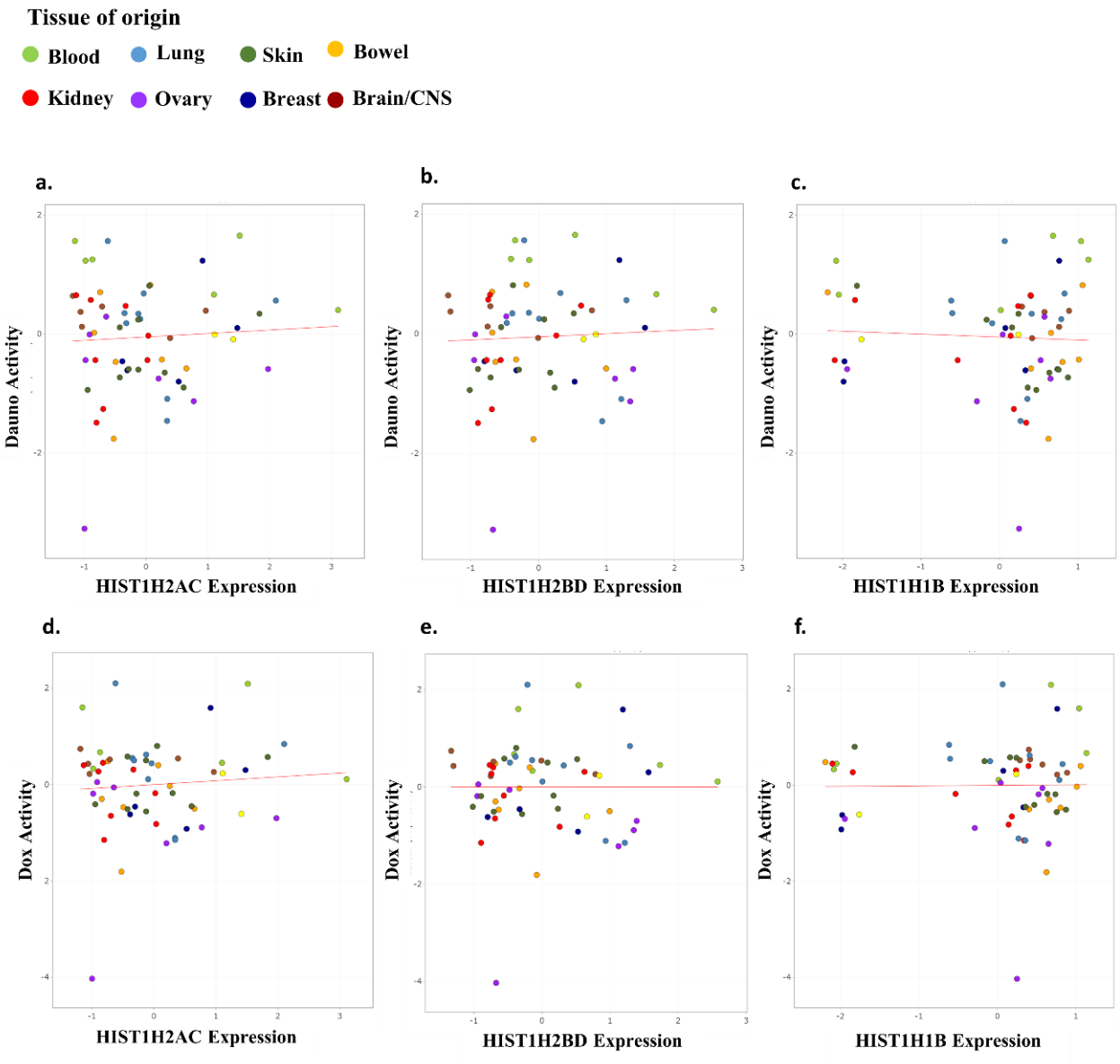

Figure B1. Activity of Dauno and Dox across 60 cell lines and their correlation with mRNA expression of H2A, H2B and H1.5 histone genes

On the y-axes activity of Dauno (a, b, c) and Dox (d, e, f) across 60 cell lines of various tissues of origin is presented. On the x-axes, mRNA expression of H2A (a, d), H2B (b, e) and H1.5 (c, f) histone is designated. Data are extracted from CellminerCDB, NCI-60 data set.

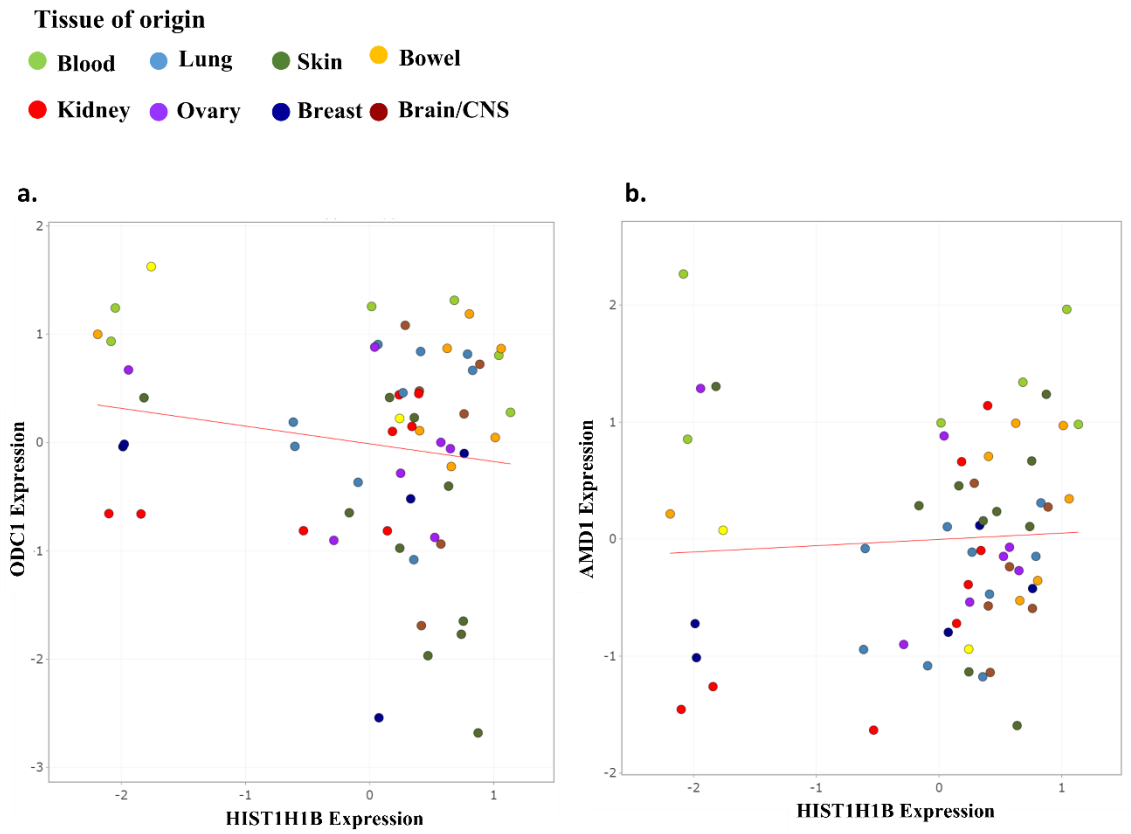

Figure B2. Anti-correlation between mRNA expression of H1.5 histone and ODC1 and AMD1 genes

*On the y-axis of both panel **a** and **b,** the mRNA expression of H1.5 histone across 60 cell lines of various tissues of origin is presented. On the x-axes, mRNA expression of ODC1 (**a**) and AMD1 (**b**) is designated. Data are extracted from CellminerCDB, NCI-60 data set.*

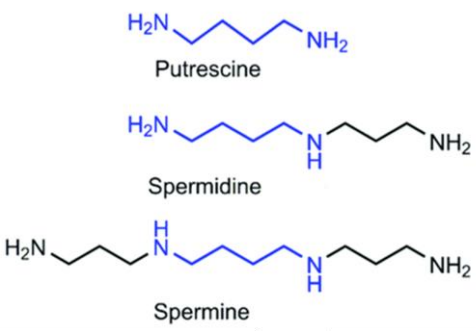

Figure B3. Chemical structure of natural PAs

II.AIM OF THE STUDY

The study aims to determine how PAs, when used at high, still biologically relevant concentrations, impact nucleosome stability?

III.METHODS

Preparation of the solutions:

Except for the permeabilizing solution (1% Triton/PBS/EDTA) that was prepared freshly, all the other solutions were prepared 24 hrs before the day of experimentation. In the case of **Figure B4**, the pH of the ice-cold PBS/EDTA (pH=7.8) solutions was alkalized to the corresponding pH of the solutions containing 2.5, 5 and 10 mM Spermidine (pH equals 9.6, 10.2, and 10.4, respectively) with NaOH. In the case of figure B5, the pH of the NaCl solutions (with slightly different pH values as shown in **Figure B4**) containing 5 and 10 mM Spermidine were neutralized with HCl to achieve pH= 7.8. It is worth mentioning that the addition of HCl was minuscule so salt concentration did not increase by more than 5 mM.

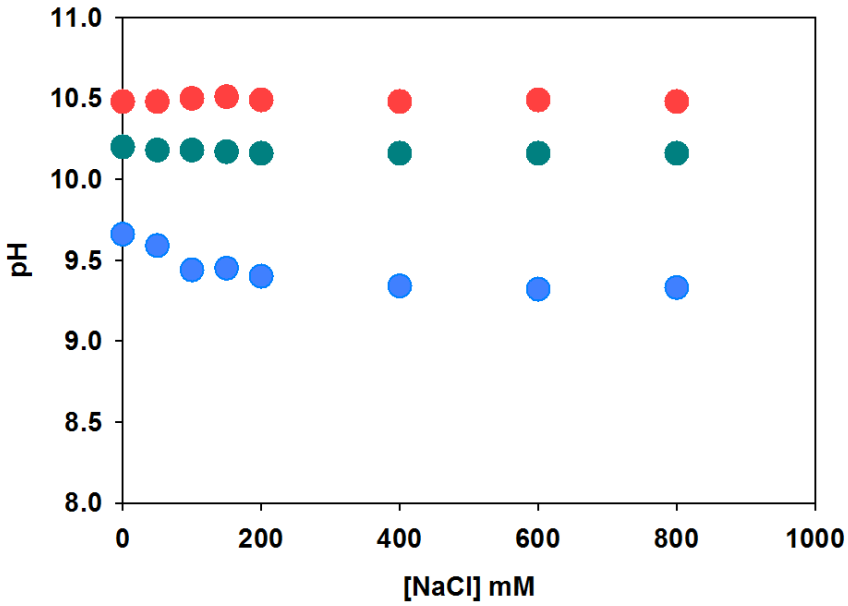

Figure B4. The pH of the NaCl solutions containing Spermidine

The pH of the solutions was set to the values shown in the X axis by the addition of HCl or NaOH. Blue, green and red circles represent solutions containing 2.5, 5 and 1 mM Spermidine, respectively. The pH is adjusted by addition of HCl or NaOH while limiting the change of NaCl cc. to maximum ±5 mM.

Preparation of nuclei/ permeabilization and histone eviction by salt

Embedding the cells in low melting agarose in Ibidi-wells, and permeabilization of cells is explained section 3.2.4 and work of Imre.et.al from our lab[117]. After permeabilization, nuclei were washed with 400 µl ice cold 1×PBS/EDTA three times for 3min. Then nuclei were treated with the solutions containing various NaCl concentration with or without Spermidine, for 60 min, on ice. After this step, the nuclei were washed with 400 µl ice cold 1×PBS/EDTA 3 times for 5 min. Since NaCl was dissolved in 1×PBS/EDTA, the salt concentrations indicated on the X axes of the graphs in **Figures B4** and **B5**, show the additional NaCl concentrations regardless of NaCl present in the PBS buffer which is ~150 mM. EDTA was included in PBS to avoid complex effects involving divalent cations[194].

Data visualization:

Plotting and analysis of the curves was made by SigmaPlot 11.0, 'Standard curves: Four Parameter Logistic Curve' curve-fitting subroutines. The number of analyzed G1 nuclei were between 200-1500/well, out of the about 800-3000 cells scanned. All the SEM values indicated in the Figure legends were calculated from the datapoints of the cell population analyzed in the given experiment.

IV. RESULTS

The effect of PAs on the stability of nucleosomes was analyzed in permebilized nuclei of H2B-GFP expressing HeLa cells by utilizing our QINESIn[195] method. As **Figure B5** shows, addition of Spermidine to the agarose-embedded nuclei at a concentration of 10 mM martkedly lowered the concentration of salt required to destabilize the nucleosomes releasing H2B-GFP. However, the pH of the PBS/EDTA buffer was strongly alkalinized by Spermidine addition, so destabilization could be partly attributed to the shift of pH toward the isoelectric point of the histones[196,197] (~10 for H2B, ~10.5 for H2A and ~11 for H3 and H4). Therefore, to determine if Spermidine itself exert a destabilizing effect, the salt elution curves were compared in the presence and in the absence of the Spermidine at the pH measured after adding the Spermidine to the PBS/EDTA + NaCl solution. As shown in **Figure B5**, Spermidine at a concentration as low as 2.5 mM, augments NaCl-induced histone eviction. Comparison of the NaCl solutions with their pH adjusted to match the pH of NaCl solutions containing Spermidine indicates that the increment in histone eviction is not merely due to alkaline pH, but also to Spermidine itself. Although 5 mM Spermidine solution in the absence of NaCl is unable to destabilize histone, the addition of 400 mM NaCl to the system is suffice to boost eviction of histones (in other words, the negligible histone eviction induced by 400 mM NaCl at alkaline pH is augmented by the addition of 5 mM Spermidine) .The same holds true for a 10 mM Spermidine solution supplemented with only 50 mM NaCl, in which histone eviction is augmented significantly in comparison to eviction elicited by alkaline NaCl solutions. As shown in **Figure B6**, although Spermidine and low concentration of NaCl, each alone, are incapable to evict histones at even pH=10.5, but their combination synergize with each other and results in histone eviction to be achieved at lower pH (starting from pH=9).

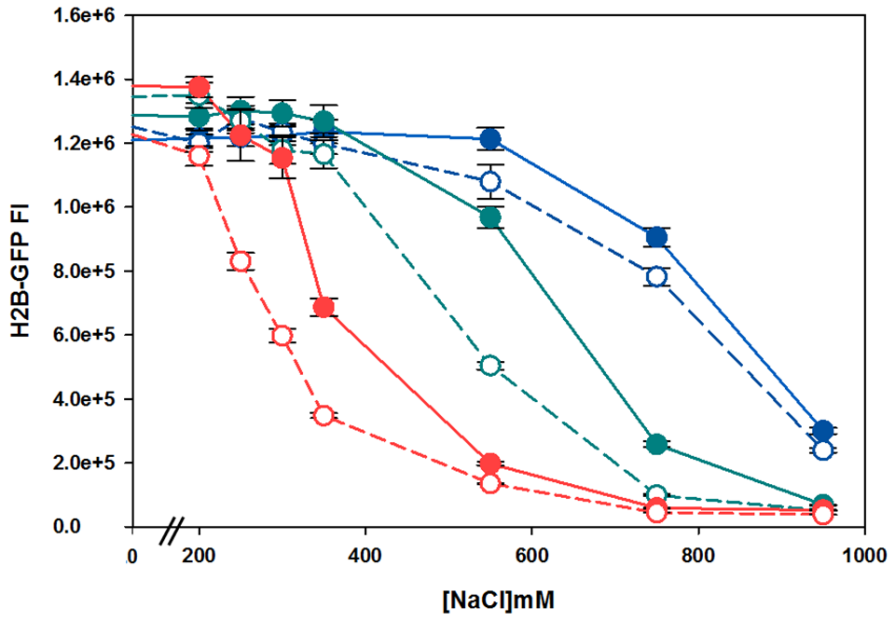

Figure B5. Spermidine augments eviction of histones induced by NaCl at the pH determined by the polyamine

Nuclei of H2B-GFP expressor HeLa cells were treated with a concentration series of NaCl solution alone, with the pH of the buffer set to the value of the corresponding solution containing also spermidine (solid lines), or in combination with spermidine used at three different concentrations (dashed lines). The pH values of each solution are shown in ***Figure B4****. The PBS/EDTA + NaCl solutions were alkalized to the pH of the corresponding 2.5, 5 and 10 mM Spermidine-PBS/EDTA + NaCl solutions with NaOH. The concentrations shown in the x-axis represent the final salt concentration after addition to PBS-EDTA. PBS/EDTA + NaCl concentration series set to the pH of the corresponding 2.5, 5 and 10 mM Spermidine containing solutions are represented by blue, green and red symbols, respectively. Spermidine-containing PBS/EDTA + NaCl concentration series with 2.5, 5 and 10 mM Spermidine are represented by empty blue, gree, and red circles, respectively. Green fluorescence intensity of ~1000 nuclei was recorded by LSC. The mean values were plotted as a function of the NaCl concentration set above that of PBS. The bars show SEM.*

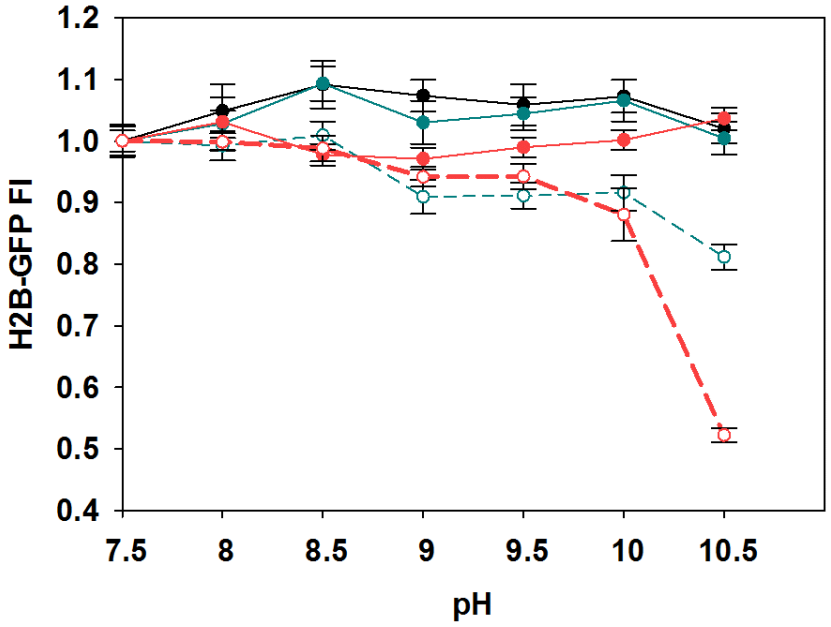

Figure B6. Spermidine induced histone eviction is pH-dependent.

Nuclei of H2B-GFP expressor HeLa cells were treated with 5 or 10 mM Spermidine alone (filled green and red symbols connected with solid lines) or in combination with 400 mM (at 5 mM Spermidine) or 200 mM (at 10 mM Spermidine) NaCl (empty green and red symbols, dashed lines). Black circle denote data achieved as a result of treatment with PBS-EDTA supplemented with 400 mM NaCl, respectively.

V.DISCUSSION

The millimolar concentration range of the nucleosome destabilizing effect observed in our experiments is attained by PAs in various physiological and pathological scenarios [198, 199, 200,201]. For instance, PAs level can reach 10-12 mM in prostate cancer [193]. Also, PAs are present in millimolar concentration in plants and have diverse functions [202], what can be modulated by their exogenous application in high concentration [203,204]. Since expression of ODC1 and AMD1 correlate (Pearson correlation r =0.38) across the 60 lines, the high ODC1 and AMD1 expressor cells likely have higher intracellular PA levels in comparison with the other 50 cell lines (**Figure B2**).

Chromatin compaction in permeabilized nuclei treated with polyamines ensued at 0.2 and 0.5 mM of Spermine or Spermidine, which has not changed further above 0.8 and 1.5 mM concentration, respectively [190]. The nucleosome destabilizing effect I observed, an unexpected finding with possible ramification not contemplated earlier, appears at higher, still biologically relevant PA concentrations. Within the physiological range, up to pH=8.0, nucleosomes are expected to be stable [205]. Alkalization to near the isoelectric point of the histones sensitized the nucleosomes to salt induced disruption, as **Figures B5** and **B6** show, effectively decreasing the electrostatic binding forces. Alkaline conditions alone, at physiological ionic strength, did not dissociate H2B-GFP from the nucleosomes (**Figure B5**). Both alkaline pH and elevated salt concentration were necessary to demonstrate the destabilizing effect of PAs. The nucleosome destabilizing effect described herein (**FigureS B5** and **B6**) is apparently superimposed on PAs' contribution to the condensed state of chromatin as well as on other, indirect effects on chromatin structure and function; these include the up-regulation of histone acetylation [206] and activation of DNA methyltransferase [207], also ensuing at the elevated PA concentrations following ODC1 overexpression, or PA feeding, respectively. Therefore we suggest that elevated PA concentration in the nucleus leading to nucleosome destabilization may contribute to epigenetic diversification, possibly through alteration in the fine balance of factors regulating remodeling[208]. It is also quite likely, in view of the effect of nucleosome eviction on Cisplatin binding (part A of the thesis) or on intercalator binding [209] that the effect of these drugs is augmented by high PA levels, a scenario relevant e.g. in the case of prostate cancer[193].

VI. SUMMARY

The role and molecular interactions of PAs in the nucleus are little understood, either when present at physiological concentration or when overproduced. Whether they alter nucleosome stability, a key regulatory factor in eukaryotic gene control, what is generally assessed by exposing preparations of nucleosomes to challenging conditions, has not yet been reported. Here their effect on nucleosome stability was demonstrated, as measured *in situ*, in a close to native state of chromatin, preserving the nucleosome constrained topology of the genomic DNA. A robust destabilizing effect was observed in the millimolar concentration range in the case of Spermidine, it was strongly pH and salt concentration dependent and manifest also at neutral pH. These observations raise the possibility that the polyamines, reaching high enough intracellular levels, influence DNA dependent processes by interfering with histone-DNA interactions.

7. REFERENCES

1 Bruckner, H. W. *et al.* Improved chemotherapy for ovarian cancer with cis-diamminedichloroplatinum and adriamycin. *Cancer* **47**, 2288-2294, doi:10.1002/1097-0142(19810501)47:9<2288::aid-cncr2820470931>3.0.co;2-3 (1981).

2 Signorelli, M. *et al.* Platinum, anthracycline, and alkylating agent-based chemotherapy for ovarian carcinosarcoma. *International journal of gynecological cancer : official journal of the International Gynecological Cancer Society* **19**, 1142-1146, doi:10.1111/IGC.0b013e3181a8ef22 (2009).

3 O'Brien, M. E. *et al.* Randomised phase II study of amrubicin as single agent or in combination with cisplatin versus cisplatin etoposide as first-line treatment in patients with extensive stage small cell lung cancer - EORTC 08062. *European journal of cancer (Oxford, England : 1990)* **47**, 2322-2330, doi:10.1016/j.ejca.2011.05.020 (2011).

4 van Wijk, F. H. *et al.* Doxorubicin versus doxorubicin and cisplatin in endometrial carcinoma: definitive results of a randomised study (55872) by the EORTC Gynaecological Cancer Group. *Annals of oncology : official journal of the European Society for Medical Oncology* **14**, 441-448, doi:10.1093/annonc/mdg112 (2003).

5 Xu, M. J., Alberts, D. S., Liu, R., Leibovitz, A. & Liu, Y. In vitro evaluation of cisplatin interaction with doxorubicin or 4-hydroperoxycyclophosphamide against human gynecologic cancer cell lines. *Cancer chemotherapy and pharmacology* **25**, 89-94, doi:10.1007/bf00692345 (1989).

6 Rosenberg, B., Vancamp, L. & Krigas, T. INHIBITION OF CELL DIVISION IN ESCHERICHIA COLI BY ELECTROLYSIS PRODUCTS FROM A PLATINUM ELECTRODE. *Nature* **205**, 698-699, doi:10.1038/205698a0 (1965).

7 Rosenberg, B., VanCamp, L., Trosko, J. E. & Mansour, V. H. Platinum compounds: a new class of potent antitumour agents. *Nature* **222**, 385-386, doi:10.1038/222385a0 (1969).

8 Gately, D. P. & Howell, S. B. Cellular accumulation of the anticancer agent cisplatin: a review. *British journal of cancer* **67**, 1171-1176, doi:10.1038/bjc.1993.221 (1993).

9 Safaei, R. & Howell, S. B. Copper transporters regulate the cellular pharmacology and sensitivity to Pt drugs. *Critical reviews in oncology/hematology* **53**, 13-23, doi:10.1016/j.critrevonc.2004.09.007 (2005).

10 Ishida, S., Lee, J., Thiele, D. J. & Herskowitz, I. Uptake of the anticancer drug cisplatin mediated by the copper transporter Ctr1 in yeast and mammals. *Proceedings of the National Academy of Sciences of the United States of America* **99**, 14298-14302, doi:10.1073/pnas.162491399 (2002).

11 Yonezawa, A. *et al.* Association between tubular toxicity of cisplatin and expression of organic cation transporter rOCT2 (Slc22a2) in the rat. *Biochemical pharmacology* **70**, 1823-1831, doi:10.1016/j.bcp.2005.09.020 (2005).

12 Komatsu, M. *et al.* Copper-transporting P-Type Adenosine Triphosphatase (ATP7B) Is Associated with Cisplatin Resistance. *Cancer research* **60**, 1312 (2000).

13 Cui, Y. *et al.* Drug resistance and ATP-dependent conjugate transport mediated by the apical multidrug resistance protein, MRP2, permanently expressed in human and canine cells. *Molecular pharmacology* **55**, 929-937 (1999).

14 Zhang, Y., Guo, Z. & You, X. Z. Hydrolysis theory for cisplatin and its analogues based on density functional studies. *Journal of the American Chemical Society* **123**, 9378-9387, doi:10.1021/ja0023938 (2001).

15 Bancroft, D. P., Lepre, C. A. & Lippard, S. J. Platinum-195 NMR kinetic and mechanistic studies of cis- and trans-diamminedichloroplatinum(II) binding to DNA. *Journal of the American Chemical Society* **112**, 6860-6871, doi:10.1021/ja00175a020 (1990).

16 Malinge, J. M., Giraud-Panis, M. J. & Leng, M. Interstrand cross-links of cisplatin induce striking distortions in DNA. *Journal of inorganic biochemistry* **77**, 23-29, doi:10.1016/s0162-0134(99)00148-8 (1999).

17 Fichtinger-Schepman, A. M., van Oosterom, A. T., Lohman, P. H. & Berends, F. cis-Diamminedichloroplatinum(II)-induced DNA adducts in peripheral leukocytes from seven cancer patients: quantitative immunochemical detection of the adduct induction and removal after a single dose of cis-diamminedichloroplatinum(II). *Cancer research* **47**, 3000-3004 (1987).

18 Eastman, A. Characterization of the adducts produced in DNA by cis-diamminedichloroplatinum(II) and cis-dichloro(ethylenediamine)platinum(II). *Biochemistry* **22**, 3927-3933, doi:10.1021/bi00285a031 (1983).

19 Pullman, A. & Pullman, B. Molecular electrostatic potential of the nucleic acids. *Quarterly reviews of biophysics* **14**, 289-380, doi:10.1017/s0033583500002341 (1981).

20 Mansy, S., Rosenberg, B. & Thomson, A. J. Binding of cis- and trans-dichlorodiammineplatinum(II) to nucleosides.i. Location of the binding sites. *Journal of the American Chemical Society* **95**, 1633-1640, doi:10.1021/ja00786a045 (1973).

21 Rice, J. A., Crothers, D. M., Pinto, A. L. & Lippard, S. J. The major adduct of the antitumor drug cis-diamminedichloroplatinum(II) with DNA bends the duplex by approximately equal to 40 degrees toward the major groove. *Proceedings of the National Academy of Sciences of the United States of America* **85**, 4158-4161, doi:10.1073/pnas.85.12.4158 (1988).

22 Bellon, S. F., Coleman, J. H. & Lippard, S. J. DNA unwinding produced by site-specific intrastrand crosslinks of the antitumor drug cis-diamminedichloroplatinum(II). *Biochemistry* **30**, 8026-8035, doi:10.1021/bi00246a021 (1991).

23 Anin, M. F. & Leng, M. Distortions induced in double-stranded oligonucleotides by the binding of cis- or trans-diammine-dichloroplatinum(II) to the d(GTG) sequence. *Nucleic acids research* **18**, 4395-4400, doi:10.1093/nar/18.15.4395 (1990).

24 Takahara, P. M., Frederick, C. A. & Lippard, S. J. Crystal Structure of the Anticancer Drug Cisplatin Bound to Duplex DNA. *Journal of the American Chemical Society* **118**, 12309-12321, doi:10.1021/ja9625079 (1996).

25 Takahara, P. M., Rosenzweig, A. C., Frederick, C. A. & Lippard, S. J. Crystal structure of double-stranded DNA containing the major adduct of the anticancer drug cisplatin. *Nature* **377**, 649-652, doi:10.1038/377649a0 (1995).

26 Gelasco, A. & Lippard, S. J. NMR solution structure of a DNA dodecamer duplex containing a cis-diammineplatinum(II) d(GpG) intrastrand cross-link, the major adduct of the anticancer drug cisplatin. *Biochemistry* **37**, 9230-9239, doi:10.1021/bi973176v (1998).

27 Yang, D., van Boom, S. S. G. E., Reedijk, J., van Boom, J. H. & Wang, A. H. J. Structure and Isomerization of an Intrastrand Cisplatin-Cross-Linked Octamer DNA Duplex by NMR Analysis. *Biochemistry* **34**, 12912-12920, doi:10.1021/bi00039a054 (1995).

28 Huang, H., Zhu, L., Reid, B. R., Drobny, G. P. & Hopkins, P. B. Solution structure of a cisplatin-induced DNA interstrand cross-link. *Science (New York, N.Y.)* **270**, 1842-1845, doi:10.1126/science.270.5243.1842 (1995).

29 Malinge, J. M., Pérez, C. & Leng, M. Base sequence-independent distorsions induced by interstrand cross-links in cis-diamminedichloroplatinum (II)-modified DNA. *Nucleic acids research* **22**, 3834-3839, doi:10.1093/nar/22.19.3834 (1994).

30 Treiber, D. K., Zhai, X., Jantzen, H. M. & Essigmann, J. M. Cisplatin-DNA adducts are molecular decoys for the ribosomal RNA transcription factor hUBF (human upstream binding factor). *Proceedings of the National Academy of Sciences* **91**, 5672, doi:10.1073/pnas.91.12.5672 (1994).

31 Kartalou, M. & Essigmann, J. M. Recognition of cisplatin adducts by cellular proteins. *Mutation research* **478**, 1-21, doi:10.1016/s0027-5107(01)00142-7 (2001).

32 Wang, D. & Lippard, S. J. Cisplatin-induced post-translational modification of histones H3 and H4. *The Journal of biological chemistry* **279**, 20622-20625, doi:10.1074/jbc.M402547200 (2004).

33 Prigent, C. & Dimitrov, S. Phosphorylation of serine 10 in histone H3, what for? *Journal of Cell Science* **116**, 3677, doi:10.1242/jcs.00735 (2003).

34 Zhang, R., Erler, J. & Langowski, J. Histone Acetylation Regulates Chromatin Accessibility: Role of H4K16 in Inter-nucleosome Interaction. *Biophysical journal* **112**, 450-459, doi:10.1016/j.bpj.2016.11.015 (2017).

35 Rosenberg, J. & Sato, P. Messenger RNA loses the ability to direct in vitro peptide synthesis following incubation with cisplatin. *Molecular pharmacology* **33**, 611-616 (1988).

36 Hostetter, A. A., Osborn, M. F. & DeRose, V. J. RNA-Pt adducts following cisplatin treatment of Saccharomyces cerevisiae. *ACS Chem Biol* **7**, 218-225, doi:10.1021/cb200279p (2012).

37 Burger, A. M., Double, J. A. & Newell, D. R. Inhibition of telomerase activity by cisplatin in human testicular cancer cells. *European journal of cancer (Oxford, England : 1990)* **33**, 638-644, doi:10.1016/s0959-8049(96)00521-7 (1997).

38 Melnikov, S. V., Soll, D., Steitz, T. A. & Polikanov, Y. S. Insights into RNA binding by the anticancer drug cisplatin from the crystal structure of cisplatin-modified ribosome. **44**, 4978-4987, doi:10.1093/nar/gkw246 (2016).

39 Martinho, N., Santos, T. C. B., Florindo, H. F. & Silva, L. C. Cisplatin-Membrane Interactions and Their Influence on Platinum Complexes Activity and Toxicity. *Frontiers in physiology* **9**, 1898, doi:10.3389/fphys.2018.01898 (2018).

40 Tulub, A. A. & Stefanov, V. E. Cisplatin stops tubulin assembly into microtubules. A new insight into the mechanism of antitumor activity of platinum complexes. *International journal of biological macromolecules* **28**, 191-198, doi:10.1016/s0141-8130(00)00159-8 (2001).

41 Casini, A. & Reedijk, J. Interactions of anticancer Pt compounds with proteins: an overlooked topic in medicinal inorganic chemistry? *Chemical Science* **3**, 3135-3144, doi:10.1039/C2SC20627G (2012).

42 Timerbaev, A. R., Hartinger, C. G., Aleksenko, S. S. & Keppler, B. K. Interactions of antitumor metallodrugs with serum proteins: advances in characterization using modern analytical methodology. *Chemical reviews* **106**, 2224-2248, doi:10.1021/cr040704h (2006).

43 Reedijk, J. New clues for platinum antitumor chemistry: kinetically controlled metal binding to DNA. *Proceedings of the National Academy of Sciences of the United States of America* **100**, 3611-3616, doi:10.1073/pnas.0737293100 (2003).

44 Mistry, P., Kelland, L. R., Abel, G., Sidhar, S. & Harrap, K. R. The relationships between glutathione, glutathione-S-transferase and cytotoxicity of platinum drugs and melphalan in eight human ovarian carcinoma cell lines. *British journal of cancer* **64**, 215-220, doi:10.1038/bjc.1991.279 (1991).

45 Holford, J., Beale, P. J., Boxall, F. E., Sharp, S. Y. & Kelland, L. R. Mechanisms of drug resistance to the platinum complex ZD0473 in ovarian cancer cell lines. *European journal of cancer (Oxford, England : 1990)* **36**, 1984-1990, doi:10.1016/s0959-8049(00)00192-1 (2000).

46 Akaboshi, M. *et al.* The number of platinum atoms binding to DNA, RNA and protein molecules of HeLa cells treated with cisplatin at its mean lethal concentration. *Japanese journal of cancer research : Gann* **83**, 522-526, doi:10.1111/j.1349-7006.1992.tb01959.x (1992).

47 Oshita, F. & Eastman, A. Gene-specific damage produced by cisplatin, ormaplatin and UV light in human cells as assayed by the polymerase chain reaction. *Oncology research* **5**, 111-118 (1993).

48 Wang, L. C. & Gautier, J. The Fanconi anemia pathway and ICL repair: implications for cancer therapy. *Critical reviews in biochemistry and molecular biology* **45**, 424-439, doi:10.3109/10409238.2010.502166 (2010).

49 Ceccaldi, R., Sarangi, P. & D'Andrea, A. D. The Fanconi anaemia pathway: new players and new functions. *Nature reviews. Molecular cell biology* **17**, 337-349, doi:10.1038/nrm.2016.48 (2016).

50 Hu, J., Lieb, J. D., Sancar, A. & Adar, S. Cisplatin DNA damage and repair maps of the human genome at single-nucleotide resolution. *Proceedings of the National Academy of Sciences* **113**, 11507, doi:10.1073/pnas.1614430113 (2016).

51 Yimit, A., Adebali, O., Sancar, A. & Jiang, Y. Differential damage and repair of DNA-adducts induced by anti-cancer drug cisplatin across mouse organs. *Nature communications* **10**, 309, doi:10.1038/s41467-019-08290-2 (2019).

52 Galea, A. M. & Murray, V. The interaction of cisplatin and analogues with DNA in reconstituted chromatin. *Biochimica et biophysica acta* **1579**, 142-152, doi:10.1016/s0167-4781(02)00535-3 (2002).

53 Bubley, G. J. *et al.* Effect of DNA conformation on cisplatin adduct formation. *Biochemical pharmacology* **51**, 717-721 (1996).

54 Houssier, C., Depauw-Gillet, M. C., Hacha, R. & Fredericq, E. Alteration in the nucleosome and chromatin structures upon interaction with platinum coordination complexes. *Biochimica et biophysica acta* **739**, 317-325, doi:10.1016/0167-4781(83)90107-0 (1983).

55 Millard, J. T. & Wilkes, E. E. cis- and trans-diamminedichloroplatinum(II) interstrand cross-linking of a defined sequence nucleosomal core particle. *Biochemistry* **39**, 16046-16055, doi:10.1021/bi0022285 (2000).

56 Bouayadi, K. & Salles, B. Influence of DNA supercoiling on cisplatin toxicity in Escherichia coli K-12. *Mutation research* **348**, 25-31, doi:10.1016/0165-7992(95)90017-9 (1995).

57 Vrâna, O., Boudny, V. & Brabec, V. Superhelical Torsion Controls DNA Interstrand Cross-Linking by Antitumor Cis - Diamminedichloroplatinum(II). *Nucleic acids research* **24**, 3918-3925, doi:10.1093/nar/24.20.3918 (1996).

58 Cech, T. & Pardue, M. L. Cross-linking of DNA with trimethylpsoralen is a probe for chromatin structure. *Cell* **11**, 631-640 (1977).

59 Bosire, R. *et al.* Intercalation of small molecules into DNA in chromatin is primarily controlled by superhelical constraint. **14**, e0224936, doi:10.1371/journal.pone.0224936 (2019).

60 Clauson, C., Schärer, O. D. & Niedernhofer, L. Advances in understanding the complex mechanisms of DNA interstrand cross-link repair. *Cold Spring Harbor perspectives in biology* **5**, a012732, doi:10.1101/cshperspect.a012732 (2013).

61 Spanswick, V. J., Hartley, J. M. & Hartley, J. A. Measurement of DNA interstrand crosslinking in individual cells using the Single Cell Gel Electrophoresis (Comet) assay. *Methods in molecular biology (Clifton, N.J.)* **613**, 267-282, doi:10.1007/978-1-60327-418-0_17 (2010).

62 Luger, K., Dechassa, M. L. & Tremethick, D. J. New insights into nucleosome and chromatin structure: an ordered state or a disordered affair? *Nature Reviews Molecular Cell Biology* **13**, 436-447, doi:10.1038/nrm3382 (2012).

63 Luijsterburg, M. S., White, M. F., van Driel, R. & Dame, R. T. The major architects of chromatin: architectural proteins in bacteria, archaea and eukaryotes. *Critical reviews in biochemistry and molecular biology* **43**, 393-418, doi:10.1080/10409230802528488 (2008).

64 Sinden, R. R. in *DNA Structure and Function* (ed Richard R. Sinden) 95-133 (Academic Press, 1994).

65 Esposito, F. & Sinden, R. R. DNA supercoiling and eukaryotic gene expression. *Oxford surveys on eukaryotic genes* **5**, 1-50 (1988).

66 Corless, S. & Gilbert, N. Investigating DNA supercoiling in eukaryotic genomes. *Briefings in functional genomics* **16**, 379-389, doi:10.1093/bfgp/elx007 (2017).

67 Bates, A. D. *DNA topology / Andrew D. Bates, Anthony Maxwell*. (IRL Press at Oxford University Press, 1993).

68 Travers, A. & Muskhelishvili, G. DNA supercoiling - a global transcriptional regulator for enterobacterial growth? *Nature reviews. Microbiology* **3**, 157-169, doi:10.1038/nrmicro1088 (2005).

69 Luger, K., Mäder, A. W., Richmond, R. K., Sargent, D. F. & Richmond, T. J. Crystal structure of the nucleosome core particle at 2.8 Å resolution. *Nature* **389**, 251-260, doi:10.1038/38444 (1997).

70 Travers, A. & Muskhelishvili, G. A common topology for bacterial and eukaryotic transcription initiation? *EMBO reports* **8**, 147-151, doi:10.1038/sj.embor.7400898 (2007).

71 Localized torsional tension in the DNA of human cells. *Proceedings of the National Academy of Sciences* **89**, 9364, doi:10.1073/pnas.89.19.9364-c (1992).

72 Liu, L. F. & Wang, J. C. Supercoiling of the DNA template during transcription. *Proceedings of the National Academy of Sciences of the United States of America* **84**, 7024-7027, doi:10.1073/pnas.84.20.7024 (1987).

73 Pommier, Y., Leo, E., Zhang, H. & Marchand, C. DNA topoisomerases and their poisoning by anticancer and antibacterial drugs. *Chemistry & biology* **17**, 421-433, doi:10.1016/j.chembiol.2010.04.012 (2010).

74 Fogg, J. M., Catanese, D. J., Randall, G. L., Swick, M. C. & Zechiedrich, L. in *Mathematics of DNA Structure, Function and Interactions.* (eds Craig John Benham *et al.*) 73-121 (Springer New York).

75 Travers, A. & Muskhelishvili, G. DNA structure and function. *The FEBS journal* **282**, 2279-2295, doi:10.1111/febs.13307 (2015).

76 Seol, Y. & Neuman, K. C. The Dynamic Interplay Between DNA Topoisomerases and DNA Topology. *Biophysical reviews* **8**, 221-231, doi:10.1007/s12551-016-0206-x (2016).

77 Deweese, J. E., Osheroff, M. A. & Osheroff, N. DNA Topology and Topoisomerases: Teaching a "Knotty" Subject. *Biochemistry and molecular biology education : a bimonthly publication of the International Union of Biochemistry and Molecular Biology* **37**, 2-10, doi:10.1002/bmb.20244 (2008).

78 Vologodskii, A. V. & Cozzarelli, N. R. Conformational and thermodynamic properties of supercoiled DNA. *Annual review of biophysics and biomolecular structure* **23**, 609-643, doi:10.1146/annurev.bb.23.060194.003141 (1994).

79 Gentry, A. C., Juul, S., Veigaard, C., Knudsen, B. R. & Osheroff, N. The geometry of DNA supercoils modulates the DNA cleavage activity of human topoisomerase I. *Nucleic acids research* **39**, 1014-1022, doi:10.1093/nar/gkq822 (2010).

80 Podtelezhnikov, A. A., Cozzarelli, N. R. & Vologodskii, A. V. Equilibrium distributions of topological states in circular DNA: interplay of supercoiling and knotting. *Proceedings of the National Academy of Sciences of the United States of America* **96**, 12974-12979, doi:10.1073/pnas.96.23.12974 (1999).

81 Boles, T. C., White, J. H. & Cozzarelli, N. R. Structure of plectonemically supercoiled DNA. *Journal of molecular biology* **213**, 931-951, doi:https://doi.org/10.1016/S0022-2836(05)80272-4 (1990).

82 Koster, D. A., Crut, A., Shuman, S., Bjornsti, M. A. & Dekker, N. H. Cellular strategies for regulating DNA supercoiling: a single-molecule perspective. *Cell* **142**, 519-530, doi:10.1016/j.cell.2010.08.001 (2010).

83 Witz, G. & Stasiak, A. DNA supercoiling and its role in DNA decatenation and unknotting. *Nucleic acids research* **38**, 2119-2133, doi:10.1093/nar/gkp1161 (2010).

84 Bauer, W. R. STRUCTURE AND REACTIONS OF CLOSED DUPLEX DNA. *Annual Review of Biophysics and Bioengineering* **7**, 287-313, doi:10.1146/annurev.bb.07.060178.001443 (1978).

85 Keck, M. V. & Lippard, S. J. Unwinding of supercoiled DNA by platinum-ethidium and related complexes. *Journal of the American Chemical Society* **114**, 3386-3390, doi:10.1021/ja00035a033 (1992).

86 Minotti, G., Menna, P., Salvatorelli, E., Cairo, G. & Gianni, L. Anthracyclines: molecular advances and pharmacologic developments in antitumor activity and cardiotoxicity. *Pharmacological reviews* **56**, 185-229, doi:10.1124/pr.56.2.6 (2004).

87 Siegfried, J. M., Burke, T. G. & Tritton, T. R. Cellular transport of anthracyclines by passive diffusion: Implications for drug resistance. *Biochemical pharmacology* **34**, 593-598, doi:https://doi.org/10.1016/0006-2952(85)90251-5 (1985).

88 Regev, R., Yeheskely-Hayon, D., Katzir, H. & Eytan, G. D. Transport of anthracyclines and mitoxantrone across membranes by a flip-flop mechanism. *Biochemical pharmacology* **70**, 161-169, doi:10.1016/j.bcp.2005.03.032 (2005).

89 Escriba, P. V., Ferrer-Montiel, A. V., Ferragut, J. A. & Gonzalez-Ros, J. M. Role of membrane lipids in the interaction of daunomycin with plasma membranes from tumor cells: implications in drug-resistance phenomena. *Biochemistry* **29**, 7275-7282, doi:10.1021/bi00483a017 (1990).

90 Escribá, P. V., Sastre, M. & García-Sevilla, J. A. Disruption of cellular signaling pathways by daunomycin through destabilization of nonlamellar membrane structures. *Proceedings of the National Academy of Sciences of the United States of America* **92**, 7595-7599, doi:10.1073/pnas.92.16.7595 (1995).

91 Alves, A. C. *et al.* A biophysical approach to daunorubicin interaction with model membranes: relevance for the drug's biological activity. *J R Soc Interface* **14**, doi:10.1098/rsif.2017.0408 (2017).

92 Jaffrézou, J. P. *et al.* Daunorubicin-induced apoptosis: triggering of ceramide generation through sphingomyelin hydrolysis. *EMBO J* **15**, 2417-2424 (1996).

93 Escriba, P. V. *et al.* Membranes: a meeting point for lipids, proteins and therapies. *Journal of cellular and molecular medicine* **12**, 829-875, doi:10.1111/j.1582-4934.2008.00281.x (2008).

94 Berlin, V. & Haseltine, W. A. Reduction of adriamycin to a semiquinone-free radical by NADPH cytochrome P-450 reductase produces DNA cleavage in a reaction mediated by molecular oxygen. *The Journal of biological chemistry* **256**, 4747-4756 (1981).

95 Gewirtz, D. A. A critical evaluation of the mechanisms of action proposed for the antitumor effects of the anthracycline antibiotics adriamycin and daunorubicin. *Biochemical pharmacology* **57**, 727-741, doi:10.1016/s0006-2952(98)00307-4 (1999).

96 Zweier, J. L., Gianni, L., Muindi, J. & Myers, C. E. Differences in O2 reduction by the iron complexes of adriamycin and daunomycin: the importance of the sidechain hydroxyl group. *Biochimica et Biophysica Acta (BBA) - General Subjects* **884**, 326-336, doi:https://doi.org/10.1016/0304-4165(86)90181-9 (1986).

97 Taatjes, D. J. & Koch, T. H. Nuclear targeting and retention of anthracycline antitumor drugs in sensitive and resistant tumor cells. *Current medicinal chemistry* **8**, 15-29, doi:10.2174/0929867013374029 (2001).

98 Skladanowski, A. & Konopa, J. Relevance of interstrand DNA crosslinking induced by anthracyclines for their biological activity. *Biochemical pharmacology* **47**, 2279-2287, doi:https://doi.org/10.1016/0006-2952(94)90266-6 (1994).

99 Kato, S. *et al.* Mass spectrometric measurement of formaldehyde generated in breast cancer cells upon treatment with anthracycline antitumor drugs. *Chemical research in toxicology* **13**, 509-516, doi:10.1021/tx000008m (2000).

100 Kasukabe, T., Rephaeli, A. & Honma, Y. An anti-cancer derivative of butyric acid (pivalyloxmethyl buterate) and daunorubicin cooperatively prolong survival of mice inoculated with monocytic leukaemia cells. *British journal of cancer* **75**, 850-854, doi:10.1038/bjc.1997.151 (1997).

101 Swift, L. P., Rephaeli, A., Nudelman, A., Phillips, D. R. & Cutts, S. M. Doxorubicin-DNA Adducts Induce a Non-Topoisomerase II–Mediated Form of Cell Death. *Cancer research* **66**, 4863, doi:10.1158/0008-5472.CAN-05-3410 (2006).

102 McClendon, A. K., Rodriguez, A. C. & Osheroff, N. Human topoisomerase IIalpha rapidly relaxes positively supercoiled DNA: implications for enzyme action ahead of replication forks. *The Journal of biological chemistry* **280**, 39337-39345, doi:10.1074/jbc.M503320200 (2005).

103 Pommier, Y. Topoisomerase I inhibitors: camptothecins and beyond. *Nature Reviews Cancer* **6**, 789-802, doi:10.1038/nrc1977 (2006).

104 Bodley, A. *et al.* DNA topoisomerase II-mediated interaction of doxorubicin and daunorubicin congeners with DNA. *Cancer research* **49**, 5969-5978 (1989).

105 Di Marco, A., Silvestrini, R., Di Marco, S. & Dasdia, T. Inhibiting effect of the new cytotoxic antibiotic daunomycin on nucleic acids and mitotic activity of HeLa cells. *The Journal of cell biology* **27**, 545-550, doi:10.1083/jcb.27.3.545 (1965).

106 Goodman, M. F., Bessman, M. J. & Bachur, N. R. Adriamycin and daunorubicin inhibition of mutant T4 DNA polymerases. *Proceedings of the National Academy of Sciences of the United States of America* **71**, 1193-1196, doi:10.1073/pnas.71.4.1193 (1974).

107 Zunina, F., Gambetta, R. & Di Marco, A. The inhibition in vitro of DNA polymerase and RNA polymerases by daunomycin and adriamycin. *Biochemical pharmacology* **24**, 309-311, doi:10.1016/0006-2952(75)90300-7 (1975).

108 Tanaka, M. & Yoshida, S. Mechanism of the inhibition of calf thymus DNA polymerases alpha and beta by daunomycin and adriamycin. *Journal of biochemistry* **87**, 911-918, doi:10.1093/oxfordjournals.jbchem.a132821 (1980).

109 Munger, C. *et al.* Evidence for inhibition of growth related to compromised DNA synthesis in the interaction of daunorubicin with H-35 rat hepatoma. *Cancer research* **48**, 2404-2411 (1988).

110 Frederick, C. A. *et al.* Structural comparison of anticancer drug-DNA complexes: adriamycin and daunomycin. *Biochemistry* **29**, 2538-2549, doi:10.1021/bi00462a016 (1990).

111 Chaires, J. B., Dattagupta, N. & Crothers, D. M. Studies on interaction of anthracycline antibiotics and deoxyribonucleic acid: equilibrium binding studies on interaction of daunomycin with deoxyribonucleic acid. *Biochemistry* **21**, 3933-3940, doi:10.1021/bi00260a005 (1982).

112 Quigley, G. J. *et al.* Molecular structure of an anticancer drug-DNA complex: daunomycin plus d(CpGpTpApCpG). *Proceedings of the National Academy of Sciences of the United States of America* **77**, 7204-7208, doi:10.1073/pnas.77.12.7204 (1980).

113 Aubel-Sadron, G. & Londos-Gagliardi, D. Daunorubicin and doxorubicin, anthracycline antibiotics, a physicochemical and biological review. *Biochimie* **66**, 333-352, doi:https://doi.org/10.1016/0300-9084(84)90018-X (1984).

114 Gupta, P., Zlatanova, J. & Tomschik, M. Nucleosome assembly depends on the torsion in the DNA molecule: a magnetic tweezers study. *Biophysical journal* **97**, 3150-3157, doi:10.1016/j.bpj.2009.09.032 (2009).

115 Clark, D. J. & Felsenfeld, G. Formation of nucleosomes on positively supercoiled DNA. *EMBO J* **10**, 387-395 (1991).

116 Pang, B. *et al.* Drug-induced histone eviction from open chromatin contributes to the chemotherapeutic effects of doxorubicin. *Nature communications* **4**, 1908, doi:10.1038/ncomms2921 (2013).

117 Imre, L. *et al.* Nucleosome stability measured in situ by automated quantitative imaging. **7**, 12734, doi:10.1038/s41598-017-12608-9 (2017).

118 Rabbani, A., Iskandar, M. & Ausio, J. Daunomycin-induced unfolding and aggregation of chromatin. *The Journal of biological chemistry* **274**, 18401-18406, doi:10.1074/jbc.274.26.18401 (1999).

119 Rabbani, A., Finn, R. M., Thambirajah, A. A. & Ausio, J. Binding of antitumor antibiotic daunomycin to histones in chromatin and in solution. *Biochemistry* **43**, 16497-16504, doi:10.1021/bi048524p (2004).

120 Nánási, P., Jr. *et al.* Doxorubicin induces large-scale and differential H2A and H2B redistribution in live cells. *PloS one* **15**, e0231223, doi:10.1371/journal.pone.0231223 (2020).

121 Hayball, M. CalcuSyn for Windows: Multiple-Drug Dose-Effect Analyzer and Manual. (1997).

122 Chou, T. & Martin, N. CompuSyn for drug combinations: PC software and user's guide: a computer program for quantitation of synergism and antagonism in drug combinations, and the determination of IC50 and ED50 and LD50 values. *ComboSyn, Paramus, NJ* (2005).

123 Chou, T. C. Derivation and properties of Michaelis-Menten type and Hill type equations for reference ligands. *Journal of theoretical biology* **59**, 253-276, doi:10.1016/0022-5193(76)90169-7 (1976).

124 Michaelis, L., Menten, M. L., Johnson, K. A. & Goody, R. S. The original Michaelis constant: translation of the 1913 Michaelis-Menten paper. *Biochemistry* **50**, 8264-8269, doi:10.1021/bi201284u (2011).

125 Chou, T. C. Theoretical basis, experimental design, and computerized simulation of synergism and antagonism in drug combination studies. *Pharmacological reviews* **58**, 621-681, doi:10.1124/pr.58.3.10 (2006).

126 O'Brien, J., Wilson, I., Orton, T. & Pognan, F. Investigation of the Alamar Blue (resazurin) fluorescent dye for the assessment of mammalian cell cytotoxicity. *European journal of biochemistry* **267**, 5421-5426, doi:10.1046/j.1432-1327.2000.01606.x (2000).

127 Chou, T. C. Drug combination studies and their synergy quantification using the Chou-Talalay method. *Cancer research* **70**, 440-446, doi:10.1158/0008-5472.can-09-1947 (2010).

128 Yang, F., Teves, S. S., Kemp, C. J. & Henikoff, S. Doxorubicin, DNA torsion, and chromatin dynamics. *Biochimica et biophysica acta* **1845**, 84-89, doi:10.1016/j.bbcan.2013.12.002 (2014).

129 Hegedus, E., Kokai, E., Kotlyar, A., Dombradi, V. & Szabo, G. Separation of 1-23-kb complementary DNA strands by urea-agarose gel electrophoresis. *Nucleic acids research* **37**, e112, doi:10.1093/nar/gkp539 (2009).

130 Materna, T., Weber, S., Kofler-Mongold, V. & Phares, W. Electrophoretic separation of both single- and double-stranded nucleic acids in the same urea-containing agarose gel. *Analytical biochemistry* **255**, 161-163, doi:10.1006/abio.1997.2464 (1998).

131 Szentesi, G. *et al.* Computer program for determining fluorescence resonance energy transfer efficiency from flow cytometric data on a cell-by-cell basis. *Computer methods and programs in biomedicine* **75**, 201-211, doi:10.1016/j.cmpb.2004.02.004 (2004).

132 Kimura, H. & Cook, P. R. Kinetics of core histones in living human cells: little exchange of H3 and H4 and some rapid exchange of H2B. *The Journal of cell biology* **153**, 1341-1353, doi:10.1083/jcb.153.7.1341 (2001).

133 Van Malderen, S. J. M., van Elteren, J. T. & Vanhaecke, F. Development of a fast laser ablation-inductively coupled plasma-mass spectrometry cell for sub-μm scanning of layered materials. *Journal of Analytical Atomic Spectrometry* **30**, 119-125, doi:10.1039/C4JA00137K (2015).

134 Pozebon, D., Scheffler, G. L. & Dressler, V. L. Recent applications of laser ablation inductively coupled plasma mass spectrometry (LA-ICP-MS) for biological sample analysis: a follow-up review. *Journal of Analytical Atomic Spectrometry* **32**, 890-919, doi:10.1039/C7JA00026J (2017).

135 Van Acker, T. *et al.* High-resolution laser ablation-inductively coupled plasma-mass spectrometry imaging of cisplatin-induced nephrotoxic side effects. *Analytica chimica acta* **945**, 23-30, doi:10.1016/j.aca.2016.10.014 (2016).

136 Van Acker, T. *et al.* High-resolution imaging and single-cell analysis via laser ablation-inductively coupled plasma-mass spectrometry for the determination of membranous receptor expression levels in breast cancer cell lines using receptor-specific hybrid tracers. *Analytica chimica acta* **1074**, 43-53, doi:10.1016/j.aca.2019.04.064 (2019).

137 Coldwell, K. E., Cutts, S. M., Ognibene, T. J., Henderson, P. T. & Phillips, D. R. Detection of Adriamycin-DNA adducts by accelerator mass spectrometry at clinically relevant Adriamycin concentrations. *Nucleic acids research* **36**, e100-e100, doi:10.1093/nar/gkn439 (2008).

138 Olive, P. L. & Banáth, J. P. Kinetics of H2AX phosphorylation after exposure to cisplatin. *Cytometry Part B: Clinical Cytometry* **76B**, 79-90, doi:10.1002/cyto.b.20450 (2009).

139 Wu, F., Lin, X., Okuda, T. & Howell, S. B. DNA polymerase zeta regulates cisplatin cytotoxicity, mutagenicity, and the rate of development of cisplatin resistance. *Cancer research* **64**, 8029-8035, doi:10.1158/0008-5472.can-03-3942 (2004).

140 Spencer, D. M. S. *et al.* DNA repair in response to anthracycline–DNA adducts: A role for both homologous recombination and nucleotide excision repair. *Mutation Research/Fundamental and Molecular Mechanisms of Mutagenesis* **638**, 110-121, doi:https://doi.org/10.1016/j.mrfmmm.2007.09.005 (2008).

141 Wang, A. H. J., Gao, Y. G., Liaw, Y. C. & Li, Y. K. Formaldehyde crosslinks daunorubicin and DNA efficiently: HPLC and x-ray diffraction studies. *Biochemistry* **30**, 3812-3815, doi:10.1021/bi00230a002 (1991).

142 Kim, E. S. *et al.* Phase II study of a multidisciplinary approach with induction chemotherapy, followed by surgical resection, radiation therapy, and consolidation chemotherapy for unresectable malignant thymomas: final report. *Lung cancer (Amsterdam, Netherlands)* **44**, 369-379, doi:10.1016/j.lungcan.2003.12.010 (2004).

143 Nakamura, K., Okuyama, R., Saida, T. & Uhara, H. Platinum and anthracycline therapy for advanced cutaneous squamous cell carcinoma. *International journal of clinical oncology* **18**, 506-509, doi:10.1007/s10147-012-0411-y (2013).

144 Guardiola, E. *et al.* Combination of cisplatin-doxorubicin-cyclophosphamide in adenocarcinoma of unknown primary site: a phase II trial. *American journal of clinical oncology* **24**, 372-375, doi:10.1097/00000421-200108000-00012 (2001).

145 Lee, S.-M., O'Halloran, T. V. & Nguyen, S. T. Polymer-Caged Nanobins for Synergistic Cisplatin−Doxorubicin Combination Chemotherapy. *Journal of the American Chemical Society* **132**, 17130-17138, doi:10.1021/ja107333g (2010).

146 Chou, T. C. & Talalay, P. Quantitative analysis of dose-effect relationships: the combined effects of multiple drugs or enzyme inhibitors. *Advances in enzyme regulation* **22**, 27-55, doi:10.1016/0065-2571(84)90007-4 (1984).

147 Peterson, C., Baurain, R. & Trouet, A. The mechanism for cellular uptake, storage and release of daunorubicin. Studies on fibroblasts in culture. *Biochemical pharmacology* **29**, 1687-1692, doi:10.1016/0006-2952(80)90126-4 (1980).

148 Belloc, F. *et al.* Intercalation of anthracyclines into living cell DNA analyzed by flow cytometry. *Cytometry* **13**, 880-885, doi:10.1002/cyto.990130811 (1992).

149 Arndt-Jovin, D. J. & Jovin, T. M. Analysis and sorting of living cells according to deoxyribonucleic acid content. *J Histochem Cytochem* **25**, 585-589, doi:10.1177/25.7.70450 (1977).

150 Szabo, G., Jr., Kiss, A. & Damjanovich, S. Flow cytometric analysis of the uptake of Hoechst 33342 dye by human lymphocytes. *Cytometry* **2**, 20-23, doi:10.1002/cyto.990020104 (1981).

151 Goda, K., Bacsó, Z. & Szabó, G. Multidrug resistance through the spectacle of P-glycoprotein. *Curr Cancer Drug Targets* **9**, 281-297, doi:10.2174/156800909788166493 (2009).

152 Pfuhler, S. & Wolf, H. U. Detection of DNA-crosslinking agents with the alkaline comet assay. *Environmental and molecular mutagenesis* **27**, 196-201, doi:10.1002/(sici)1098-2280(1996)27:3<196::aid-em4>3.0.co;2-d (1996).

153 Peters, G. J. *et al.* Interaction between cisplatin and gemcitabine in vitro and in vivo. *Seminars in oncology* **22**, 72-79 (1995).

154 Arancia, G., Calcabrini, A., Meschini, S. & Molinari, A. Intracellular distribution of anthracyclines in drug resistant cells. *Cytotechnology* **27**, 95-111, doi:10.1023/a:1008040117882 (1998).

155 Rajapakse, V. N. *et al.* CellMinerCDB for Integrative Cross-Database Genomics and Pharmacogenomics Analyses of Cancer Cell Lines. *iScience* **10**, 247-264, doi:10.1016/j.isci.2018.11.029 (2018).

156 Holbeck, S. L. *et al.* The National Cancer Institute ALMANAC: A Comprehensive Screening Resource for the Detection of Anticancer Drug Pairs with Enhanced Therapeutic Activity. *Cancer research* **77**, 3564-3576, doi:10.1158/0008-5472.can-17-0489 (2017).

157 Fritzsche, H. *et al.* Anthracycline antibiotics. Interaction with DNA and nucleosomes and inhibition of DNA synthesis. *Biochemistry* **26**, 1996-2000, doi:10.1021/bi00381a032 (1987).

158 Johnston, F. P., Jorgenson, K. F., Lin, C. C. & van de Sande, J. H. Interaction of anthracyclines with DNA and chromosomes. *Chromosoma* **68**, 115-129, doi:10.1007/BF00287144 (1978).

159 Jamieson, E. R. & Lippard, S. J. Structure, Recognition, and Processing of Cisplatin-DNA Adducts. *Chemical reviews* **99**, 2467-2498 (1999).

160 Spingler, B., Whittington, D. A. & Lippard, S. J. 2.4 A crystal structure of an oxaliplatin 1,2-d(GpG) intrastrand cross-link in a DNA dodecamer duplex. *Inorganic chemistry* **40**, 5596-5602 (2001).

161 Japaridze, A. *et al.* Hyperplectonemes: A Higher Order Compact and Dynamic DNA Self-Organization. **17**, 1938-1948, doi:10.1021/acs.nanolett.6b05294 (2017).

162 Vrana, O., Boudny, V. & Brabec, V. Superhelical torsion controls DNA interstrand cross-linking by antitumor cis- diamminedichloroplatinum(II). *Nucleic acids research* **24**, 3918-3925, doi:10.1093/nar/24.20.3918 (1996).

163 Corless, S. & Gilbert, N. Effects of DNA supercoiling on chromatin architecture. **8**, 245-258 (2016).

164 Bednar, J. *et al.* The twist, writhe and overall shape of supercoiled DNA change during counterion-induced transition from a loosely to a tightly interwound superhelix. Possible implications for DNA structure in vivo. *Journal of molecular biology* **235**, 825-847, doi:10.1006/jmbi.1994.1042 (1994).

165 Bishop, T. C. Geometry of the nucleosomal DNA superhelix. *Biophysical journal* **95**, 1007-1017, doi:10.1529/biophysj.107.122853 (2008).

166 Burgess, D. J. *et al.* Topoisomerase levels determine chemotherapy response in vitro and in vivo. *Proceedings of the National Academy of Sciences of the United States of America* **105**, 9053-9058, doi:10.1073/pnas.0803513105 (2008).

167 Braunstein, M. *et al.* Downregulation of histone H2A and H2B pathways is associated with anthracycline sensitivity in breast cancer. *Breast Cancer Res* **18**, 16-16, doi:10.1186/s13058-016-0676-6 (2016).

168 Kapfhamer, D. *et al.* Ornithine decarboxylase, the rate-limiting enzyme of polyamine synthesis, modifies brain pathology in a mouse model of tuberous sclerosis complex. *Human Molecular Genetics* **29**, 2395-2407, doi:10.1093/hmg/ddaa121 (2020).

169 Zabala-Letona, A. *et al.* mTORC1-dependent AMD1 regulation sustains polyamine metabolism in prostate cancer. *Nature* **547**, 109-113, doi:10.1038/nature22964 (2017).

170 Paz, E. A., Garcia-Huidobro, J. & Ignatenko, N. A. in *Advances in Clinical Chemistry* Vol. 54 (ed Gregory S. Makowski) 45-70 (Elsevier, 2011).

171 Ernestus, R. I. *et al.* Polyamine metabolism in brain tumours: diagnostic relevance of quantitative biochemistry. *J Neurol Neurosurg Psychiatry* **71**, 88-92, doi:10.1136/jnnp.71.1.88 (2001).

172 Bale, S. & Ealick, S. E. Structural biology of S-adenosylmethionine decarboxylase. *Amino Acids* **38**, 451-460, doi:10.1007/s00726-009-0404-y (2010).

173 Nishimura, K. *et al.* Effects of polyamines on two strains of Trypanosoma brucei in infected rats and in vitro culture. *The Journal of parasitology* **92**, 211-217, doi:10.1645/ge-633r.1 (2006).

174 Perdeh, J. *et al.* Critical functions of the polyamine putrescine for proliferation and viability of Leishmania donovani parasites. *Amino Acids* **52**, 261-274, doi:10.1007/s00726-019-02736-z (2020).

175 Morrison, L. D. & Kish, S. J. Brain polyamine levels are altered in Alzheimer's disease. *Neuroscience letters* **197**, 5-8, doi:10.1016/0304-3940(95)11881-v (1995).

176 Saiki, S. *et al.* A metabolic profile of polyamines in parkinson disease: A promising biomarker. **86**, 251-263, doi:10.1002/ana.25516 (2019).

177 Minois, N., Carmona-Gutierrez, D. & Madeo, F. Polyamines in aging and disease. *Aging* **3**, 716-732, doi:10.18632/aging.100361 (2011).

178 López-Contreras, F. *et al.* Searching for Drug Synergy Against Cancer Through Polyamine Metabolism Impairment: Insight Into the Metabolic Effect of Indomethacin on Lung Cancer Cells. *Frontiers in pharmacology* **10**, 1670, doi:10.3389/fphar.2019.01670 (2019).

179 Gamble, L. D. *et al.* Inhibition of polyamine synthesis and uptake reduces tumor progression and prolongs survival in mouse models of neuroblastoma. *Science Translational Medicine* **11**, eaau1099, doi:10.1126/scitranslmed.aau1099 (2019).

180 Evageliou, N. F. *et al.* Polyamine Antagonist Therapies Inhibit Neuroblastoma Initiation and Progression. *Clinical cancer research : an official journal of the American Association for Cancer Research* **22**, 4391-4404, doi:10.1158/1078-0432.ccr-15-2539 (2016).

181 Meyskens, F. L., Jr. *et al.* Difluoromethylornithine plus sulindac for the prevention of sporadic colorectal adenomas: a randomized placebo-controlled, double-blind trial. *Cancer prevention research (Philadelphia, Pa.)* **1**, 32-38, doi:10.1158/1940-6207.capr-08-0042 (2008).

182 Fischer, S. M., Conti, C. J., Viner, J., Aldaz, C. M. & Lubet, R. A. Celecoxib and difluoromethylornithine in combination have strong therapeutic activity against UV-

induced skin tumors in mice. *Carcinogenesis* **24**, 945-952, doi:10.1093/carcin/bgg046 (2003).

183 Burns, M. R., Graminski, G. F., Weeks, R. S., Chen, Y. & O'Brien, T. G. Lipophilic lysine-spermine conjugates are potent polyamine transport inhibitors for use in combination with a polyamine biosynthesis inhibitor. *Journal of medicinal chemistry* **52**, 1983-1993, doi:10.1021/jm801580w (2009).

184 Pegg, A. E. Mammalian polyamine metabolism and function. *IUBMB life* **61**, 880-894, doi:10.1002/iub.230 (2009).

185 Yamashita, T. *et al.* Role of polyamines at the G1/S boundary and G2/M phase of the cell cycle. *The international journal of biochemistry & cell biology* **45**, 1042-1050, doi:10.1016/j.biocel.2013.02.021 (2013).

186 Ueda, A., Araie, M. & Kubota, S. Polyamine depletion induces G1 and S phase arrest in human retinoblastoma Y79 cells. *Cancer Cell Int* **8**, 2-2, doi:10.1186/1475-2867-8-2 (2008).

187 Pelta, J., Livolant, F. & Sikorav, J. L. DNA aggregation induced by polyamines and cobalthexamine. *The Journal of biological chemistry* **271**, 5656-5662, doi:10.1074/jbc.271.10.5656 (1996).

188 Smirnov, I. V., Dimitrov, S. I. & Makarov, V. L. Polyamine-DNA interactions. Condensation of chromatin and naked DNA. *Journal of biomolecular structure & dynamics* **5**, 1149-1161, doi:10.1080/07391102.1988.10506455 (1988).

189 Ni, X. & Cole, R. D. Effects of Various Salts and pH on the Stability of the Nucleosome in Chromatin Fragments. *Biochemistry* **33**, 9276-9284, doi:10.1021/bi00197a031 (1994).

190 Visvanathan, A. *et al.* Modulation of Higher Order Chromatin Conformation in Mammalian Cell Nuclei Can Be Mediated by Polyamines and Divalent Cations. *PloS one* **8**, e67689, doi:10.1371/journal.pone.0067689 (2013).

191 Sauvé, D. M., Anderson, H. J., Ray, J. M., James, W. M. & Roberge, M. Phosphorylation-induced rearrangement of the histone H3 NH2-terminal domain during mitotic chromosome condensation. *The Journal of cell biology* **145**, 225-235, doi:10.1083/jcb.145.2.225 (1999).

192 Raspaud, E., Chaperon, I., Leforestier, A. & Livolant, F. Spermine-Induced Aggregation of DNA, Nucleosome, and Chromatin. *Biophysical journal* **77**, 1547-1555, doi:https://doi.org/10.1016/S0006-3495(99)77002-5 (1999).

193 Schipper, R. G., Romijn, J. C., Cuijpers, V. M. & Verhofstad, A. A. Polyamines and prostatic cancer. *Biochemical Society transactions* **31**, 375-380, doi:10.1042/bst0310375 (2003).

194 Ohyama, T. New Aspects of Magnesium Function: A Key Regulator in Nucleosome Self-Assembly, Chromatin Folding and Phase Separation. *International journal of molecular sciences* **20**, doi:10.3390/ijms20174232 (2019).

195 Imre, L. *et al.* Nucleosome stability measured in situ by automated quantitative imaging. **7**, 12734, doi:10.1038/s41598-017-12608-9 (2017).

196 Nishida, H. Relationship between chromosomal GC content and isoelectric points of histones in fungi. *The Journal of general and applied microbiology* **61**, 24-26, doi:10.2323/jgam.61.24 (2015).

197 Chung, S. Y., Hill, W. E. & Doty, P. Characterization of the histone core complex. *Proceedings of the National Academy of Sciences of the United States of America* **75**, 1680-1684, doi:10.1073/pnas.75.4.1680 (1978).

198 Brooks, W. H. Increased polyamines alter chromatin and stabilize autoantigens in autoimmune diseases. *Frontiers in immunology* **4**, 91, doi:10.3389/fimmu.2013.00091 (2013).

199 Sarhan, S. & Seiler, N. On the subcellular localization of the polyamines. *Biological chemistry Hoppe-Seyler* **370**, 1279-1284, doi:10.1515/bchm3.1989.370.2.1279 (1989).

200 Svensson, K. J. *et al.* Hypoxia-mediated induction of the polyamine system provides opportunities for tumor growth inhibition by combined targeting of vascular endothelial growth factor and ornithine decarboxylase. *Cancer research* **68**, 9291-9301, doi:10.1158/0008-5472.can-08-2340 (2008).

201 Murai, N., Murakami, Y., Tajima, A. & Matsufuji, S. Novel ubiquitin-independent nucleolar c-Myc degradation pathway mediated by antizyme 2. *Scientific reports* **8**, 3005, doi:10.1038/s41598-018-21189-0 (2018).

202 Takahashi, T. Plant Polyamines. *Plants (Basel, Switzerland)* **9**, doi:10.3390/plants9040511 (2020).

203 Soda, K. Polyamine Metabolism and Gene Methylation in Conjunction with One-Carbon Metabolism. *International journal of molecular sciences* **19**, doi:10.3390/ijms19103106 (2018).

204 Chen, D., Shao, Q., Yin, L., Younis, A. & Zheng, B. Polyamine Function in Plants: Metabolism, Regulation on Development, and Roles in Abiotic Stress Responses. *Frontiers in plant science* **9**, 1945, doi:10.3389/fpls.2018.01945 (2018).

205 Ni, X. & Cole, R. D. Effects of various salts and pH on the stability of the nucleosome in chromatin fragments. *Biochemistry* **33**, 9276-9284, doi:10.1021/bi00197a031 (1994).

206 Hobbs, C. A. & Gilmour, S. K. High levels of intracellular polyamines promote histone acetyltransferase activity resulting in chromatin hyperacetylation. *Journal of cellular biochemistry* **77**, 345-360 (2000).

207 Fukui, T. & Soda, K. Extracellular Spermine Activates DNA Methyltransferase 3A and 3B. **20**, doi:10.3390/ijms20051254 (2019).

208 Paul, S. & Bartholomew, B. Regulation of ATP-dependent chromatin remodelers: accelerators/brakes, anchors and sensors. **46**, 1423-1430, doi:10.1042/bst20180043 (2018).

209 Bosire, R. *et al.* Intercalation of small molecules into DNA in chromatin is primarily controlled by superhelical constraint. **14**, e0224936, doi:10.1371/journal.pone.0224936 (2019).

UNIVERSITY AND NATIONAL LIBRARY
UNIVERSITY OF DEBRECEN
H-4002 Egyetem tér 1, Debrecen
Phone: +3652/410-443, email: publikaciok@lib.unideb.hu

Registry number: DEENK/128/2021.PL
Subject: PhD Publication List

Candidate: Erfaneh Firouzi Niaki
Doctoral School: Doctoral School of Molecular Cellular and Immune Biology

List of publications related to the dissertation

1. Nánási, P. P. i., Imre, L., **Firouzi Niaki, E.**, Bosire, R., Mocsár, G., Türk-Mázló, A., Ausio, J., Szabó, G.: Doxorubicin induces large-scale and differential H2A and H2B redistribution in live cells.
   PLoS One. 15 (4), e0231223-, 2020.
   DOI: http://dx.doi.org/10.1371/journal.pone.0231223
   IF: 2.74 (2019)
2. **Firouzi Niaki, E.**, Van Acker, T., Imre, L., Nánási, P. P. i., Tarapcsák, S., Bacsó, Z., Vanhaecke, F., Szabó, G.: Interactions of Cisplatin and Daunorubicin at the Chromatin Level.
   Sci. Rep. 10 (1), 1-12, 2020.
   DOI: http://dx.doi.org/10.1038/s41598-020-57702-7
   IF: 3.998 (2019)
3. Imre, L., Simándi, Z., Horváth, A., Fenyőfalvi, G., Nánási, P. P. i., **Firouzi Niaki, E.**, Hegedűs, É., Bacsó, Z., Weyemi, U., Mauser, R., Ausio, J., Jeltsch, A., Bonner, W., Nagy, L., Kimura, H., Szabó, G.: Nucleosome stability measured in situ by automated quantitative imaging.
   Sci Rep. 7 (1), 1-15, 2017.
   DOI: http://dx.doi.org/10.1038/s41598-017-12608-9
   IF: 4.122

Total IF of journals (all publications): 10,86
Total IF of journals (publications related to the dissertation): 10,86

The Candidate's publication data submitted to the iDEa Tudóstér have been validated by DEENK on the basis of the Journal Citation Report (Impact Factor) database.

30 March, 2021

8. KEY WORDS

Chromatin, Cisplatin, Daunorubicin, combination therapy, mode of drug interaction, polyamines, histone eviction, alkaline comet/halo assay

9. ACKNOWELDGMENTS

First I would like to express my deepest gratitude to my supervisor Professor. Dr. Gabor Szabo. The door to his office as well as his heart was always open whenever I ran into a trouble spot or had a question. I am extremely thankful and indebted to him for sharing expertise, sincere and valuable guidance.

I am grateful to all of those with whom I have had the pleasure to work during my journey specially Adel Nagy Vezendine.

This work would not have been possible without the financial support of the Richter Gedeon Talentum Alapítvány scholarship, I gratefully acknowledge the scholarship received towards my PhD.

I greatly appreciate the support received through the collaborative work undertaken with the Chemistry Department of Ghent University, Belgium.

Finally, I must express my very profound gratitude to my family, for providing me with unfailing support and continuous encouragement throughout my years of study and through the process of researching and writing this thesis. This accomplishment would not have been possible without them.

10. Appendix